

OXFORD

PRINCIPLES
OF MATERIALS
CHARACTERIZATION
AND METROLOGY

KANNAN M. KRISHNAN



PRINCIPLES OF MATERIALS CHARACTERIZATION AND METROLOGY

Principles of Materials Characterization and Metrology

Kannan M. Krishnan

University of Washington, Seattle

OXFORD
UNIVERSITY PRESS

OXFORD

UNIVERSITY PRESS

Great Clarendon Street, Oxford, OX2 6DP,
United Kingdom

Oxford University Press is a department of the University of Oxford.
It furthers the University's objective of excellence in research, scholarship,
and education by publishing worldwide. Oxford is a registered trade mark of
Oxford University Press in the UK and in certain other countries

© Kannan M. Krishnan 2021

The moral rights of the author have been asserted

First Edition published in 2021

Impression: 1

All rights reserved. No part of this publication may be reproduced, stored in
a retrieval system, or transmitted, in any form or by any means, without the
prior permission in writing of Oxford University Press, or as expressly permitted
by law, by licence or under terms agreed with the appropriate reprographics
rights organization. Enquiries concerning reproduction outside the scope of the
above should be sent to the Rights Department, Oxford University Press, at the
address above

You must not circulate this work in any other form
and you must impose this same condition on any acquirer

Published in the United States of America by Oxford University Press
198 Madison Avenue, New York, NY 10016, United States of America

British Library Cataloguing in Publication Data

Data available

Library of Congress Control Number: 2020952840

ISBN 978-0-19-883025-2 (hbk.)

ISBN 978-0-19-883026-9 (pbk.)

DOI: 10.1093/oso/9780198830252.001.0001

Printed and bound by
CPI Group (UK) Ltd, Croydon, CR0 4YY

Links to third party websites are provided by Oxford in good faith and
for information only. Oxford disclaims any responsibility for the materials
contained in any third party website referenced in this work.

To

Amma,

Appa,

MN,

and my students—past, present, and future

Preface

Materials science and engineering (MSE) is a multidisciplinary field, impacting every aspect of our technological society today. At the heart of MSE is understanding the relationship between structure and properties of materials. In fact, it is now well established that, by optimizing composition and structure ranging from the macroscopic to atomic dimensions, the properties of materials can be not only well controlled but also tailored for any specific application. In this endeavor, *materials characterization* and *analysis* involving a range of *diffraction*, *imaging*, and *spectroscopy* methods, at relevant length scales, has enabled the structure–property–processing–performance tetrahedron that epitomizes the field.

Traditionally, an *undergraduate* curriculum in MSE emphasizes the practical application of optical microscopy and spectroscopy, imparts a working knowledge of X-ray diffraction and, where resources are available, scanning and transmission electron microscopy, and atomic force microscopy. However, recent advances in developing materials for a wide range of applications, emphasizing atomic-scale tailoring of microstructure and exploiting size-dependent properties, require an interdisciplinary approach to materials development where a judicious use of available characterization methods becomes important. This requires a coherent discussion of the underlying *physical principles* of materials characterization and metrology using the wide range of electrons, photons, ions, neutrons, and scanning probes.

Following a broad introduction (§1), this book lays the foundations of characterization, analysis, and metrology and builds on concepts that should be familiar to an upper-division student in any branch of science or engineering. Starting with atomic structure, we develop spectroscopy methods based on intra-atomic electronic transitions (§2), followed by bonding and the electronic structure of molecules and solids motivating a number of spectroscopy methods (§3). We then discuss the periodic arrangement of atoms and develop principles of crystallography (§4), which leads to an introduction to diffraction in both real and reciprocal space. Next, we address different probes and present relevant details of the generation and use of photons, electrons, ions, neutrons, and scanning probes (§5), followed by a presentation of ion-based scattering methods (§5). A concise introduction to optics, optical microscopy, polarization of light, and ellipsometry follows (§6). The second part of the book includes a comprehensive discussion of diffraction and imaging methods that emphasize techniques widely used in the characterization and analysis of materials. This includes X-ray (§7), electron (§8), and neutron (§8) diffraction, as well as transmission and analytical electron (§9), scanning electron (§10), and scanning probe (§11) microscopies. Throughout the text, the characterization techniques are also used to introduce

and illustrate fundamental properties and materials science concepts encountered in a wide range of materials. The book is generously illustrated throughout with figures, data tables, comparison between related methods, worked examples, and concludes (§12) with three unique and comprehensive tables summarizing the salient points of all the spectroscopy, diffraction, and imaging methods presented.

To keep the overall extent of the book to a manageable length, I have mainly emphasized *probe-based techniques*. Other methods, such as thermal characterization and property measurements, including mechanical testing, are deliberately not included. However, I do include numerous applications of materials and structures in fields ranging from science, technology, art, and biology. Each chapter also includes a number of worked examples to help tie together the concepts introduced therein, an extensive set of test-your-knowledge questions to help readers consolidate understanding of the subject matter based on the text, problem sets to further deepen learning, a summary highlighting the key concepts and ideas presented in each chapter, and an extensive bibliography for further reading.

While specialized books do exist for most of the techniques discussed here, including encyclopedias of materials characterization, a coherent textbook on materials characterization and metrology at the undergraduate or early graduate level, emphasizing fundamental physical principles, such as this one, is both lacking and highly desirable. Combining discussions of the underlying principles with practical examples, and detailed sets of exercises, this book will ideally serve as a text for a *year-long course* at the undergraduate and/or early graduate level. Completion of such a course should give students an entry into the interdisciplinary field of Materials Science and Engineering, and a solid foundation in characterization and analysis methods, with the ability to select and apply the appropriate technique for any characterization problem at hand. Alternatively, the book can be adapted to a *semester-length course*, taking a more traditional approach by devoting about five weeks each to spectroscopy (Chapters 2, 3, 9, and 10), diffraction (Chapters 4, 7, and 8), and imaging (Chapters 6, 9–11). If one is further constrained in time to a *10-week quarter or term*, as in many US universities, and which is the case for the course I have been teaching (syllabus available on request) for many years at UW—where UG students take this course after prior exposure to X-ray diffraction and the electronic structure of solids—this book may be adopted by teaching, selectively, the essential concepts of Chapters 1–6 at the approximate pace of one chapter per week, and in the last four weeks, covering scanning electron (Chapter 10) and scanning probe (Chapter 11) microscopies. Assigning term paper topics for self-study, involving more specialized techniques and their applications, including transmission electron microscopy (Chapter 9), would further strengthen student learning.

For those students from different disciplines other than MSE, this book provides what they will essentially need to know in materials characterization, including additional background, at an early stage of their study. Overall, this book is expected to potentially have a wide readership and academic relevance

for teaching a course on characterization, analysis, and metrology, across multiple disciplines of engineering, physics, chemistry, geology, biology, art conservation, etc. The examples in the book are selected to reinforce this breadth of disciplines. Finally, even though this textbook is tailored for the teaching of upper-division undergraduate or early-stage graduate students, it is also written for self-study by experienced researchers, including those in industry, who realize that, to deliver a program/product satisfactorily, they need to know more about the microstructure of their materials than they currently do!

In writing this book, I benefitted from discussions with numerous colleagues and teachers who generously shared their knowledge in multiple disciplines with me over the last four decades. Some of them also reviewed sections of this manuscript at various stages of development. Alphabetically they include: S. D. Bader, P. Blomqvist, S. Brück, J. N. Chapman, D. E. Cox, U. Dahmen, C. J. Echer, R. Egerton, M. Farle, P. J. Fischer, E.E. Fullerton, C. Hetherington, F. Hofer, W. Grogger, R. Gronsky, R. Kilaas, C.A. Lucas, R. K. Mishra, Y. Murakami, C. Nelson, S. Paciornik, S. J. Pennycook, L. Rabenberg, P. Rez, D. Shindo, I. K. Schuller, S.G.E. te Velthuis, N. Thangaraj, S. Thevuthasan, G. Thomas, M. Varela, D. O. Welch, T. Wen, and T. Young. I also offer a special note of thanks to my former students, Eric Teeman and Ryan Hufshmid, who have independently created, for the exercises in the book, a solution manual (available from OUP to those who adopt this book for teaching a course), and the anonymous reviewer who provided a chapter-by-chapter review of the entire book. Also, I benefitted immensely from interactions with many generations of graduate students and post-doctoral fellows at both UCB and UW who, driven by their own curiosity and interests, provided me the motivation to learn and apply a wide range of characterization methods in our research. The list is too long to acknowledge them individually here, but many of their contributions are reflected in this book. Finally, over the past many years, students of my course on Principles of Materials Characterization (MSE333) at UW have used draft chapters of this book as it has evolved over time with subsequent revisions. Their constructive feedback and relentless criticisms have significantly improved the book, making it more accessible and tailored to student teaching and learning. I am deeply indebted to all of the people mentioned here; however, I am entirely responsible for any remaining omissions, errors, or mistakes, and if they are brought to my attention, I will be more than happy to address them in subsequent revisions. This book has been many years in the making and parts of it were written during multiple residencies in a number of places. I am particularly beholden to the Whitely Center, an idyllic writing retreat at Friday Harbor, the Brahm Prakash Visiting Professorship at the Indian Institute of Science, Bangalore, the JSPS Senior Fellowship at the University of Tohoku, and the Humboldt Career Research Award at the University of Duisburg-Essen, all of which provided the right atmosphere to make substantial progress in writing this book.

Kannan M. Krishnan
Seattle, August 2020

Contents

1. Introduction to Materials Characterization, Analysis, and Metrology	1
1.1 Microstructure, Characterization, and the Materials Engineering Tetrahedron	2
1.2 Examples of Characterization and Analysis	7
1.2.1 Ni-Based Superalloys: Ultrahigh Temperature Materials for Jet Engines	8
1.2.2 Unraveling the Structure of Deoxyribonucleic Acid (DNA)	10
1.2.3 Characterizing a Picasso Painting Reveals Hidden Secrets	12
1.2.4 Failure Analysis: Metallurgy of the <i>RMS Titanic</i>	13
1.2.5 Beneath Our Feet: Microstructure of Rocks and Minerals	15
1.2.6 Ceramic Materials: Sintering and Grain Boundary Phases	17
1.2.7 Microstructure and the Properties of Materials: An Engineering Example	20
1.3 Probes for Characterization and Analysis: An Overview	22
1.3.1 Probes and Signals	22
1.3.2 Probes Based on the Electromagnetic Spectrum and Their Attributes	22
1.3.3 Wave–Particle Duality	24
1.3.4 Nature and Propagation of Electromagnetic Waves	27
1.3.5 Interactions of Probes with Matter and Criteria for Technique Selection	29
1.4 Methods of Characterization: Spectroscopy, Diffraction, and Imaging	34
1.4.1 Spectroscopy: Absorption, Emission, and Transition Processes	34
1.4.2 Scattering and Diffraction	37
1.4.3 Imaging and Microscopy	41
1.4.4 Digital Imaging	48
1.4.5 <i>In Situ</i> Methods across Spatial and Temporal Scales	56
1.5 Features of Materials Used for Characterization	57
Summary	59
Further Reading	59
References	61
Exercises	63

2. Atomic Structure and Spectra	68
2.1 Introduction	69
2.2 Atomic Structure	69
2.2.1 Bohr–Rutherford–Sommerfeld Model	69
2.2.2 Quantum Mechanical Model	70
2.3 Atomic Spectra: Transitions, Emissions, and Secondary Processes	78
2.3.1 Dipole Selection Rules and Allowed Transitions of Electrons in Atoms	78
2.3.2 Characteristic X-Ray Emissions and their Nomenclature	85
2.3.3 Non-Radiative Auger Electron Emission	91
2.3.4 Electron Photoemission	97
2.4 X-Rays as Probes: Generation and Transmission of X-Rays	97
2.4.1 Laboratory Sources and Methods of X-Ray Generation	98
2.4.2 X-Ray Absorption and Filtering	102
2.4.3 Synchrotron Sources of X-Ray Radiation	105
2.5 X-Rays as Signals: Core-Level Spectroscopy with X-Rays	107
2.5.1 Instrumentation for Detecting X-Rays	107
2.5.2 Chemical X-Ray Microanalysis	113
2.6 Surface Analysis: Spectroscopy with Electrons	119
2.6.1 Instrumentation for Surface Analysis with Electron Spectroscopy	120
2.6.2 Auger Electron Spectroscopy	123
2.6.3 X-Ray Photoelectron Spectroscopy	128
2.6.4 Surface Compositional Analysis with AES and XPS	134
2.6.5 Comparison of AES and XPS	136
2.7 Select Applications	137
2.7.1 XRF Analysis of Dental and Medical Specimens	137
2.7.2 Environmental Science: Contamination in Ground Water Colloids	138
Summary	139
Further Reading	140
References	142
Exercises	143
3. Bonding and Spectra of Molecules and Solids	147
3.1 Introduction	148
3.2 Bonds and Bands	149
3.3 Interatomic Bonding in Solids	152
3.3.1 Ionic Bonding	153
3.3.2 Covalent Bonding	154
3.3.3 Metallic Bonding	156

3.4	Molecular Spectra	158
3.4.1	Vibrational and Rotational Modes	158
3.4.2	Ultraviolet and Visible Spectroscopy (UV-Vis)	162
3.4.3	Classical Model of Rayleigh and Raman Scattering	166
3.4.4	Selection Criteria for Infrared and Raman Activity	169
3.5	Infrared Spectroscopy	172
3.5.1	Instrumentation for Raman and IR Spectroscopy	173
3.5.2	Michelson Interferometer and the Fourier Transform Infrared (FTIR) Method	174
3.5.3	Practice and Application of FTIR	177
3.6	Raman Spectroscopy	179
3.6.1	Raman, Resonant Raman, and Fluorescence	179
3.6.2	Instrumentation for Raman Spectroscopy and Imaging	181
3.6.3	Application of Raman Spectroscopy in Chemical and Materials Analysis	182
3.6.4	Surface-Enhanced Raman Spectroscopy (SERS)	183
3.7	Probing the Electronic Structure of Solids	185
3.8	Photoemission and Inverse Photoemission from Solids	188
3.9	Absorption Spectroscopies—Probing Unoccupied States	197
3.9.1	X-Ray Absorption Spectroscopy (XAS)	197
3.9.2	Near-Edge and Extended X-Ray Absorption Fine Structure (NEXAFS and EXAFS)	200
3.10	Select Applications	206
3.10.1	Structure of Proteins Resolved by FTIR	206
3.10.2	Analysis of Catalytic Particles by XAS and XPS	208
	Summary	208
	Further Reading	211
	References	212
	Exercises	214
4.	Crystallography and Diffraction	220
4.1	The Crystalline State	222
4.1.1	Lattices	223
4.1.2	Generalized Crystal Systems and Bravais Lattices	224
4.1.3	Lattice Points, Lines, Directions, and Planes	227
4.1.4	Zonal Equations	231
4.1.5	Atomic Size, Coordination, and Close Packing	233
4.1.6	Describing Crystal Structures—Some Examples	236
4.1.7	Symmetry and the International Tables for Crystallography	239
4.1.8	The Stereographic Projection	244
4.1.9	Imperfections in Crystals	247

4.2	The Reciprocal Lattice	250
4.3	Diffraction	256
4.3.1	Bragg's Law: Interpreting Diffraction in Real Space	257
4.3.2	The Ewald Construction: Interpreting Diffraction in Reciprocal Space	259
4.3.3	Comparison of X-Ray and Electron Diffraction	262
4.4	Quasicrystals and the Definition of a Crystalline Material	266
	Summary	267
	Further Reading	268
	References	269
	Exercises	270
5.	Probes: Sources and Their Interactions with Matter	277
5.1	Introduction	278
5.2	Probes and Their Generation	278
5.2.1	Photons: Lamps and Lasers	278
5.2.2	Electrons: Thermionic and Field-Emission Sources	282
5.2.3	Neutrons	287
5.2.4	Ions	288
5.3	Interactions of Probes with Matter, Including Damage	292
5.3.1	Photons	293
5.3.2	Electrons	294
5.3.3	Neutrons	303
5.3.4	Protons	303
5.3.5	Ions	304
5.4	Ion-Based Characterization Methods	315
5.4.1	Rutherford Back-Scattering Spectroscopy (RBS)	315
5.4.2	Low-Energy Ion Scattering Spectroscopy (LEISS)	325
5.4.3	Secondary Ion Mass Spectrometry (SIMS)	328
5.4.4	Induction-Coupled Plasma Mass Spectrometry (ICP-MS)	331
5.4.5	Particle-Induced X-Ray Emission (PIXE)	336
	Summary	337
	Further Reading	338
	References	339
	Exercises	339
6.	Optics, Optical Methods, and Microscopy	345
6.1	Introduction	346
6.2	Wave Equation for Simple Harmonic Motion	346

6.2.1	The Phase Angle	347
6.2.2	The Superposition Principle	348
6.2.3	Phasor Representation and the Addition of Waves	350
6.2.4	Complex Representation of a Simple Harmonic Wave	350
6.2.5	Superposition of Two Waves of the Same Frequency	351
6.2.6	Addition of Waves on Orthogonal Planes and Polarization	353
6.3	Huygens' Principle	356
6.4	Young Double-Slit Experiment	357
6.5	Reflection and Refraction	359
6.6	Diffraction	361
6.6.1	Fraunhofer Diffraction from a Single Slit	363
6.6.2	Fraunhofer Diffraction from Double and Multiple Slits	366
6.6.3	Resolving Power of a Diffraction Grating	369
6.6.4	Fresnel Diffraction	370
6.6.5	Fresnel Half-Period Zones	371
6.6.6	Diffraction by a Circular Aperture or Disc	372
6.6.7	Zone Plates and Their Applications in X-Ray Microscopy	373
6.7	Visually Observable: Characteristics of the Human Eye	375
6.8	Optical Microscopy	376
6.8.1	Resolution: Rayleigh and Abbe Criteria	376
6.8.2	Geometric Optics and Aberrations	378
6.8.3	The Optical Microscope	381
6.8.4	Confocal Scanning Optical Microscopy (CSOM)	386
6.8.5	Metallography	388
6.9	Ellipsometry	392
6.9.1	p- and s-Polarized Light Waves, and Fresnel Equations of Reflection	394
6.9.2	Optical Elements Used in Ellipsometry	397
6.9.3	Ellipsometry Measurements	398
	Summary	400
	Further Reading	401
	References	402
	Exercises	402
7.	X-Ray Diffraction	408
7.1	Introduction	409
7.2	Interaction of X-Rays with Electrons	409
7.2.1	Thomson Coherent Scattering	410
7.2.2	Compton Incoherent Scattering	413

7.3	Scattering by an Atom: Atomic Scattering Factor	415
7.4	Scattering by a Crystal: Structure Factor	422
7.5	Examples of Structure Factor Calculations	425
7.5.1	Face-Centered Cubic (FCC) Structure	425
7.5.2	Body-Centered Cubic (BCC) Structure	427
7.5.3	Hexagonal Close Packed (HCP) Structure	428
7.5.4	Cesium Chloride (CsCl) Structure	429
7.6	Symmetry and Structure Factor	431
7.6.1	Crystals with Inversion Symmetry	431
7.6.2	Friedel Law	431
7.6.3	Systematic Absences	431
7.7	The Inverse Problem of Determining Structure from Diffraction Intensities	432
7.8	Broadening of Diffracted Beams and Reciprocal Lattice Points	433
7.9	Methods of X-Ray Diffraction	437
7.9.1	The Laue Method for Single Crystals	438
7.9.2	Diffractometry of Powders and Single Crystals	439
7.9.3	Debye–Scherrer Method for Powders	443
7.9.4	Thin Films and Multilayers: Diffractometry, Reflectivity, and Pole Figures	445
7.9.5	Practical Considerations: Collimators and Monochromators	449
7.10	Factors Influencing X-Ray Diffraction Intensities	451
7.10.1	Temperature Factor	451
7.10.2	Absorption or Transmission Factor	453
7.10.3	Lorentz Polarization Factor	455
7.10.4	Multiplicity	457
7.10.5	Corrected Intensities for Diffractometry and the Debye–Scherrer Camera	457
7.11	Applications of X-Ray Diffraction	459
7.11.1	Measurement of Lattice Parameters	460
7.11.2	Crystallite or Grain Size and Lattice Strain Measurements	460
7.11.3	Phase Identification and Structure Refinement	461
7.11.4	Chemical Order–Disorder Transitions	464
7.11.5	Short-Range Order (SRO) and Diffuse Scattering	467
7.11.6	<i>In Situ</i> X-Ray Diffraction at Synchrotrons	468
7.11.7	X-Ray Diffraction Measurements on Mars	469
	Summary	471
	Further Reading	472
	References	473
	Exercises	474

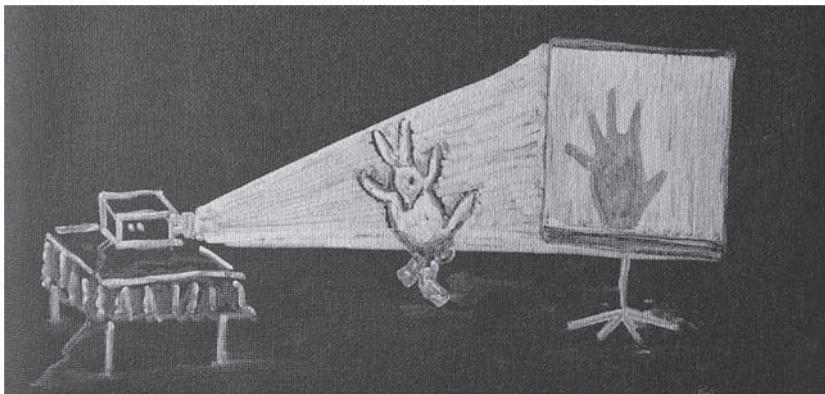
8. Diffraction of Electrons and Neutrons	481
8.1 Introduction	482
8.2 The Atomic Scattering Factor for Electrons	482
8.3 Basics of Electron Diffraction from Surfaces	485
8.3.1 Surface Reconstruction, Surface Nets, and Their Notation	486
8.3.2 Reciprocal Lattice Nets and Ewald Sphere Construction in Two Dimensions	487
8.4 Surface Electron Diffraction Methods and Applications	489
8.4.1 Low-Energy Electron Diffraction (LEED)	490
8.4.2 Adsorption Studies on Surfaces Using LEED	493
8.4.3 Reflection High-Energy Electron Diffraction (RHEED)	494
8.4.4 RHEED Oscillations: <i>In Situ</i> Monitoring of Thin Film Growth	498
8.5 Transmission High-Energy Electron Diffraction	501
8.5.1 Coherent, Incoherent, Elastic, and Inelastic Scattering	504
8.5.2 Basics of Electron Diffraction in a Transmission Electron Microscope	505
8.5.3 Kinematical Theory of Electron Diffraction	506
8.5.4 The Column Approximation, Dynamical Diffraction, and Diffraction from Imperfect Crystals	509
8.6 Transmission Electron Diffraction Methods	514
8.6.1 Selected Area Diffraction: Ring and Spot Patterns	514
8.6.2 Kikuchi Lines, Maps, and Patterns	519
8.6.3 Convergent Beam Electron Diffraction (CBED)	523
8.7 Examples of Transmission Electron Diffraction of Materials	527
8.7.1 Indexing a Single Crystal Diffraction Pattern	527
8.7.2 Polycrystalline Materials and Nanoparticle Arrays	527
8.7.3 Orientation Relationships Between Crystals or Phases	529
8.7.4 Chemical Order in Materials	529
8.7.5 Diffraction from Long-Period Multilayers	531
8.7.6 Twinning	532
8.8 Interactions of Neutrons with Matter	535
8.8.1 Nuclear Interactions	535
8.8.2 Magnetic Interactions	537
8.8.3 <i>In Situ</i> Kinetic Studies Using Neutrons: Hydration of Cement	538
Summary	540
Further Reading	542
References	543
Exercises	544

9. Transmission and Analytical Electron Microscopy	552
9.1 Introduction	553
9.2 Elements and Operations of a Transmission Electron Microscope	558
9.2.1 Electron Sources: Thermionic, Field, and Schottky Emission	558
9.2.2 Electromagnetic Lenses	560
9.2.3 The Illumination Section	565
9.2.4 The Imaging Section: Objective Lens and Aperture	568
9.2.5 Specimen Handling and Manipulation	570
9.2.6 The Magnification Section	571
9.2.7 Imaging and Diffraction Modes	573
9.2.8 Scanning Transmission Mode and the Principle of Reciprocity	584
9.2.9 Correction of Lens Aberrations	587
9.2.10 Image Recording and Detection of Electrons	588
9.3 Beam–Solid Interactions, Contrast Mechanisms, and Imaging Methods	588
9.3.1 Elastic Interactions	589
9.3.2 Mass–Thickness Contrast	592
9.3.3 Diffraction Contrast	595
9.3.4 High-Angle Incoherent Scattering: <i>Z</i> -Contrast Imaging	598
9.3.5 High-Resolution Electron Microscopy (HREM): Phase Contrast Imaging in Practice	601
9.3.6 Magnetic Contrast: Lorentz Microscopy	609
9.3.7 Electron Holography	613
9.4 Analytical Electron Microscopy (AEM) and Related Spectroscopies	617
9.4.1 Inelastic Scattering and Spectroscopy	619
9.4.2 Electron Energy-Loss Spectroscopy (EELS) in a TEM	623
9.4.3 Quantitative Microanalysis with Energy-Dispersive X-Ray Spectrometry	641
9.4.4 Microdiffraction	648
9.5 Select Applications of TEM	650
9.5.1 Electron Tomography	650
9.5.2 Analysis of Defects: Dislocations and Stacking Faults	655
9.5.3 Thin Films and Multilayers: An Example	658
9.5.4 TEM in Semiconductor Manufacturing: Metrology, Process Development, and Failure Analysis	660
9.5.5 Dynamic Measurements in a TEM	664
9.6 Preparation of Specimens for TEM Observations	666
9.6.1 Chemical and Electrochemical Polishing	668
9.6.2 Ion-Beam Milling	669
9.6.3 Ultramicrotomy and Preparation of Biological Materials	669
9.6.4 Preparation of Cross-Section Specimens	669
9.6.5 Focused Ion-Beam (FIB) Milling	670

Summary	671
Further Reading	674
References	675
Exercises	684
10. Scanning Electron Microscopy	693
10.1 Introduction	694
10.2 The Scanning Electron Microscope	694
10.2.1 The Instrument	694
10.2.2 The Everhart–Thornley Electron Detector	698
10.2.3 Beam–Solid Interactions and Signals	699
10.2.4 The Incident Probe Size and Spatial Resolution	701
10.2.5 Depth of Field	703
10.2.6 Noise and Contrast in Imaging	706
10.2.7 Elastic and Inelastic Scattering, and Beam Broadening	707
10.3 Image Contrast in a Scanning Electron Microscope	709
10.3.1 Factors Influencing Secondary Electron Emission	710
10.3.2 Topographical Contrast in Secondary Electron Imaging	713
10.3.3 Angular Dependence of Back-Scattered Electrons and Topographic Information	715
10.3.4 Comparison of SEM Images with Different Operating Parameters	718
10.4 Channeling and Electron Back-Scattered Diffraction Patterns (EBSD)	720
10.5 Imaging Magnetic Domains	722
10.5.1 Type I and Type II Magnetic Contrast	722
10.5.2 Scanning Electron Microscopy with Polarization Analysis (SEMPA)	723
10.6 Probing Sample Composition and Electronic Structure	726
10.6.1 Basics of X-Ray Microanalysis in an SEM	726
10.6.2 Cathodoluminescence	731
10.7 Variations of Scanning Electron Microscopy	732
10.7.1 Environmental Scanning Electron Microscopy (ESEM)	732
10.7.2 Combined Focused Ion-Beam (FIB) and Scanning Electron Microscope	734
10.8 Preparing Specimens for SEM	736
Summary	737
Further Reading	738
References	739
Exercises	740
11. Scanning Probe Microscopy	745
11.1 Introduction	746
11.2 Physics of Scanning Tunneling Microscopy (STM)	749

11.2.1	Elastic Tunneling Through a One-Dimensional Barrier	749
11.2.2	Quantum Mechanical Tunneling Model of the STM	750
11.3	Basic Operation of the Scanning Tunneling Microscope	752
11.3.1	Imaging	753
11.3.2	Tunneling Spectroscopy	755
11.3.3	Manipulation of Adsorbed Atoms on Clean Surfaces	757
11.4	Physics of Scanning Force Microscopy	759
11.4.1	Mechanical Characteristics of the Cantilever	760
11.4.2	Cantilever as a Force Sensor	763
11.4.3	Tip–Specimen Forces Encountered in an SFM	765
11.5	Operation of the Scanning Force Microscope	767
11.5.1	Static Contact Mode for Topographic Imaging	769
11.5.2	Lateral Force Microscopy	772
11.5.3	Dynamic Noncontact Modes of Atomic Force Microscopy	773
11.6	Scanning Force Microscopy Instrumentation	776
11.7	Artifacts in Scanning Probe Microscopy	777
11.7.1	Probe Artifacts	777
11.7.2	Instrument Artifacts	780
11.8	Select Applications of Scanning Force Microscopy	780
11.8.1	Atomic Fingerprinting in Frequency Modulated Atomic Force Microscopy	781
11.8.2	Magnetic Force Microscopy (MFM)	782
11.8.3	Scanning Thermal Microscopy (SThM)	785
11.8.4	Applications of Atomic Force Microscopy in the Life Sciences	786
11.8.5	Dip-Pen Nanolithography (DPN)	793
	Summary	794
	Further Reading	795
	References	796
	Exercises	799
12.	Summary Tables	803
Table 12.1	Spectroscopy and Chemical Methods	804
Table 12.2	Diffraction and Scattering Methods	814
Table 12.3	Imaging Methods	818
	Index	825
	Table of values	847
	Periodic Table of the Elements	848

Introduction to Materials Characterization, Analysis, and Metrology



This illustration, by the author, based on a cartoon by John O'Brien (*The New Yorker*, February 25, 1991), succinctly describes the challenges in materials characterization. We are often called upon to describe the material microstructure (rabbit) based on the measured signals (hand) in diffraction, spectroscopy, or imaging methods. Needless to say, a poor understanding of the fundamental principles underlying the characterization methods generally lead to bad experimental design, hasty interpretations, and/or erroneous conclusions.

1.1 Microstructure, Characterization, and the Materials Engineering Tetrahedron	2
1.2 Examples of Characterization and Analysis	7
1.3 Probes for Characterization and Analysis: An Overview	22
1.4 Methods of Characterization: Spectroscopy, Diffraction, and Imaging	34
1.5 Features of Materials Used for Characterization	57
Summary	59
Further Reading	59
References	61
Exercises	63

1.1 Microstructure, Characterization, and the Materials Engineering Tetrahedron

Materials science and engineering (MSE) is an enabling and multidisciplinary field, impacting nearly every aspect of society today. The reach of MSE is enormous—advanced semiconductors have stretched the limit of high-performance computers; optical fibers have dramatically increased the bandwidth and speed of intercontinental data transmission; magnetic materials in data storage have revolutionized information access, including the proliferation of the Internet; light-weight metals, polymers, and composites have transformed aircraft design and fuel efficiency; novel batteries and fuel-cell materials power things from cell phones to public buses; and increasingly, innovation in materials is at the heart of biomedicine. As the late William Baker, past president of Bell Laboratories, put it so elegantly: “everything is made of something and always will be!” In other words, MSE exemplifies the use-inspired fundamental studies of “Pasteur’s Quadrant” (Stokes, 1997). The dramatic societal impact of the work of materials scientists and engineers can be illustrated by numerous examples; a few of them, included in Figure 1.1.1, are adapted from a special report by a distinguished panel of members of the U.S. National Academy of Engineering [1].

When we engineer any material, we tailor its properties for a specific application. This requires that it perform in a predictable and reliable manner when it is fabricated in the desirable shape or *form*. The latter may be a bulk material, a composite, a coating, a thin film or heterostructure, a wire or rod, a nanoparticle or its dispersion in a matrix, a surface, a nanoscale structure, a lithographically patterned element or array, etc. In other words, we make materials with sizes ranging from the atomic to the macroscopic, and dimensionality ranging from zero to three. Sometimes, the critical feature of interest in the material may be deep inside; an example is the buried interface in many modern semiconductor, magnetic, or photonic devices that are designed and fabricated in the form of thin film heterostructures.

Characterization and analysis of materials is central to the practice of materials sciences and engineering. The properties of all materials are determined by their *structure*, by which we broadly mean the composition, electronic structure, thermodynamic state/phase, and the arrangements of their internal components. The structure of materials can be described at various *length scales* or levels of detail. At the *atomic* level, it describes the bonding and organization of atoms or molecules relative to one another. At the *mesoscopic* level, it refers to an intermediate-length scale, between the atomic and microscopic, where material properties are different from the bulk, often determined by quantum mechanics, and dominated by surface effects. This is also the length scale of particular interest in nanoscience and nanotechnology (Owens and Poole, 2008). At

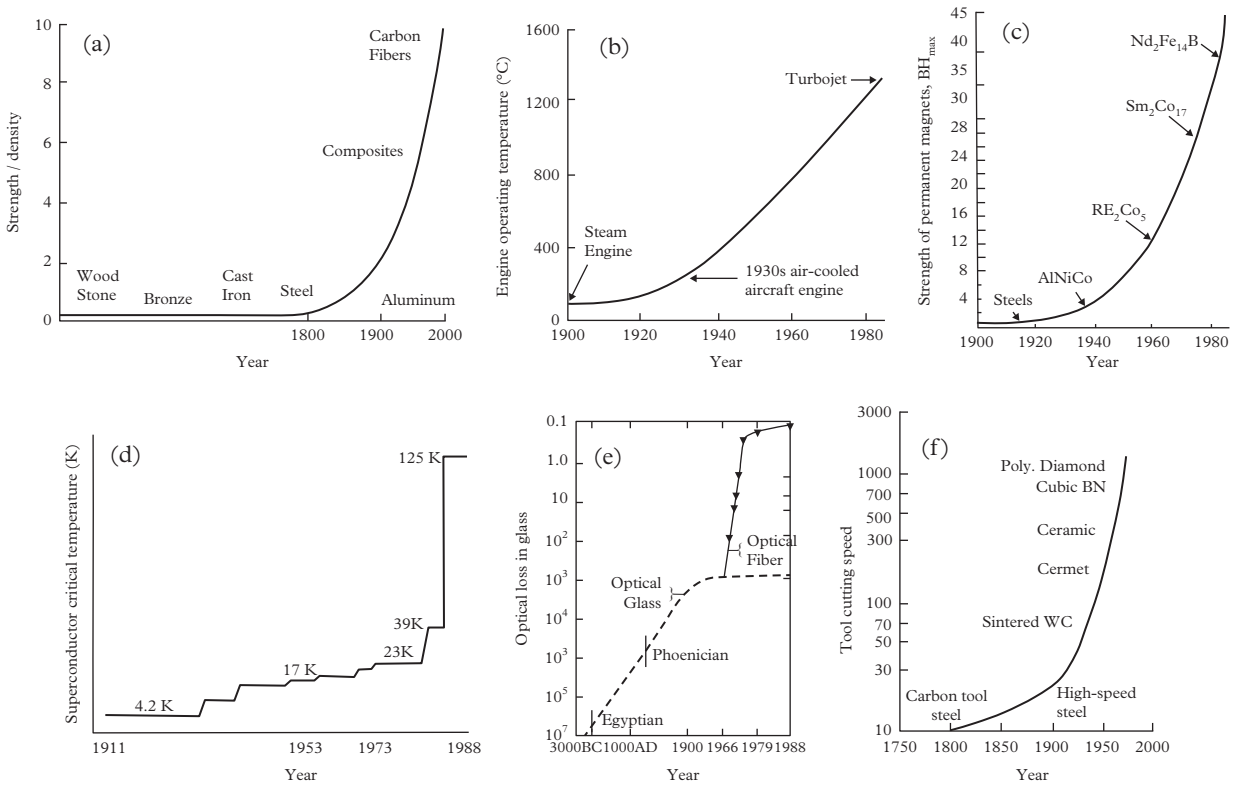


Figure 1.1.1 The societal impact of materials science and engineering is illustrated by a few representative examples. (a) Strength-to-density ratio of structural materials has increased fiftyfold, compared to cast iron used two centuries ago, with application ranging from light-weight eye glasses to composite airplanes. (b) The design of high-efficiency engines with reduced environmental impact requires materials that are strong at high temperature—superalloys and specialty ceramics can operate at temperature as high as 1,100–1,400°C, with theoretical efficiencies of ~80%. (c) The strength of a permanent magnet, given by its energy product, determines the design of smaller and more powerful motors—a 100-fold increase from the 1930s is evident. (d) Progress in the critical temperature of superconducting materials. (e) Optical fibers are now 100 times more transparent than they were in the 1960s. (f) New hard abrasive materials have increased cutting tool speeds by a factor of 100 from the early twentieth century, making manufacturing processes cheaper and more efficient.

Adapted from [1].

the *microscopic*—that which can be observed by some type of microscope—level, it refers to the arrangements of larger groups of atoms, such as grains and thermodynamic phases, including their morphology, chemistry, and crystallographic relationships. As materials scientists/engineers, when we use

4 Introduction to Materials Characterization and Analysis

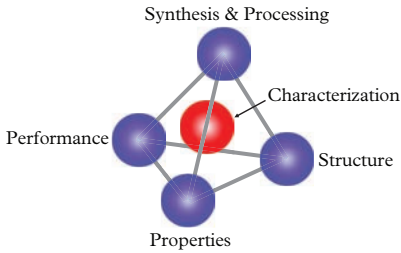


Figure 1.1.2 The materials engineering tetrahedron, where characterization plays a central role.

the term *microstructure*, we generally mean *all* relevant structural details described here, from the atomic up to the microscopic-length scale. Lastly, at the *macroscopic* level, we refer to structure that can be viewed with the naked eye.

The core activities of a materials scientist/engineer can be represented by a tetrahedron (Fig. 1.1.2). Naturally, we begin with the *synthesis* of any material and then *process* it to achieve the desired *structure*, which in turn, determines its *properties* and its required *performance* in an economical and socially acceptable manner. Note that *characterization*, or *evaluating the microstructure at the appropriate length scale*, plays a critical role in tailoring the synthesis and processing of materials to achieve the desired properties and performance of any engineering component. So, we conveniently place characterization in the center of this tetrahedron. Note that characterization, as discussed in this book, does not include measurements of properties—mechanical, magnetic, electrical, thermal, etc.—that can be found in other specialized textbooks.

A range of characterization methods is required to elucidate the *processing–structure–property–performance* tetrahedron exhibited by the wide variety of materials that are tailor-made for specific functionality today. The list is long and includes metals/alloys, ceramics, polymers, amorphous materials and glasses that do not express any long-range crystallographic order, semiconductors, biological or biomimetic materials, composites, and natural materials like wood and paper. Alternatively, we can also classify materials in terms of their application, i.e. where structural, mechanical, functional (electrical, magnetic, optical), nuclear, biocompatibility properties, either individually or in some combination, become important. It may well be a soft material that is susceptible to damage when probed. Irrespective of the class of material that may be of interest, understanding the role of microstructure and tailoring it to optimize its properties is central to MSE. The microstructure of interest may be a combination of chemical, electronic, structural, crystallographic, or magnetic (*domains*) features, and has to be elucidated at the appropriate length scale that describes the behavior of the material. The characterization methods are many and the one to be applied for a specific problem has to be chosen judiciously among those readily available. Table 1.1.1 provides a list of *probe-based* characterization methods discussed in this book, especially those commonly identified by acronyms.

Broadly, the methods of characterization using different *probes* are classified as *diffraction*, *spectroscopy*, and *imaging*. The physical principles underlying these methods are the foundations of this book. Various techniques follow from these principles and are presented, with varying detail, as appropriate for this comprehensive presentation; naturally, detailed discussions of individual techniques abound in more advanced texts, including encyclopedias of materials characterization (see Further Reading). For working engineers, the American Society of Testing and Materials, now known as ASTM International, provides detailed standards¹ for a variety of materials characterization

¹ <https://www.astm.org/studentmember/metallurgybycommittee.html>

Table 1.1.1 Probe-based characterization methods, including acronyms where appropriate, discussed in this book, with sections indicated. Many of these techniques are mentioned in this chapter.

Technique	Acronym/Abbreviation	Section
Analytical electron microscopy	AEM	§9.4
Auger electron spectroscopy	AES	§2.6.2
Atomic force microscopy	AFM	§11.8
Atom probe field ion microscopy	AP-FIM	§1.4.3
Back-scattered electron imaging		§10.3.3
Biological force spectroscopy	BFS	§11.8.4.5
Cathodoluminescence	CL	§10.6.2
Confocal scanning optical microscopy	CSOM	§6.8.4
Convergent beam electron diffraction	CBED	§8.6.3
Dip-pen nanolithography	DPN	§11.8.5
Energy dispersive X-ray spectrometry	EDXS	§2.5.1.1
Electron back-scattered diffraction	EBSD	§10.4
Electron energy-loss spectroscopy	EELS	§9.4.2
Electron holography		§9.3.7
Electron probe microanalysis	EPMA	§2.5.2.2
Electron tomography		§9.5.1
Ellipsometry		§6.9
Energy filtered imaging in a TEM	EFTEM	§9.4.2.6
Environmental scanning electron microscopy	ESEM	§10.7.1
Extended X-ray absorption fine structure	EXAFS	§3.9.2
Field ion microscopy	FIM	§1.4.3
Focused ion beam milling	FIB	§9.6.5
Fourier transform infrared spectroscopy	FTIR	§3.5.2
High-angle annular dark field imaging	HAADF	§9.3.4

continued

Table 1.1.1 Continued

Technique	Acronym/Abbreviation	Section
High-resolution electron microscopy	HREM	§9.3.5
Inductively coupled plasma mass spectrometry	ICP-MS	§5.4.4
Inductively coupled plasma optical emission spectrometry	ICP-OES	§5.4.4
Interference contrast microscopy		§6.8.3.3
Inverse photoemission spectroscopy	IPES	§3.8
Lateral force microscopy	LFM	§11.5.2
Local electrode atom probe	LEAP	§1.4.3
Lorentz microscopy		§9.3.6
Low-energy electron diffraction	LEED	§8.4.1
Low-energy ion scattering spectroscopy	LEISS	§5.4.2
Magnetic force microscopy	MFM	§11.8.2
Metallography		§6.8.6
Neutron scattering		§8.8
Optical microscopy		§6.8
Particle induced X-ray emission	PIXE	§5.4.5
Photoemission spectroscopy	PES	§3.8
Raman spectroscopy		§3.6
Rayleigh scattering		§3.4.2
Reflection high-energy electron diffraction	RHEED	§8.4.3
Rutherford back-scattering spectroscopy	RBS	§5.4.1
Scanning electron microscopy	SEM	§10
Scanning electron microscopy with polarization analysis	SEMPA	§10.5.2
Scanning force microscopy	SFM	§11.4
Scanning probe microscopy	SPM	§11
Scanning thermal microscopy	SThM	§11.8.3
Scanning transmission electron microscopy	STEM	§9.2.8
Scanning tunneling microscopy	STM	§11.2
Secondary ion mass spectrometry	SIMS	§5.4.3
Selected area diffraction	SAD	§8.6.1
Transmission electron microscopy	TEM	§9
Ultraviolet and visible spectroscopy	UV-Vis	§3.4.2
Ultraviolet photoelectron spectroscopy	UPS	§3.8
Wavelength dispersive (X-ray) spectroscopy	WDS	§2.5.1.2
X-ray absorption near edge structure	XANES	§3.9.2
X-ray absorption spectroscopy	XAS	§3.9.1
X-ray diffraction	XRD	§7
X-ray fluorescence spectroscopy	XRF	§2.5.2.1
X-ray magnetic circular dichroism	XMCD	
X-ray photoelectron spectroscopy	XPS	§2.6.5
X-ray transmission microscopy	XTM	§6.6.7
Z-contrast imaging		§9.3.4

methods encountered in their professional practice; familiarity with them and adhering to these standard practices will help advance the career of those in industry.

First and foremost, this book is not a catalog of characterization techniques, but, as already mentioned, it emphasizes the physical principles underlying each of the measurement techniques. The study of measurements, broadly known as *metrology*, is also of much industrial relevance with many companies having separate metrology departments to monitor the production and characterization of materials, devices, and components. The contents of this book are also relevant to *failure analysis*, an interdisciplinary engineering subject that is discussed at length in other specialized textbooks (Brooks and Choudhury, 2001). Finally, any reader who is convinced of the importance and breadth of materials characterization may skip this introductory chapter, but mastery of the basic concepts introduced here are critical for making progress through the rest of the book.

1.2 Examples of Characterization and Analysis

Materials scientists and engineers are called upon to work with and characterize a wide range of materials (Callister and Rethwisch, 2009). These include metals/alloys, ceramics, polymers, semiconductors, composites, amorphous or glassy materials, wood, paper, etc. An alternative way to classify materials of interest is in terms of their *application or function*; for example, these include structural or mechanical properties, functional (electronic, optical, magnetic) behavior, biomaterials optimized for specific *in vivo* applications that raise additional issues of biocompatibility and toxicity, “smart” materials that are able to sense changes in their environment and respond to them in a predetermined manner, nanomaterials, etc.

In general, the microstructural questions to be resolved are particular to the morphology of the material. For a bulk material, we may be interested in identifying its crystal structure (*point or space group*, Bravais lattice, unit cell dimensions, distribution of atoms in the unit cell; all described in §4), composition, chemical homogeneity, grain size and distribution, and if multi-phase, the orientation relationship between the matrix phases and the distribution of secondary phases, if any, especially at grain boundaries. We may also be interested in identifying the nature, extent, and distribution of defects (§4.1.9), be they planar, line, or point, and their effect on the properties of interest. In addition, in thin films, multilayers, and superlattices, we may wish to investigate the crystallographic relationships between the layers, i.e. texture and *epitaxy*.² Questions about the nature of the

² The nature or artificial growth of crystalline materials on single crystal substrates determining their orientation.

interfaces, especially the buried ones, such as roughness, compositional mixing, and in the case of magnetic materials, the spin lattice at the interface, may also be of interest. Further, elucidation of their growth mode—e.g. columnar, layer-by-layer—could also be relevant (§8.4.4). For surfaces, additional questions of the surface electronic structure and changes in crystallography due to surface reconstruction also arise (§8.3.1). For zero-dimensional objects like *nanoparticles*, resolving their crystallography and defects, compositional homogeneity, phase purity, size, size-distribution, and shape, especially when they are on the nanoscale, is an ongoing challenge (Fig. 9.3.14). Last, but not least, for glassy or amorphous materials without long-range order, identifying a good descriptor or a method to quantify such structures is an enduring question.

It is really impossible to find a *single* technique or an *Eierlegende Wollmilchsau*,³ to address these wide range of microstructural questions. To be effective, we have to identify the best technique, or set of techniques, to resolve the microstructural questions at hand. Sometimes, the optimal technique may not be readily available and one may have to make do with a less-effective alternative.

Here, we begin with some typical examples of characterization and analysis of materials used in a variety of fields including engineering, biology, art, and geology. Each of these examples requires a judicious selection of characterization methods. Then, in subsequent chapters, we elucidate the fundamental principles behind these methods of *spectroscopy*, *diffraction*, and *imaging*, building on elementary concepts that should be familiar to the reader, i.e. atomic structure (§2), then moving to molecules (§3) and their vibration modes, and finally to crystalline solids (§4).

1.2.1 Ni-Based Superalloys: Ultrahigh Temperature Materials for Jet Engines

The efficiency and performance of jet engines are strongly dependent on the highest temperature attainable in their high-pressure turbine section (Fig. 1.2.1). Higher thrust requires higher operating temperatures, and for higher efficiency the engine must be made lighter without loss of thrust. Even though Ni-based superalloys in single crystal form have the required properties—high melting point ($\sim 1,650^\circ\text{C}$), good thermal conductivity, low density, and intrinsic corrosion resistance—their *microstructure* and the ensuing thermo-mechanical properties depend on the alloying elements, their concentrations, and their processing conditions.

Ni-based superalloys usually have a dual-phase microstructure (Fig. 1.2.2c) consisting of a $L1_2$ ordered γ' phase, existing in cuboidal shapes with $\{100\}$ faces, separated by narrow channels of the FCC γ phase in between, and creating a coherent $\gamma|\gamma'$ interface (Fig. 1.2.3c). The chemically ordered $L1_2$ structure

³ This is an old term in German for an imaginary animal, which provides everything for every purpose. A literal translation is oviparous-wooly-milking-sow. Here it means an animal that can lay eggs, give milk, and provides wool and meat. Needless to say, such an animal does not exist.

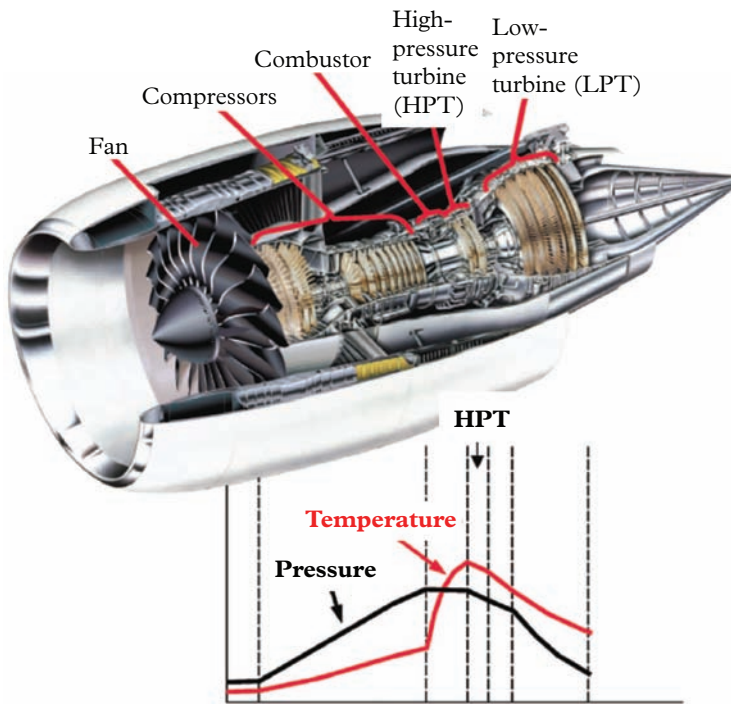


Figure 1.2.1 Illustration of the various components of a GE 90-115B jet engine. The variation of temperature and pressure from the back to the front of the engine is shown below.

Adapted from [34].

(Fig. 1.2.3j) of the γ' phase renders it highly rigid with low dislocation tolerance; hence the dislocations are confined to the γ channels, providing the required strength and high temperature creep properties. However, when subject to thermo-mechanical loads, the microstructure evolves—forming dislocation networks, coarsening the γ' cuboids (Fig. 1.2.2d–f), and precipitating topologically close-packed phases—and deteriorates the creep resistance of the alloy. Various alloying elements and heat treatments are used to control the microstructure and its evolution upon thermo-mechanical loading: precipitation elements (Al, Ta, Ti, Re) stabilize the γ' phase, solid-solution elements (Cr, Co, Mo) strengthen the γ phase by increasing the solidus temperature and resistance to dislocation movement, grain boundary elements (C, B) form carbides and borides along the grain boundaries to prevent casting pores and strengthen low-angle grain boundaries, and oxidation resistance elements (Al) form a protective Al_2O_3 surface layer.

Figure 1.2.3 shows a typical microstructure analysis carried out on a single crystal superalloy after heat treatment; in practice, this is correlated with mechanical behavior like creep as described in [3]. However, in the context of characterization it is important to point out that the analysis outlined here

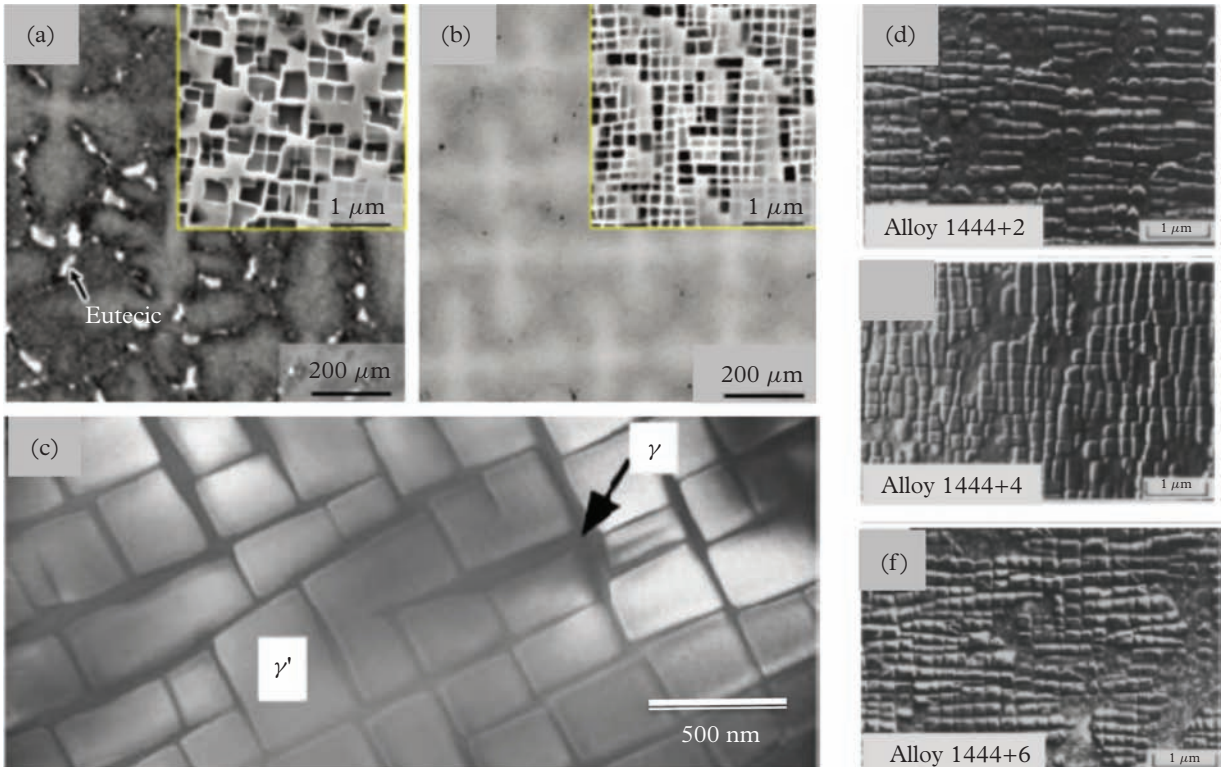


Figure 1.2.2 Microstructure of Ni-based single crystal superalloys (a) in the as-cast state, and (b) after the formation of the γ' phase following heat treatment, with the morphology of the two phases shown in greater detail (c). The rate of coarsening of the γ' phase, when the samples are aged for 2 hours at 1,065°C, is slowed down by the addition of Re, as shown in (d) 2% Re, (e) 4% Re, and (f) 6% Re. These images were obtained using transmission electron microscopy (TEM), a technique discussed further in §9.

Adapted from [2].

emphasizes the use of electron-based imaging, diffraction (§8), and spectroscopy methods in both transmission (§9) and scanning (§10) geometries.

1.2.2 Unraveling the Structure of Deoxyribonucleic Acid (DNA)

“It has not escaped our notice that the specific pairing we have postulated immediately suggests a possible copying material for this genetic material”. With this characteristic understatement, the first paper [6] describing the structure of the genetic building blocks of life was published. The model of DNA proposed by

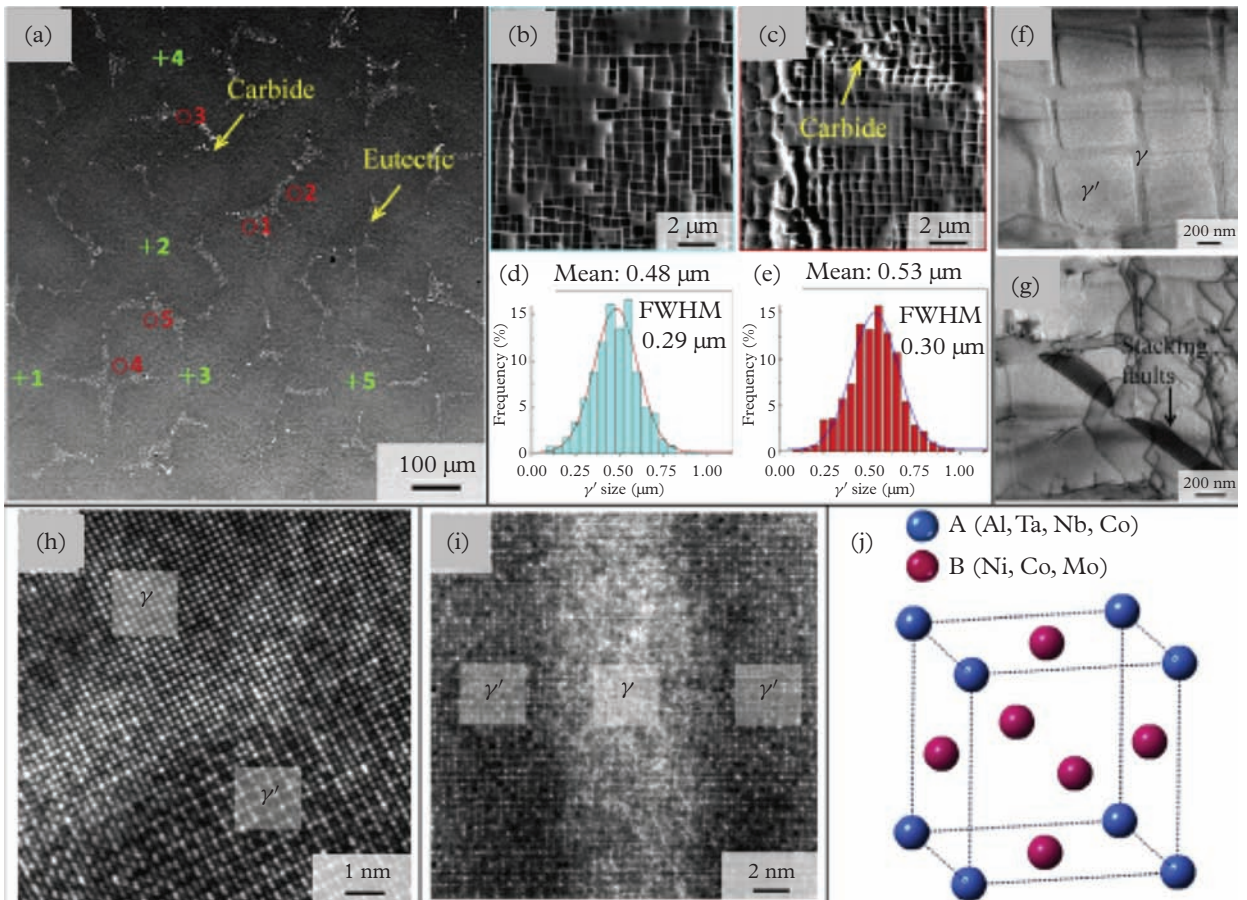


Figure 1.2.3 Typical microstructure analysis of a superalloy after heat treatment showing (a) secondary electron image of the microstructure seen from the transverse directions, identifying dendritic (green, b) and interdendritic (red, c) regions, where the γ' precipitate size distribution was determined, as shown in (d) and (e), respectively. The bright field TEM image of the alloy in different regions is shown in (f) and (g). (h) A high-resolution TEM, and (i) a high-angle annular dark field scanning TEM, HAADF-STEM image of the $\gamma | \gamma'$ interface illustrating the high level of coherency. (j) Schematic of the L_{12} ordered unit cell of the γ' phase. These methods are discussed in later chapters of electron diffraction (§8), TEM (§9), and SEM (§10).

Adapted from [3].

Watson and Crick (Fig. 1.2.4a) shows two phosphate-sugar, right-handed, helical chains, each coiled around the same axis, with the horizontal rods indicating the pairs of bases that holds the chains together. In particular, the bases are on the inside of the helix and the phosphates on the outside.

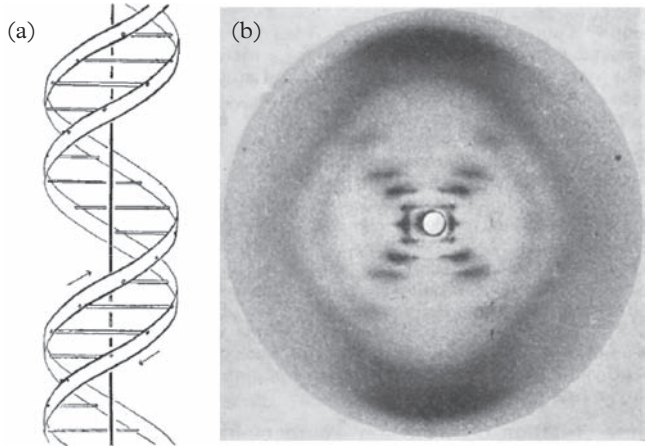


Figure 1.2.4 (a) The Watson–Crick model of DNA proposed in 1953. (b) The crucial X-ray diffraction (XRD, §7) photograph that was key to identifying the helical structure of DNA.

Adapted from [7].

The crucial experiment that provided key evidence for the correctness of the Watson–Crick⁴ model of DNA was the X-ray diffraction (XRD) photograph (Fig. 1.2.4b) published in the same issue of the journal [7]. The specimen is a fiber with high water content and containing many millions of DNA strands aligned along the fiber axis; supposedly, this is the form of DNA in living cells. The X-ray beam is incident normal to the fiber and the X-ray photograph shows, in a striking manner, the characteristic features of helical structures. The key features of the diffraction pattern are four diamond-shaped outlines of fuzzy diffraction halos and separated by two arms of spots radiating from the center. The two arms are characteristic of helical structures, and the angle between the arms is proportional to the ratio of the width of the molecule (20 Å) to the repeat period (34 Å) of the helix. Further, careful study of the sequence of spots along the arms indicates an absence of the fourth spot, which confirms that there are only two intertwined helices involved in the structure.

1.2.3 Characterizing a Picasso Painting Reveals Hidden Secrets

Characterization and analysis play a significant role in art conservation, and are often used for authentication and to rule out forgery of paintings and sculptures when their provenance is questionable. Sometimes they reveal hidden secrets. Figure 1.2.5a shows Picasso’s *La Misèreuse accroupie*, painted early in his Blue Period era of work. Using X-ray fluorescence (§2.5.2.1) measurements in a specialized set up (Fig. 1.2.5b) to scan such large paintings, it was discovered that the current Picasso painting was painted over a landscape painting (Fig. 1.2.8c) by another artist.

⁴ F. H. C. Crick, J. D. Watson and M. H. F. Wilkins shared the 1962 Nobel Prize in Physiology in Medicine, and were cited “for their discoveries concerning the molecular structure of nucleic acids and its significance for information transfer in living material.”



Figure 1.2.5 (a) The current Picasso *La Miséreuse accroupie*. (b) Mounting of the painting for element-specific, spatially-resolved X-ray fluorescence measurements. (c) The hidden landscape painting buried underneath the current painting detected by element-specific X-ray fluorescence (XRF, §2) images.

Adapted from the *New York Times*, February 21, 2018.

In X-ray fluorescence, the incident probe of X-rays is absorbed by the various elements in the pigments, which then re-emit their characteristic X-rays (or fluoresce) at specific wavelengths (§2.5.2). This element-specific X-ray fluorescence can be locally excited and mapped spatially to obtain their two-dimensional distribution in the painting. Maps of iron (Fig. 2.Frontispiece.d) representing the use of Prussian blue, which is an iron-based pigment, and chromium (Fig. 2.Frontispiece.e), which is used in yellow pigments, matches the structure of the painting as seen today. However, the distributions of cadmium (Fig. 2.Frontispiece.f) used in multiple colored pigments, including red, yellow, and orange, and lead (Fig. 2.Frontispiece.g), used as a white pigment, clearly shows a different painting underneath.

1.2.4 Failure Analysis: Metallurgy of the *RMS Titanic*

In the early part of the twentieth century, passengers and mail between Europe and North America crossed the Atlantic Ocean by passenger steamship. One of the most luxurious steamships to be built for this purpose was the *RMS Titanic* (Fig. 1.2.6a), which, on its maiden voyage in 1912, struck an iceberg that damaged its hull and broke the ship in two. Within three hours, it sank, and more than 1,500

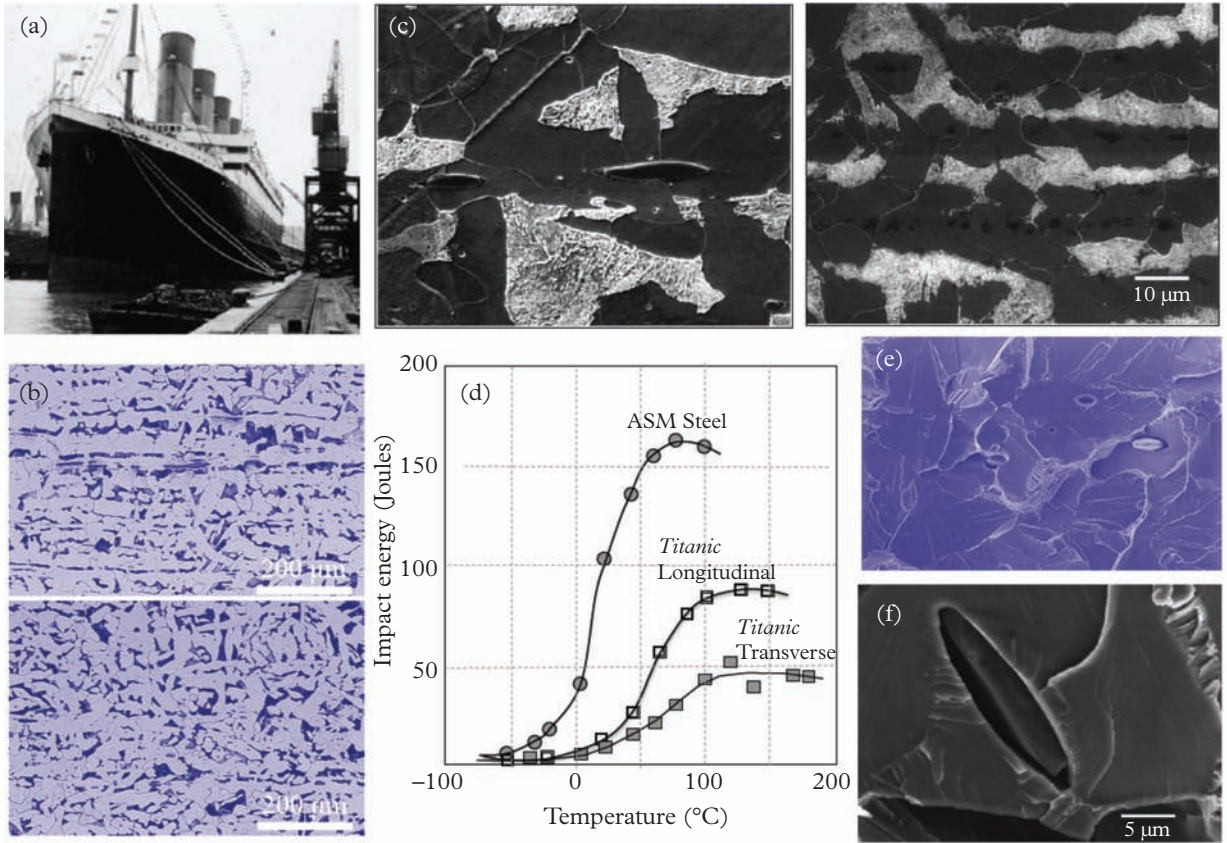


Figure 1.2.6 (a) The *HMSTitanic* before its maiden voyage. (b) Optical micrographs (§6) of the steel from the *Titanic* hull in the longitudinal (top) and transverse (bottom), showing the banding with elongated pearlite colonies and MnS precipitates. (c) An SEM micrograph of the *Titanic* hull plate (longitudinal section) and the ASTM standard. (d) Charpy impact energy as a function of temperature for longitudinal and transverse specimens of the *Titanic* hull and ASTM A36 standard. (e) An SEM micrograph of a Charpy impact fracture surface newly created at 0°C shows cleavage planes with ledges and MnS particles; the latter is shown magnified in (f).

Adapted from [8].

of its passengers died. An oft-cited culprit for this disaster was the quality of the steel used in its construction. A metallurgical analysis of the hull steel recovered from the wreckage provides interesting insight into its failure.

The first analysis of the steel looking at its overall composition Table 1.2.1 revealed a low nitrogen content, indicating that the steel was not made by the Bessemer process, which was known to render the steel against being brittle, especially at freezing temperatures. Instead, it was made by the then-alternative

Table 1.2.1 The composition (at %) of steels from the *Titanic*, a lock gate of the same era, and ASTM A36 steel

	C	Mn	P	S	Si	Cu	O	N	Mn:S ratio
<i>Titanic</i> Hull Plate	0.21	0.47	0.045	0.069	0.017	0.024	0.013	0.0035	6.8:1
Lock gate	0.25	0.52	0.01	0.03	0.02	-	0.018	0.0035	17.3:1
ASTM A36	0.20	0.55	0.012	0.037	0.007	0.01	0.079	0.0032	14.9:1

open-hearth process, as suggested by the relatively high oxygen and low silicon content. In addition, it contained a higher than normal phosphorus content, a very high sulfur content, and a low manganese content; the ratio of Mn:S was 6.8:1, a very low ratio by modern standards. The overall composition suggests that this steel was prone to embrittlement, or loss of ductility, especially at the freezing conditions encountered by the ship on that fateful night.

Metallographic preparation for optical microscopy, consisting of grinding, polishing, and etching with 2% Nital (§6.8.5), revealed the microstructure of the steel by optical microscopy (Fig. 1.2.6b). The steel is clearly banded in the longitudinal direction (top) with an average grain size of $\sim 60 \mu\text{m}$, and the pearlite phase cannot be resolved. A scanning electron micrograph (§10) reveals the pearlite colonies, ferrite grains, small non-metallic inclusions, and MnS particles (Fig. 1.2.6c) identified by energy-dispersive X-ray spectrometry (EDXS, §2.5.1.2), elongated in the direction of banding. The Charpy impact test, performed from -55°C to 179°C (Fig. 1.2.6d) shows that the ductile–brittle transition temperature is 32°C for the hull steel, and -27°C , for the comparable ASTM A36 steel. The sea water temperature at the time of the collision was -2°C ! Note that the ASTM A36 standard has a higher Mn:S ratio, and a substantially lower phosphorous content, both of which lead to reduced ductile–brittle transitions. A scanning electron microscope (SEM) image (Fig. 1.2.6e) shows a fractured lenticular MnS particle that protrudes edge-on from the fractured surface; further, slip lines radiating away from the MnS particle can be seen. Based on such analysis [8] it can be concluded that, even though the hull steel used was the best available in 1909–1911—when the *Titanic* was built—it would not meet the standards for plate steel used in ship construction today.

1.2.5 Beneath Our Feet: Microstructure of Rocks and Minerals

Common materials used in engineering are sourced from common minerals, which in turn are the major constituents of common rocks. Earth is a series of “shells”; it has a liquid core composed mainly of iron (and some nickel),

an intermediate mantle (solid rock rich in oxygen, silicon, iron, and magnesium, in the form of silicates), and an outer crust (which averages around 30 km in thickness) that is made mostly of aluminosilicates, alkali elements, and calcium. The most abundant chemical element in the Earth's crust is oxygen (47 wt%, 94 at%), followed by silicon (28 wt%, 1% at%), and aluminum (8 wt%, 0.5 at%). Needless to say, most metals and ceramics are extracted from this outer crust.

The most common minerals are chemical compounds of silicon, aluminum, and oxygen, with small amounts of other elements distributed in them. Silicates dominate the minerals in the crust, the most abundant (58%) being feldspars (Orthoclase— KAlSi_3O_8 , Albite— $\text{NaAlSi}_3\text{O}_8$, Anorthite— $\text{CaAl}_2\text{Si}_2\text{O}_8$), followed (13%) by pyroxenes and amphiboles (Diopside— $\text{CaMgSi}_2\text{O}_6$, Enstatite— MgSiO_3 , Tremolite), and to a lesser extent, $\sim 10\text{--}11\%$ each, by quartz (SiO_2) and mica (Muscovite— $\text{KAl}_2(\text{AlSi}_3\text{O}_{10})(\text{OH})_2$, Kaolinite— $\text{Al}_2\text{Si}_2\text{O}_3(\text{OH})_4$), respectively.

Petrologists study the mineralogical and chemical details of rocks, and structural geologists study the structural aspects of minerals and rocks, especially from the viewpoint of deformation processes. Detailed studies of rocks at the microscopic level provide a link between these two areas of study (Vernon, 2004). Microstructures of standard thin or polished sections of rocks are routinely observed in optical microscopes (§6.8.3) using polarized light (Fig. 1.2.7a). Cathodoluminescence (CL, §10.6.2) is used (Fig. 1.2.7b) to reveal the internal microstructure of grains, especially from those minerals (quartz, feldspar, and calcite) that appear colorless in light microscopes. Moreover, CL arises from imperfections in the crystal lattice (§4.1.9), e.g. impurity atoms, vacancies, and dislocations that are produced during the formation and growth of the minerals. Higher resolution images can be obtained in an SEM (§10), using secondary or back-scattered electrons (Fig. 1.2.7c) the latter with element sensitivity, and are used to reveal detailed microstructures of small grains, fine-grain aggregates, and intergrowths. Transmission electron microscopes (§9) can provide further details of finer features, e.g. exsolution lamellae. Computed tomography (§9.5.1) maps the variation of X-ray attenuation within a solid, along multiple directions [10]. The attenuation varies with the amount of each mineral present, and a series of cross-section or 2D images, produced along different directions, are computed to provide a 3D representation of the grains and aggregates in the rock (Fig. 1.2.7d,e). Finally, electron probe microanalysis (EPMA, §2.5.2.2) and mapping produces maps of compositional distribution, particularly in fine-grained aggregates of minerals (Fig. 1.2.7c). In general, the microstructure of rocks is a product of a complicated sequence of geological events and processes. As such, its microstructural analysis, including its chemical information, applying many of the techniques discussed in this book, can provide insight into the rock's formation, its geological history, and mineral value.

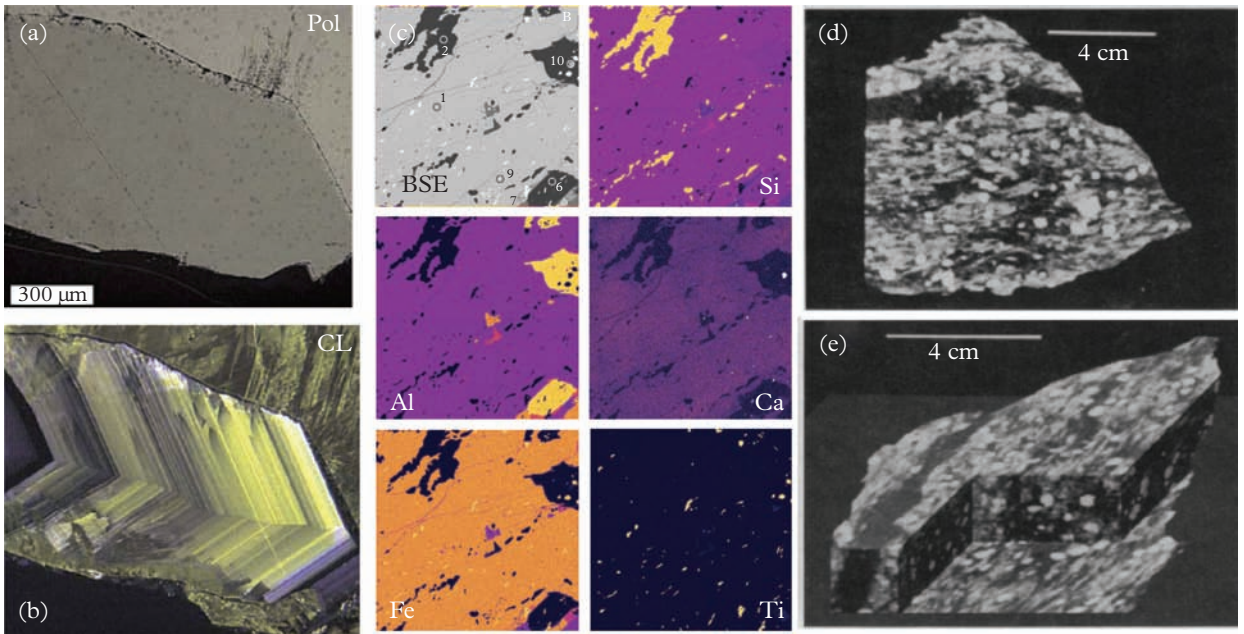


Figure 1.2.7 A specimen of hydrothermal quartz imaged by (a) polarizing and (b) cathodoluminescence (CL, §10) microscopy. Note that CL reveals internal structures and growth zoning that is not visible in the former. Adapted from [9]. (c) Back-scattered electron image (§10) of a specimen of peletic schist from Antarctica, along with composition maps for the principal elements. X-ray tomographic images of garnetiferous metamorphic rocks. (d) A single slice of a peletic schist—garnets are light gray to white ovals, kainite appears as medium gray laths, and dark gray to black regions are rich in quartz, feldspar, and muscovite. (e) A perspective view of a 3D density map. The single slice at the bottom of the stack locates the cutaway block in the interior of the specimen.

Adapted from [10].

1.2.6 Ceramic Materials: Sintering and Grain Boundary Phases

Ceramic materials are typically heterogeneous, multiphase materials, often containing crystalline and glassy (non-crystalline) phases with unique properties that make them suitable for high-temperature structural applications. As mentioned in §1.1, microstructure that may be too small to be seen with the naked eye, plays an important factor in the final property of a material. For ceramics, the microstructure is made up of small crystals called grains (Fig. 4.1.1), and in general, the smaller the grain size, the stronger and denser is the ceramic material.

Typically, ceramic materials are prepared by sintering, often in the presence of additives to introduce a liquid phase during sintering to overcome the poor solid-state diffusion, and achieve high densities. For example, in the case of silicon nitride, the liquid phase is introduced by oxide additives, which form a low-temperature eutectic⁵ liquid with the oxidized surface layers of the silicon nitride powder precursors. However, the glassy intergranular layer is often retained after sintering, causing a deterioration in the mechanical properties. An understanding of the intergranular layer and its structure is required to improve the performance of ceramic materials. The characterization of the microstructure, including the grain boundary phases, is carried out using multiple techniques, such as X-ray microanalysis (§2.5.2), scanning and transmission electron microscopy (§9 and §10), and X-ray (§7) and electron (§8) diffraction, which is then correlated with rigorous mechanical testing.

Now, we briefly introduce the microstructural evaluation of the sintering of silicon nitride with small additions of La_2O_3 , Y_2O_3 , and SrO [4]. A polished specimen is first prepared and observed in an SEM (Fig. 1.2.8a) and its composition analyzed by EDXS (Fig. 1.2.8b). The polished surface reveals Si_3N_4 grains (90%) with a distribution of a boundary phase at grain boundaries and multi-grain junction regions (pockets); the latter can be estimated to be $\sim 10\%$ of the volume.

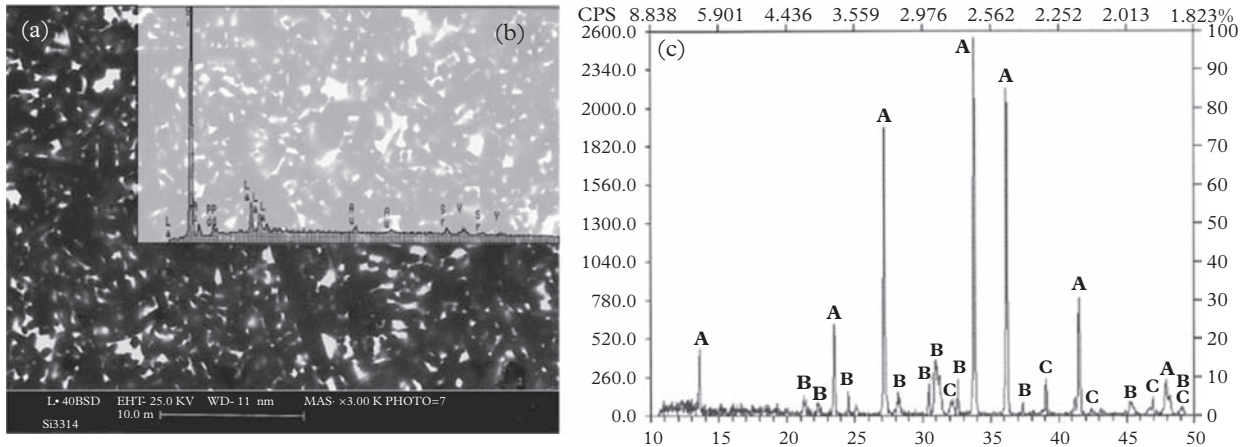


Figure 1.2.8 (a) SEM micrograph of a polished surface of a silicon nitride specimen showing the presence of the boundary phase (white), especially in the multiple grain junctions. (b) X-ray microanalysis (§2.5.2) of the polished surface shows peaks of Si and La, with very small intensities for Y and Sr. (c) X-ray diffraction (§7) patterns showing peaks that can be indexed for $\beta\text{-Si}_3\text{N}_4$ (A), $\text{La}_5\text{Si}_3\text{O}_{12}\text{N}$ (B), and $\text{Y}_5\text{Si}_3\text{O}_{12}\text{N}$ (C).

Adapted from [4].

⁵ Relating to or denoting a mixture of substances (in fixed proportions) that melts and solidifies at a single temperature that is lower than the melting points of the separate constituents or of any other mixture of them.

The EDXS spectrum reveals the presence of the major sintering aid (La_2O_3) with La peak intensities substantially more intense than that for Y and Sr. Further, routine XRD θ - 2θ scans (§7.9.2, Fig. 1.2.8c) reveal the presence of a majority β - Si_3N_4 and minority/boundary $\text{La}_5\text{Si}_3\text{O}_{12}\text{N}$ and $\text{Y}_5\text{Si}_3\text{O}_{12}\text{N}$ crystalline phases; however, it is not easy to say if the crystalline boundary phases were formed during sintering or during subsequent heat treatments.

Figure 1.2.9a is a lower magnification, bright-field transmission electron microscope (TEM) image of a two-grain region that shows a near-uniform dark contrast at the grain boundary. High-resolution electron microscopy (HREM) using phase contrast (§9.2.7) reveals further details of the microstructure at the atomic level. The HREM image from the two-grain region (Fig. 1.2.9b) shows that the β - Si_3N_4 grains are separated by a uniform amorphous phase ~ 1.8 nm in thickness. However, a HREM image (Fig. 1.2.9c) of a three-grain junction shows evidence of a crystalline phase, with two sets of orthogonal lattice fringes (0.32 nm and 0.33 nm) present in the pocket. The fringe spacing(s) is in agreement with the interatomic spacing for the (210) and ($1\bar{1}2$) lattice planes of silicon

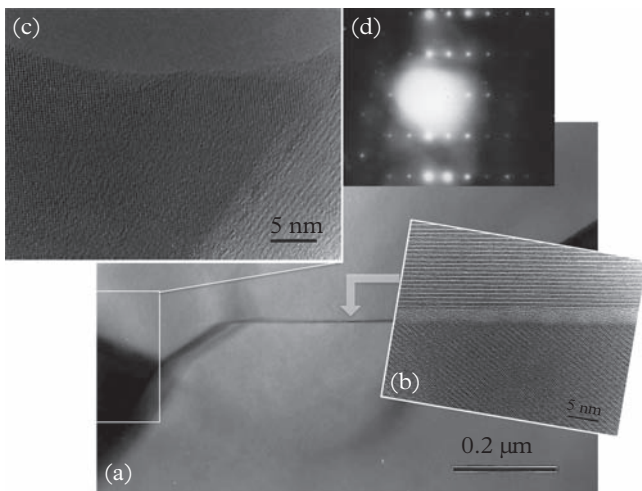


Figure 1.2.9 (a) A lower magnification bright-field TEM image showing a straight two-grain boundary. (b) An HREM micrograph of a two-grain boundary region. Using the lattice plane spacing of β - Si_3N_4 as an internal calibration, the amorphous phase thickness can be estimated to be ~ 1.8 nm. (c) The multigrain junction (pocket) shows two-dimensional lattice fringes, with orthogonal spacing of 0.32 nm and 0.33 nm, respectively, corresponding to $\text{La}_5\text{Si}_3\text{O}_{12}\text{N}$. A residual glassy phase between $\text{La}_5\text{Si}_3\text{O}_{12}\text{N}$ and the β - Si_3N_4 grain is also found. (d) The crystallized material at the grain pocket can be indexed as the $\langle 012 \rangle$ diffraction pattern of $\text{La}_5\text{Si}_3\text{O}_{12}\text{N}$.

Adapted from [4].

lanthanum oxynitride ($\text{La}_5\text{Si}_3\text{O}_{12}\text{N}$), which is further confirmed by the selected area electron diffraction (Fig. 1.2.9d). Detailed analysis of this microstructure [4] shows that it is consistent with models [5] of sintering that predict an equilibrium thickness (~ 1 nm) at two-grain boundaries. Further, the grain pockets still show the presence of an amorphous phase, suggesting that it is hard to achieve a complete recrystallization of the grain boundary phase in silicon nitride. However, the partial recrystallization of the grain boundary phase can be correlated with the superior high-temperature strength of these ceramic materials.

1.2.7 Microstructure and the Properties of Materials: An Engineering Example

We now present an engineering example that illustrates a number of microstructural features; these are of particular relevance to materials characterization. Consider a dual-phase steel alloy of iron and chromium, doped with other elements, and bulk composition $\text{Fe}_{64}\text{Cr}_{25.3}\text{Ni}_{4.7}\text{Mn}_{1.34}\text{Mo}_{0.48}\text{C}_{0.04}$, typically used in automobile body panels, wheels, and bumpers. A number of *specimens*⁶ of this alloy, all of the same bulk composition, were prepared and first annealed for one hour at $1,300^\circ\text{C}$. Then, each of them was subsequently annealed again at a different temperature, T_a , over the range, $400^\circ\text{C} < T_a < 1200^\circ\text{C}$. Their mechanical properties were measured and the ultimate tensile strength (UTS) of the alloys varied with T_a (Fig. 1.2.10a) with a minimum at $T_a = 900^\circ\text{C}$. Now, since all the alloys have the same chemical composition, the variation of mechanical properties can only be explained in terms of the *microstructure*. Figure 1.2.10b shows a typical microstructure observed in a transmission electron microscopy (§9) bright field image common to all these alloys. Clearly it has two *phases* with distinctly different features, i.e. dark particles distributed in a light matrix.

Careful *crystallographic structure* analysis by transmission electron diffraction (§8) shows that the *structural arrangement* of the *unit cells* in the two phases is different—the dark particles have a face-centered cubic (FCC) structure (Fig. 4.1.12), which is referred to as the γ -austenite phase, and they are distributed in a body-centered cubic (BCC), α -ferrite matrix phase. The volume fraction, f_γ , of the γ -austenite phase, is obtained by analyzing these images and it varies from 5% to 40% as a function of T_a , (Fig. 1.2.10c) with a maximum for $T_a = 900^\circ\text{C}$. It is clear that the ultimate tensile strength depends *inversely* on the content, f_γ , of the γ - phase. Now, it is easy to understand the mechanical behavior. Compared to the α -ferrite matrix (BCC) the γ -austenite (FCC) particles have a lower resistance to plastic deformation, a larger ductility, and lower values of the UTS. This is not the end of the story. If we carefully plot the value of UTS as a function of f_γ , we see not one but two distinct curves (Fig. 1.2.10d). It turns out that these two curves correspond to different *compositions* of the particle and matrix phases, as confirmed by appropriate *chemical analysis*, using EDXS (§2.5) in a TEM

⁶ In materials characterization, the terms *specimen* and *sample* are used interchangeably. However, in this book we will endeavor to distinguish the two. The sample is generally the overall subject of the study, and the specimen is specifically what is used or prepared to carry out a measurement or examination. For example, a chemically *inhomogeneous* sample may have a certain bulk/average composition; however, different specimens prepared from different parts of the sample may have different compositions because of the inhomogeneity.

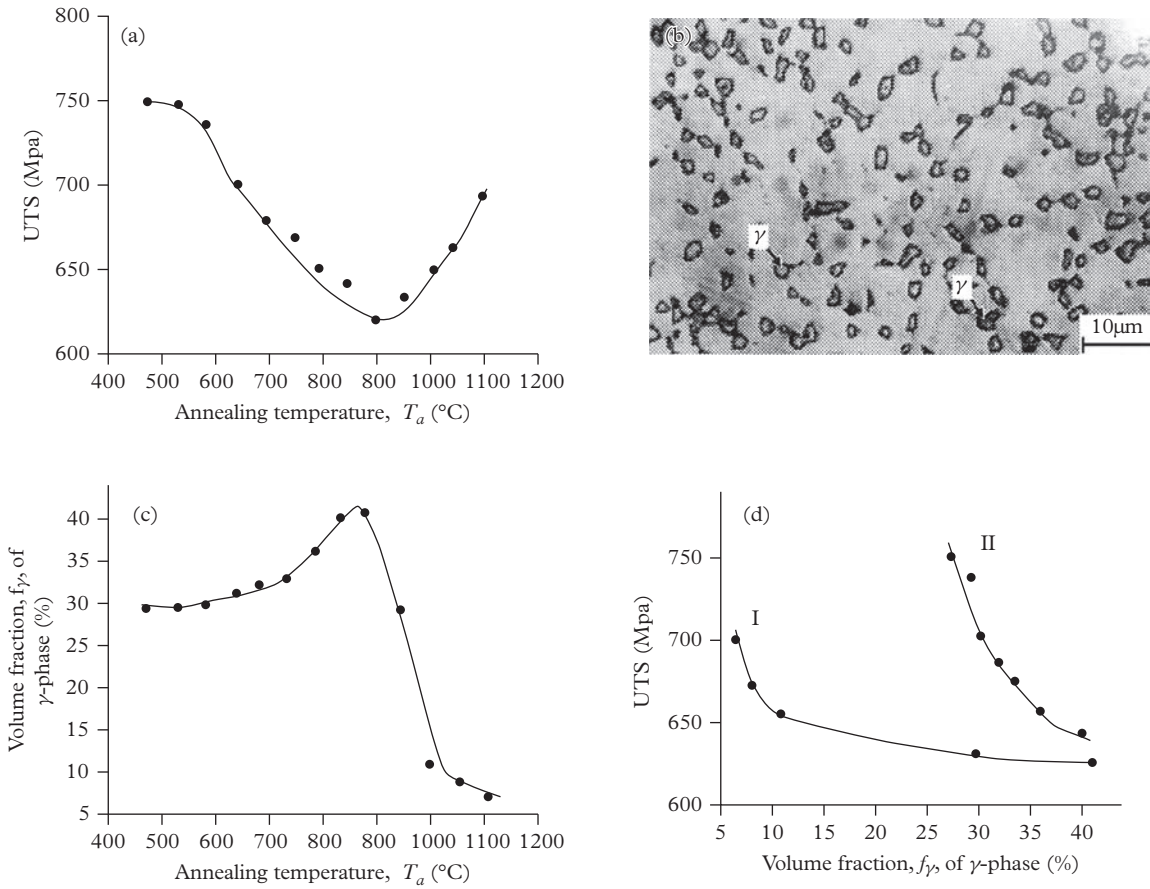


Figure 1.2.10 An example of the relationship between microstructure and properties in dual-phase steel. (a) Variation of the ultimate tensile strength (UTS) with annealing temperature. (b) The two-phase microstructure of γ -austenite (FCC) precipitates in an α -ferrite (BCC) matrix. (c) The γ -phase volume fraction, f_γ , as a function of annealing temperature. Note the inverse correlation with UTS. (d) The variation of UTS with f_γ further depends on the composition.

Adapted from Kurzydowski and Ralph (1995).

(§9.4.3). Thus, we can see that these two phases not only differ in their mechanical properties but also their alloying content. From the perspective of this book, we can see that the microstructure involves *structural* (crystallography), *chemical* (composition), and *morphological* (volume fraction) aspects, among others, that need to be understood to optimize the mechanical properties of these dual-phase steel alloys.

1.3 Probes for Characterization and Analysis: An Overview

1.3.1 Probes and Signals

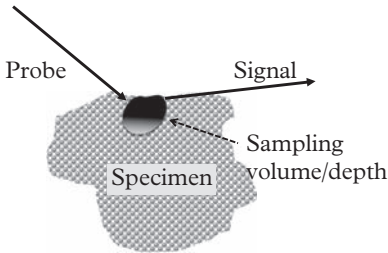


Figure 1.3.1 A general representation of materials characterization using probe and signal radiations to infer details of the microstructure of materials. In general, the probe and signal may be the same type of radiation, or they may be different.

Our general approach to materials characterization is illustrated in Figure 1.3.1. We typically use an incident radiation or *probe* to interrogate the material and then detect a *signal* that can be used to infer or interpret the microstructure of interest. The interaction of the probe with the specimen can be *elastic* or *inelastic*. By elastic, we mean that there is no difference in the energy of the probe and signal, and applies predominantly to scattering or diffraction methods. By inelastic interactions, we mean a change in energy and such dispersions of signal intensity, as a function of energy, form the basis of spectroscopy techniques. However, signals from both elastic and inelastic interactions can be spatially resolved or mapped, and such spatial intensity distributions form the basis of imaging methods.

We emphasize that the probe and signal may or may not be the same; in other words, they can be different. For example, in X-ray photoelectron spectroscopy (XPS, §2.6.3), we use X-rays or photons as the incident probe, and detect the photoelectrons as the signal. In this case, it is also important to recognize that, even though the *penetration depth* of the incident photons or X-rays may vary, the signal will be restricted to the *escape depth* of the photoelectrons, which is largely limited to the surface. A counter-example would be EDXS, where the incident probe is a high-energy or “fast” electron beam in an SEM (§10) or TEM (§9), and the detected signals are the characteristic X-rays emitted from elements constituting the specimen. Alternatively, electron energy-loss spectroscopy (EELS) in a TEM (§9.4.2), which is the electron analog of X-ray absorption spectroscopy (XAS, §3.9.1), uses fast electrons as the incident probe but then detects the energy dispersion of the inelastically scattered electrons, typically in the forward direction, after passing through the specimen.

1.3.2 Probes Based on the Electromagnetic Spectrum and their Attributes

The electromagnetic spectrum, extending from radio waves to γ -rays (Fig. 1.3.2) and including the relationship between energy (E), wavelength (λ), and frequency (f), is a good starting point to look at various probes used in materials characterization and analysis. The visible spectrum ranging from $\lambda \sim 380 - 700$ nm, with red ($\lambda = 650$ nm), green ($\lambda = 530$ nm), and blue ($\lambda = 470$ nm) indicated prominently, is used in optical imaging/microscopy and Raman spectroscopy. At larger wavelengths, we encounter infrared (IR) radiation used in probing vibration modes in molecules, followed by microwaves and radio waves; the latter, includes nuclear magnetic resonance (NMR) of wide use in chemistry and medical imaging. At wavelengths shorter than the visible, we find ultraviolet (UV)

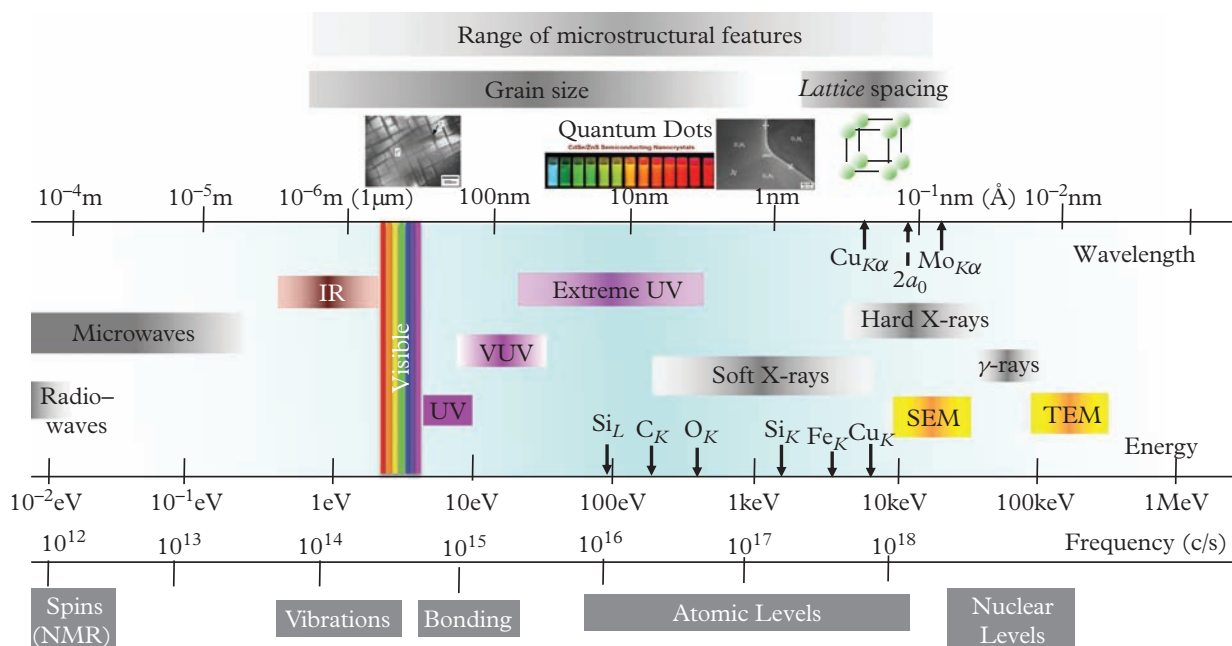


Figure 1.3.2 The electromagnetic spectrum illustrating the range of probes that can be used in materials characterization. In addition, we must also include scanning probes as well as ions and neutrons.

radiation, useful in probing bonding states of molecules, and further down we encounter extreme UV (EUV) radiations, followed by soft X-rays,⁷ hard X-rays, and γ -rays, in that order. Soft X-rays overlap in energy with the atomic levels of core electrons; for reference, the Si_L (99.2 eV, $\lambda = 12.5$ nm), C_K (284 eV, $\lambda = 4.4$ nm), O_K (532 eV, $\lambda = 2.3$ nm), Si_K (1840 eV, $\lambda = 0.674$ nm), Fe_K (7112 eV, $\lambda = 0.174$ nm), and Cu_K (8980 eV, $\lambda = 0.138$ nm) absorption edges are shown. The $Cu_{K\alpha}$ (8.05 keV, $\lambda = 0.154$ nm) and $Mo_{K\alpha}$ (17.48 keV, $\lambda = 0.071$ nm) radiations, often used as laboratory sources for X-ray diffraction, are also indicated. The radius of the $n = 1$ orbit in the Bohr model (§2.2) of the hydrogen atom is $a_0 = 0.53$ Å. Twice this Bohr radius, or the diameter, $2a_0$, is a critical dimension that represents the spatial extent within which most of the charge for all atoms is contained; this value $2a_0 = 1.06$ Å, is also indicated. However, in atoms with multiple (Z) electrons, the inner shells have radii of the order of a_0/Z because they are not shielded by the outer electrons and experience the full Coulombic interactions of the nuclear charge ($+Ze$).

Most commercial SEMs (§10.2) and TEMs (§9.2) operate in the range of 1–30 kV and 100–300 kV, respectively. The energy ranges of these “fast” electrons straddle those of γ -rays, and are also included in Figure 1.3.2. However, we

⁷ Wilhelm C. Röntgen (1845–1923) was the German physicist who discovered X-rays, also known as Röntgen rays, in 1895. He received the *first* Nobel prize in Physics in 1901 “in recognition of the extraordinary services he has rendered by the discovery of the remarkable rays subsequently named after him.”

should not forget that electrons are charged particles and that Coulomb forces are very strong. Microstructural features of interest in materials characterization range from the interatomic lattice spacing ($\sim 1 \text{ \AA}$), to intergranular phases ($\sim 1 \text{ nm}$), to grains and precipitates ($10 \text{ nm} \sim 1 \text{ }\mu\text{m}$). Representative microstructural examples (§1.2) of γ and γ' phases in bulk Ni-based super alloys, semiconductor quantum dots, and intergranular amorphous phase in a sintered silicon nitride ceramic, illustrate the spatial range of materials encountered in characterization and are included for comparison in Figure 1.3.2.

Note that in Figure 1.3.2, energy is not expressed in the standard SI or MKS unit of joule (J), but in unit of electron volts (eV), which is the kinetic energy gained by an electron accelerated from rest through a potential difference of 1 V. It is generally recognized that the unit of joule is so large that it is inconvenient for use in routine materials characterization. Using the electron charge ($e^- = -1.602 \times 10^{-19}$ Coulomb), and the fact that a joule is equal to a Coulomb-Volt, we can readily show that $1 \text{ eV} = 1.602 \times 10^{-19} \text{ J}$. Commonly, multiples of the eV, i.e. keV (10^3 eV) and MeV (10^6 eV), are also used. Further, based on the dispersion relation in vacuum, $c = f\lambda$, where $c = 299,792,458 \text{ m/s}$, is the velocity of light, f is the frequency, and λ is the wavelength, one can write the energy, E , of the photon⁸ as

$$E = hf = \frac{hc}{\lambda} = \frac{12.4 \text{ (keV)}}{\lambda(\text{\AA})} \quad (1.3.1)$$

where Planck's⁹ constant, $h = 4.136 \times 10^{-15} \text{ eV s} = 6.626 \times 10^{-34} \text{ Js}$, and λ is in units of \AA ($= 10^{-10} \text{ m}$).

1.3.3 Wave-Particle Duality

We have described probes within the electromagnetic spectrum in terms of their unique attributes of energy, wavelength, and frequency. In materials characterization we also tend to view the probe and signal radiations as discrete particles, e.g. electrons, photons, ions, and neutrons. The wave-particle duality—a concept central to modern physics—is the key to understanding this dichotomy. Historically, the behavior of electrons and photons provided key insight into the wave and particle nature of matter. Two important classical experiments are discussed here.

⁸ The word *photon* was introduced by G. N. Lewis in *Nature*, December 18, 1926.

⁹ Max Planck (1858–1947) was a German physicist who was awarded the Nobel prize in Physics in 1918 “in recognition of the services he rendered to the advancement of Physics by his discovery of energy quanta.”

The photoelectric effect: When light is incident on a clean metal surface it ejects electrons (known as photoelectrons). The intensity of the light determines the number of photoelectrons emitted but the energy of the photoelectrons depends only on the frequency, f , of the light. This is impossible to reconcile with a wave description of light because it requires that the photoelectrons be emitted

with a velocity proportional to the intensity of light. Einstein¹⁰ explained the photoelectric effect by considering the incident light as a beam of particles or photons, each with a *quantum* of energy, hf , such that a single photon would eject an electron from the metal surface with velocity, v , given by

$$\frac{1}{2}m_e v^2 = hf - \Phi \quad (1.3.2)$$

where, m_e is the mass of the electron, h is the Planck constant, and Φ is the surface work function (§3.7) required to remove a photoelectron from the solid. In this then-radical theory, increasing the intensity of light increases the number of incident photons, and leads to an increase in the number of ejected electrons without changing their velocities. In contrast, diffraction of light and X-rays, the latter from the planes of atoms in crystals, arises from interference (§6.6) and confirms their wave-like nature.

Example 1.3.1: A beam of photons illuminates a metallic surface (work function = 3.45 eV) and ejects electrons with a velocity of 765 km/s. What is the wavelength of the incident photon? What part of the electromagnetic spectrum does this photon correspond to?

Solution: First we convert the work function into SI units:

$$\Phi = 3.45 \text{ eV} = 5.527 \times 10^{-19} \text{ J}$$

Then, applying (1.3.2) and using the values of the fundamental constants, we get the frequency of the incident photon:

$$f = \frac{\frac{1}{2}m_e v^2 + \Phi}{h} = 1.236 \times 10^{15} \text{ s}^{-1}$$

From (1.3.1), we get

$$\lambda = c/f = 2.43 \times 10^{-7} \text{ m} = 243 \text{ nm},$$

where

$$c = 3 \times 10^8 \text{ m/s}$$

is the velocity of light.

Thus, the wavelength of the incident photon is 243 nm, and falls in the UV region of the electromagnetic spectrum (Fig. 1.3.2).

¹⁰ Albert Einstein (1879–1955) received the Nobel prize in Physics in 1921 for “his services to theoretical physics and especially for his discovery of the law of the photoelectric effect.”

Electron diffraction: Electrons are deflected in electric and magnetic fields consistent with a classical particle-like behavior. In fact, such deflections are used in the design of electron spectrometers (§2.6.1.2) and systems for the magnetic imaging of domains (§9.3.6). However, one can associate a wavelength, λ , and a momentum, \mathbf{p} , where $|\mathbf{p}| = p$, with the motion of the electrons as postulated by de Broglie¹¹ (1924), in his principle of *wave-particle duality*:

$$\lambda = h/p \quad (1.3.3)$$

where h is the Planck constant. In fact, such wave-like behavior of electrons was verified almost immediately by Davisson¹² and Gerner (1925), who demonstrated the diffraction of electrons (§8) from the surface of nickel single crystals.

Thus, diffraction studies of surfaces require electrons with energies of the order of 100 eV, and such surface techniques are termed low energy electron diffraction (LEED, §8.4.1) or microscopy (LEEM).¹³ See Example 1.3.2. However, to probe the internal crystal structure of materials, electrons with substantially higher energy (100–200 keV), e.g. in TEMs, with wavelengths in the range (0.037–0.0251 Å) are used (§9). Such high-energy electrons can also probe the structure of surfaces in reflection mode (RHEED, §8.4.3). In addition, scattering of protons (H^+) and He^+ ions of energy ~ 1.0 – 2.0 MeV, are also used in materials characterization (§5.4); typically, a 2.0 MeV He^+ ion has a wavelength of 10^{-5} nm.

Example 1.3.2: What is the kinetic energy of an electron suitable for electron diffraction of crystalline materials?

Solution: The distances between lattice planes in a crystal are of the order of 0.1 nm (1 Å) and for diffraction of electrons their wavelengths should be of comparable magnitude. Thus, for a wavelength of 0.1 nm, the velocity of the electron is, from (1.3.3), $\lambda = \frac{h}{p} = \frac{h}{m_e v}$.

Thus,

$$v = \frac{h}{m_e \lambda} = \frac{6.626 \times 10^{-34}}{(9.109 \times 10^{-31})(0.1 \times 10^{-9})} = 7.27 \times 10^6 \text{ m/s} \quad (1.3.4)$$

and its kinetic energy is

$$E = \frac{1}{2} m_e v^2 = 2.41 \times 10^{-17} \text{ J} \sim 150.4 \text{ eV} \quad (1.3.5)$$

where $1 \text{ eV} = 1.602 \times 10^{-19} \text{ J}$.

¹¹ L. de Broglie (1892–1987) was a French physicist who was awarded the Nobel prize in Physics in 1929 and was cited for his “his discovery of the wave nature of electrons.”

¹² C. J. Davisson (1881–1958) was an American physicist who won the Nobel prize in Physics in 1937 and was cited for “the experimental discovery of the diffraction of electrons by crystals.”

¹³ If, in addition, spin polarized (SP) electrons are used for imaging, the resulting SPLEEM microscope can be used to image surface magnetic domain structures. See Krishnan (2016), Ch. 8.

1.3.4 Nature and Propagation of Electromagnetic Waves

We briefly review the laws governing the propagation of electromagnetic waves (see §6 and/or Hecht (2002) for more details). We state here, without a detailed discussion, that Maxwell¹⁴ equations, which apply to all electromagnetic phenomena, require that the electric, \mathbf{E} , and magnetic, \mathbf{H} , fields that form the components of any electromagnetic radiation propagate as waves in free space. Both \mathbf{E} and \mathbf{H} vary along the direction of propagation, with the variation being harmonic in time, and the related displacements being always along the propagation direction. Further, the waves have only transverse and no longitudinal components. Figure 1.3.3 shows such an electromagnetic wave, propagating in the z -direction, at a particular instant of time, with \mathbf{E} confined to the xz -plane, and \mathbf{H} confined to the yz -plane. For this wave, the plane of vibration of the electric field, \mathbf{E} , is the xz -plane and its direction of vibration is the x -direction. Such plane waves are said to be *linearly* or *plane polarized*.

For a plane-polarized radiation, with the coordinates chosen such that \mathbf{E} is parallel to the x -axis, assuming that the variation of \mathbf{E} with both position, z , and time, t , are sinusoidal, we can express the electric field as

$$E_x = E_{x0} \sin 2\pi \left(\frac{z}{\lambda} - ft + \theta_x \right) \quad (1.3.6)$$

where, E_{x0} is the amplitude of the wave, λ is its wavelength, f is the frequency, and θ_x is the phase angle. Naturally, the frequency and wavelength are related, i.e. $c = f\lambda$. Note that any electromagnetic radiation, such as an X-ray beam, carries energy, and the rate of flow of this energy per unit area perpendicular to the

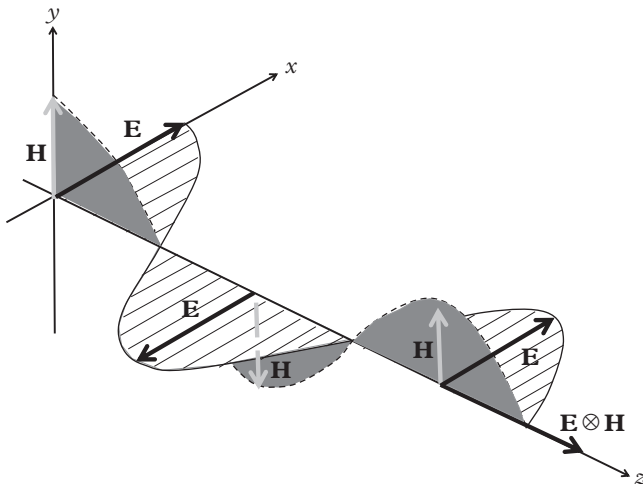


Figure 1.3.3 The variation of \mathbf{E} and \mathbf{H} , for a plane polarized electromagnetic wave propagating along the positive z -direction.

¹⁴ James Clerk Maxwell (1831–1879) was a Scottish physicist best known for his formulation of electromagnetic theory.

direction of propagation is given by its intensity that is proportional to the square of its amplitude, E_{x0}^2 . The unit of intensity is $\text{J/m}^2/\text{s}$.

The associated magnetic field, \mathbf{H} , is always perpendicular to \mathbf{E} , and in this case varies along the y -axis. Thus

$$H_y = H_{y0} \sin 2\pi \left(\frac{z}{\lambda} - ft + \theta_y \right) \quad (1.3.7)$$

where all terms have been defined earlier. If we are only concerned with the variations in time, at a specific location, z , of \mathbf{E} (or, for that matter, \mathbf{H}) we can simplify (1.3.6) for the plane wave as

$$E_x = E_{x0} \sin 2\pi (ft + \theta_x) \quad (1.3.8)$$

Further, if the phase angle, θ_x , is not of interest it can be set to zero.

Waves with other states of polarization do exist. A simple way to visualize them is to consider the combination of two waves of the same frequency, propagating in the same direction, (say, z -axis), but with the direction of vibration of the electric vector in the x -direction for one wave and the y -direction for the other. Then the resultant polarization will depend on the combination of their amplitudes, E_{x0} and E_{y0} , and their phases, θ_x and θ_y , which is given by

$$E_x = E_{x0} \sin 2\pi \left(\frac{z}{\lambda} - ft + \theta_x \right) \quad (1.3.9a)$$

and

$$E_y = E_{y0} \sin 2\pi \left(\frac{z}{\lambda} - ft + \theta_y \right) \quad (1.3.9b)$$

Following some mathematical manipulations, at any given position along the z -axis, we can show that the locus of positions with coordinates of E_x and E_y are, in general, an ellipse (§6.2.6). The characteristics of this ellipse depend on the amplitudes, E_{x0} and E_{y0} , and the phase difference, $\Delta\theta = \theta_x - \theta_y$, of the two waves. The minor, y' , and major, x' , axes of this ellipse do not lie along the original x - and y -direction, but make an angle, ψ , with the x -direction such that

$$\begin{aligned} E_{x'} &= E_x \cos \psi + E_y \sin \psi \\ E_{y'} &= -E_x \sin \psi + E_y \cos \psi \end{aligned} \quad (1.3.10)$$

where E_x and E_y can be substituted from (1.3.6). This *elliptically polarized* wave is shown in Figure 1.3.4. Further, when $E_{x0} = E_{y0}$, the ellipse simplifies to a circle and the wave is called *circularly polarized*. We discuss the application of polarized light in ellipsometry in §6.9.

A word on the nature of photons is now in order. Its nature can be illustrated with reference to Figure 1.3.5, which shows its electric field component, E , propagating in the z -direction. What we see is a pulse, or wave packet, moving with

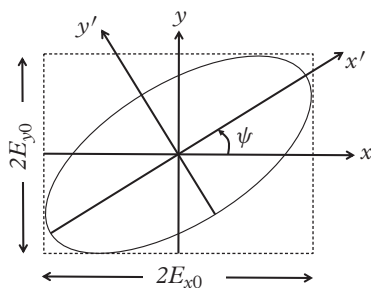


Figure 1.3.4 The vibrational ellipse of the electric vector, \mathbf{E} , of an elliptically polarized wave propagating in the z -direction (out of the plane of the paper). Note that when $E_{x0} = E_{y0}$, the ellipse becomes a circle and the radiation is called circularly polarized. Also see Figure 6.2.7.

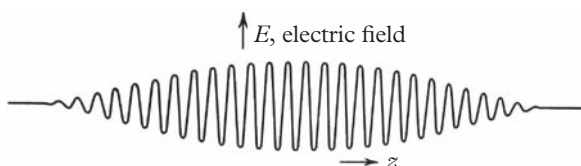


Figure 1.3.5 A photon can be considered as a wave packet, with its electric field component, $E(z)$, shown at any instant of time, t . Note that the entire wave packet moves with the velocity, c , of light.

Adapted from Sproul (1963).

the velocity, c , of light. Even though only a small number of oscillations are shown for clarity, in reality a typical photon emitted by an atom following a transition (Fig. 2.3.1) would have millions of oscillations. The motion of this photon or *wave packet*, would also follow all the properties of waves (wavelength, diffraction, polarization, etc.). Both, when light is emitted or absorbed, photons are created and absorbed as single indivisible units. Its energy is hf , where $f = c/\lambda$, and h is the Planck constant.

Example 1.3.3: How many photons of wavelength, λ (nm), are required to deliver 1 J of energy?

Solution: The energy of each photon is $E = hf = hc/\lambda$. Thus, the number (#) of photons required to deliver 1 J of energy is

$$\# = 1/E = \lambda/hc = \lambda \times 10^{-9} / (6.63 \times 10^{-34} \times 2.9979 \times 10^8) = 5.03 \times 10^{15} \lambda.$$

1.3.5 Interactions of Probes with Matter and Criteria for Technique Selection

Any characterization technique involving a probe will interact and invariably perturb the material (§5.3). Such perturbation has the potential to cause damage. Hence, the probe should be selected carefully to give maximum information with

minimum damage. Of all the available probes, electromagnetic radiation in the visible spectrum (light, in common parlance) causes the least damage, but at the same time the information it provides is restricted to the surface, and even that, only with modest resolution. Thus, initial observations of materials should be made with optical methods (§6) using either/both elastic and inelastic scattering strategies; this includes both imaging and spectroscopic methods. Subsequently, higher-energy X-rays can be used to probe the material at greater depths to provide crystallographic (§7) and chemical information (§2.5). If imaging at higher resolution is desired, it can be accomplished by either using an SEM with higher energy (5–30 keV) electrons (§10), or using a TEM (§9) with electrons of energy >100 keV to obtain information at the highest spatial resolution, provided electron transparent thin foil specimens representative of the behavior of interest can be made (§8 and §9). Before resorting to electron-based probes, e.g. SEM and TEM, when available, scanning probe methods (§11) may also provide useful information from the *specimen surface*, albeit at small areal (typically, 10 μm \times 10 μm) coverage. Finally, the materials can be investigated with ions (§5.4), or neutrons (§8.8), to provide a variety of complementary information. Chapter 5 discusses in detail in the various probes available (photons, electrons, ions, neutrons), the nature of their interactions—both elastic and inelastic—with the specimen, their generation, and factors to consider in their selection and use; where relevant the discussion continues in subsequent chapters dealing with specific techniques. Here, in brief, is a preview of some important points to be considered.

1.3.5.1 Penetration Depth and Mean Free Path Length

These define different distances travelled in the material being characterized by the probe radiation. *Penetration depth* is a measure of how deep the electromagnetic radiation can penetrate into a material; often, it is defined as the depth at which the intensity falls to $1/e$ (37%) of its original value. *Mean free path length* is the average distance traveled by a moving particle in a material between successive impacts/collisions that modify its direction or energy. For any technique, if the probe and signal radiations are not the same and have different mean free path lengths in the material, the volume analyzed (or, the *sampling depth*) will be determined by the radiation—either probe or signal—with the smaller mean free path length. In general, it is impossible to provide a single, comprehensive description of the penetration depth of the radiation across the entire electromagnetic spectrum. Instead, it is only possible to discuss it in terms of some specific wavelengths of importance in materials characterization. For example, in the vicinity of the visible spectrum, IR radiation is used to probe materials based on how they are absorbed (Fourier transform IR (FTIR) spectroscopy, see §3.5.2), visible light is used to examine the specimen surface (optical microscopy, §6.8), and UV radiation is used to resolve the surface electronic structure (UV photoelectron spectroscopy, UPS, §3.8).

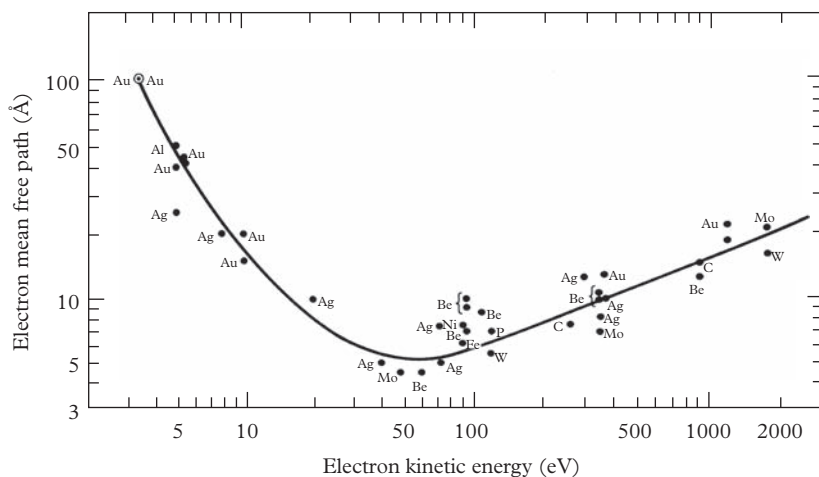


Figure 1.3.6 The mean free path of electrons as a function of energy for various metals. A universal curve, with a minimum of 4.0 Å for energies in the range ~ 50 – 100 eV, of relevance for Auger Electron Spectroscopy (AES, §2.6.2) and X-ray photoelectron spectroscopy (XPS, §3.8), is observed.

Adapted from [35].

Higher-energy probes, particularly X-ray radiation, have a uniform and predictable behavior in all materials. The absorption of X-rays, is defined by the attenuation coefficient, μ , (see Table 2.4.1) which increases with the average atomic number of the material, and determines the depth of penetration as

$$I = I_0 \exp(-\mu t) \quad (1.3.11)$$

where, I_0 is the intensity of the incident X-ray probe, and I is its intensity after being transmitted through the material of thickness, t (§2.4.2). The intensities of γ -rays show the same exponential dependence on thickness as X-rays, but with their much higher energies (~ 50 keV– 50 MeV) they penetrate much larger distances.

For electron probes, the mean free path length varies dramatically with their energy and the (average) atomic number of the material. For low energy (~ 0 – 2000 eV) electrons, the mean free path length is of the order of a few Å, and curiously, for all materials, satisfy a universal curve (Fig. 1.3.6) as a function of energy. This behavior, in simple terms, can be explained as follows.

For the range of energies of interest, the electrons in the solid can be approximated as a free electron gas. Then, the plasma frequency, which is a function of the mean electron-electron distance, r_s , determines the loss function. The inverse of the mean free path length, λ^{-1} , for electron propagation, is determined by r_s , which, to first order, is the same for all materials. For high-energy ($E \geq 5$ keV) electrons, the penetration depth, d_p , behaves as $d_p \propto E^{1.7}/Z$, where Z is the average atomic number of the material.

Neutrons have $\sim 1,000$ times the mass of electrons but do not have an electric charge. As a result, neutrons penetrate much greater distances than electrons and X-ray photons. Precise details of the penetration of neutrons in materials depend

on the specific atomic species; in fact, the scattering lengths of neutrons show an erratic variation in magnitude and sign with atomic number (§8.8).

The interaction of high-energy ions with materials is also complex. At low (\sim eV) energy they are reflected back from the surface, following simple rules of conservation of energy and momentum; at higher energies, they interact with the material, causing atomic displacements, formation of clusters and sputtering, or the removal of atoms, ions, and electrons from the specimen. In this context, it is customary to define a stopping distance, rather than a mean-free path, in the material for the ion. Further details are in §5.4.

1.3.5.2 Resolution

In the direction of the incident beam, i.e. *depth resolution*, the resolution is equivalent to the penetration depth already described in the previous section. However, the resolution in a direction normal to the direction of incidence, also known as the *spatial resolution*, depends on the diameter of the incident beam, its wavelength, and its mean free path length in the material. It also depends on the mode of imaging or signal collection. If the image is formed using an imaging system with “lenses”, utilizing either the transmitted or reflected radiation, then the spatial resolution will depend on the wavelength of the radiation, the quality of the imaging system, including the “aberrations” inherent in the lenses, and the coherence of the source. Microscopes—conventional optical, electron in diffraction or phase contrast modes, certain X-ray, and some ion—operate in this manner. To first order, the Rayleigh criterion (Fig. 1.4.10) provides a good working rule to determine the spatial resolution of these imaging modes (also see §6.8.1).

The alternative method of imaging is to focus a narrow beam of radiation onto the specimen surface and again to detect the transmitted or reflected radiation. The image is formed by rastering the incident probe on the specimen surface and recording any changes in the radiation either due to elastic or inelastic interactions. Now, the spatial resolution is determined by the diameter and wavelength of the incident radiation, and the nature of the interaction, including the degree of localization of the interaction event that constitutes the signal of interest. Confocal light microscopy using lasers (§6.8.5), SEMs (§10), and ion-based optical imaging systems are examples of this mode of imaging. It is important to recognize that the spatial resolution of a technique using such focused probes of high-intensity radiation can also be limited by the potential damage the beam can cause to the material being analyzed; this is discussed briefly in the next section and in detail in §5.3.

Complementing this, *temporal resolution*, defined as the precision of a measurement with respect to time, is a very important criterion for designing *in situ* and dynamic experiments for the study of growth, morphological evolution, and response of materials to various applied stimulus (§1.4.5). Further details of the achievable *depth*, *spatial*, and *temporal* resolution, and the factors that influence them, are discussed for specific techniques in future chapters.

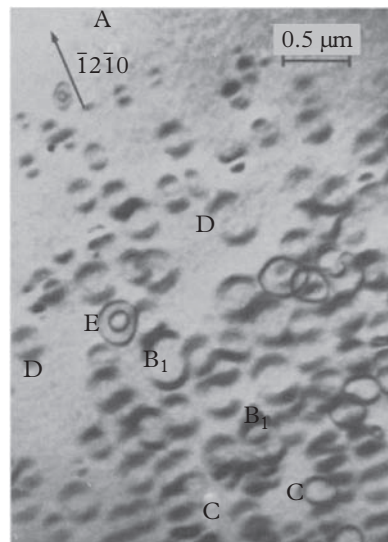
1.3.5.3 Damage

Damage to the specimen can be caused by the transfer of energy and momentum from the probe (see §5.3 for a detailed discussion). For photons, the transfer of energy in the form of heat largely causes the damage. The degree and spatial extent of the damage will be determined by the penetration of the radiation in the material, and the energy and flux of the incident photon. Specifically, for photons in the IR, visible, and UV portions of the electromagnetic spectrum, their momentum is quite small. However, higher-energy photons in the X-ray range, particularly when focused, can cause significant damage if the flux density is high, such as that obtained in synchrotron sources (§2.4.3) using zone-plate “lenses” (§6.6.7).

Electrons can behave both as particles and waves (§1.3.3), and when accelerated through several hundred keV in a TEM, they can cause significant damage by breaking interatomic bonds, particularly in polymeric materials (note: bond-breaking is not so common in inorganic or metallic materials). However, if the electrons are accelerated through higher voltages (~ 1 MeV), such as in high-voltage electron microscopes (HVEMs), the momentum transferred to the atomic nuclei by elastic large-angle scattering is sufficient to cause significant atomic displacements even in inorganic materials and alloys (Fig. 1.3.7). Similar atomic displacements are also caused by ions, and the extent of the damage is determined by the incident ion flux. For low flux, areas of displacement damage are isolated from each other, but at high flux the displacement damage is uniformly distributed in the specimen, resulting in the formation of an amorphous region even in crystalline materials. Note that an HVEM can be a powerful tool for *in situ* studies of radiation processes and the kinetics of defect formation; in fact, if it can be combined with an ion beam source such as in a tandem facility,¹⁵ where if necessary, conditions similar to that experienced in a high-flux nuclear reactor can be approximated and the ensuing damage in the material can be studied at high resolution [12].

1.3.5.4 Specimen Preparation or Requirements

These are also to be considered in probe and technique selection. While these requirements are technique specific and are described in appropriate sections throughout the book, some typical considerations are outlined here. Optical metallography (§6.8.5) often requires the polishing of surfaces, with specialized etchants (Table 6.8.1) to provide adequate contrast to resolve the features of interest. FTIR and Raman spectroscopy are quite flexible, require no vacuum, and can investigate liquids, gases, and solids. SEM requires minimal preparation, as long as the specimen is vacuum compatible, but if it is an insulator, it will require a thin (~ 10 nm) coating of a conducting layer of carbon, gold, or other metal to prevent image degradation due to charging effects (§10.8). The most important requirement for carrying out TEM experiments is the ability to prepare high-quality, electron transparent thin foil specimens, which are representative of the



1.3.7 Complex damage, showing a variety of dislocation loops, produced by 400 keV electrons in zinc irradiated to 10^{-3} displacements per atom (d.p.a) at room temperature. The electron beam direction was [0001].

Adapted from [11].

¹⁵ Intermediate Voltage Electron Microscopy (IVEM)—Tandem Facility, Argonne National Laboratory, USA.

sample microstructure. The same holds true for X-ray transmission microscopy (XTM). For atomic resolution scanning tunneling microscopy (STM, §11.3), an atomically flat specimen that is also conducting to establish a tunneling current, is required; however, scanning force microscopy (SFM), commonly known as atomic force microscopy (AFM) does not require a conducting surface, but both STM and AFM require solid surfaces that are somewhat rigid to avoid deformation during scanning. Ion scattering techniques (§5.4) require a solid specimen that is vacuum compatible.

1.4 Methods of Characterization: Spectroscopy, Diffraction, and Imaging

Three basic processes underpin the foundations of most characterization methods using probes and signals. The first, *spectroscopy*, is generally described by considering the probe radiation as a particle and involves absorption and emission processes. The second, *scattering* and/or *diffraction*, is described by considering the radiation as a wave, and monitoring its intensity in different directions. *Imaging*, a third way to characterize materials, largely follows from the first two by recording the signal in a spatially resolved fashion. Images can be formed by various contrast mechanisms arising from variations in mass, chemical composition, diffraction, and phase. In scanning probe techniques (§11), contrast is obtained by mapping various forces or registering a tunneling current between the specimen and a tip as it is moved across the surface.

1.4.1 Spectroscopy: Absorption, Emission, and Transition Processes

We start with a simple Bohr model of the atom (§2.2.1), represented by electrons orbiting around a nucleus of charge $+Ze$. In standard X-ray notation, the electron orbits are labeled as $K (n = 1)$, $L (n = 2)$, $M (n = 3) \dots$, where n is the principal quantum number of the electron. Further details of the electronic structure of atoms (§2) and molecules and solids (§3), as they pertain to various materials characterization methods, are discussed later.

Now, consider a multi-electron atom (Fig. 1.4.1). When a primary electron (probe) with sufficient energy, E_p , to overcome the binding energy, E_B , of the inner-shell electron, is incident on the atom, it removes or ejects the *core electron*. In this process, the primary electron is scattered in some new direction with reduced energy, E_p' . Note that not all primary electrons have a close encounter with one of the core electrons to result in such an ejection. The probability of such a close encounter is given by the *cross-section* or the probability of the occurrence of such a collision and ejection. Alternatively, the average distance that the primary electron

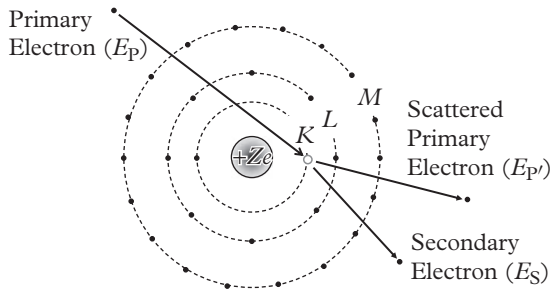


Figure 1.4.1 Interaction of a primary electron with the atom resulting in a core hole, a scattered primary electron, and a secondary electron.

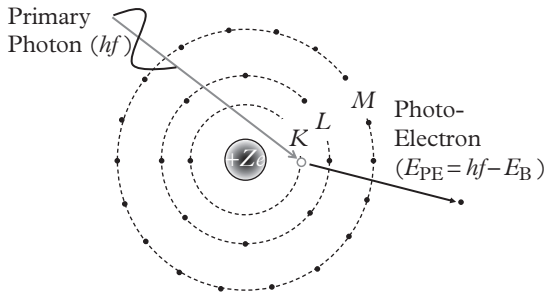


Figure 1.4.2 An incident photon causing an inner-shell ionization and the ejection of a photoelectron.

travels between such collisions in the material is called the *mean free path length* (see §5.3.5.1 for related definitions). The core electron that is removed is now free and is referred to as the *secondary electron*. Further, the primary electron may impart some kinetic energy, E_S , to the secondary electron. By conservation of energy we can easily see that the energy lost by the primary electron, $E_P - E_{P'} = E_B + E_S$, is sensitive to the binding energy of the core electron, and by measuring this loss of energy accurately, the electronic structure of the atom/material can be probed. This technique, EELS, can be implemented either to probe a surface or the bulk—the latter using a TEM (§9.4). It is also possible to map the distribution of such secondary electrons as the primary electron beam is rastered along the specimen surface, and this technique forms the basis of SEM (§10).

Alternatively, instead of the primary electron if a *photon* of sufficient energy, $E_P = hf$, is incident, the related process of photoionization can be realized (Fig. 1.4.2). The photon can be absorbed by the atom and a *photoelectron* with kinetic energy, $E_{PE} = hf - E_B$, can be emitted. As the *K*-shell electrons are bound with more energy than the *L*-shell electrons, for the same incident photon, they will emerge with lower kinetic energy. Atomic electron binding energies are tabulated in Table 2.2.2. However, even though, to first order, binding energies of core electrons are impervious to the nature of atomic bonding, they can be perturbed by the electronic states of the outer electrons; these include electronic bonding in molecules and the valence/conduction bands in solids (see §2.6.3, §3.7). Thus,

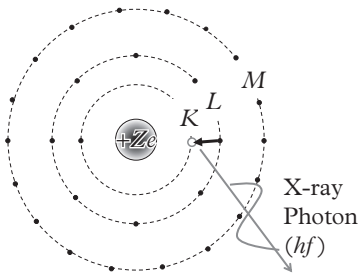


Figure 1.4.3 Characteristic X-ray fluorescence following the creation of a core hole. Note that the emitted photon would have the characteristics of a wave packet illustrated in Figure 1.3.5.

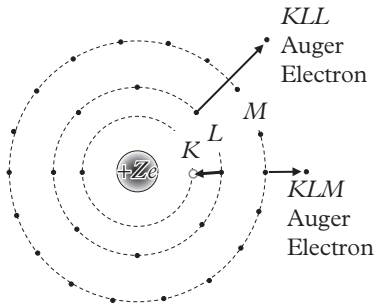


Figure 1.4.4 Atomic relaxation process by non-radiative Auger electron emission. Two alternative scenarios, to illustrate that the Auger electron need not be emitted from the same shell, are shown.

studies of the energy distribution of photoelectrons for photon incidence, i.e. XPS, is a powerful technique to study chemical states in materials. Naturally, as the *K*-shell electrons are more tightly bound and shielded, compared to the *L*-shell electrons, they are less commonly probed and *L*-shell photoelectrons are preferred in photoemission studies (§2.6).

In both ionization processes, following the ejection of the core electron, the atom is left in an excited state with an inner-shell vacancy and can rearrange its electronic configuration to minimize its energy. This is accomplished by the transition of an outer-shell electron of higher energy, aided by the strong nuclear Coulombic attractive potential, to the vacancy created by the core hole. This can be accomplished by two competing processes.

1.4.1.1 Characteristic X-Ray Emission

In this process of atomic rearrangement (Fig. 1.4.3), the transition of the electron is accompanied by the fluorescent emission of an X-ray photon with characteristic energy equal to the difference in energy between the initial and final atomic levels. As expected, these characteristic X-ray emission energies (Table 2.3.1), are element specific and their detection by energy or wavelength dispersion form the basis of elemental analysis by energy (EDXS) or wave-length dispersive X-ray spectrometry (WDS) methods. The semiconductor detectors for energy dispersion are rather compact (§2.5.1.2) and are widely implemented in the narrow confines of both SEMs and TEMs. The alternative, wavelength dispersion analysis (§2.5.1.1) requires a rather bulky crystal detector, and is implemented in dedicated instruments called electron microprobe analyzers (§2.5.2.2). Commonly referred to as microprobes, they are popularly used by geologists to analyze mineral samples (Fig. 1.2.8b).

1.4.1.2 Non-Radiative Auger Emission

In this competing process (Fig. 1.4.4), the atomic rearrangement is accompanied by a non-radiative emission of a second Auger electron, again with energies characteristic of the atom (Table 2.3.2). Since three atomic levels are involved, the emitted Auger electron is labeled with three capital letters—the first represents the shell where the original vacancy is created, the second represents the shell from which the vacancy is filled, and the third represents the shell from which the Auger electron is ejected. Figure 1.4.4 shows two representative Auger electrons, *KLL* and *KLM*.

Which of these two competing processes is favored? Figure 1.4.5 shows X-ray fluorescence and Auger electron yields, as a function of atomic number. It can be clearly seen that, between fluorescence and non-radiative Auger emission, the former (X-rays) is preferred for high atomic number (*Z*) elements, but the latter (Auger electrons) is favored by low atomic number elements.

In molecules, additional transition between rotational, vibrational, and electronic levels can also be probed (Fig. 3.4.2). If a monochromatic radiation of frequency, f_I (usually from a laser, but in the first experiments a high-intensity mercury arc lamp was used), irradiates a specimen (Fig. 1.4.6) it can be both

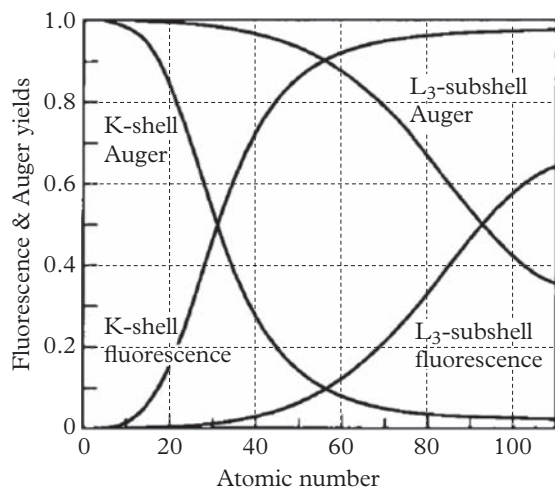


Figure 1.4.5 Auger electron and X-ray fluorescence yields, for K- and L-shell ionization, as a function of atomic number. It is clear that lower atomic number elements favor Auger emissions. See also Example 2.3.2.

Adapted from [13].

elastically (no loss of energy) or inelastically (change in energy) scattered. The scattered radiation has both intensity and polarization (§1.3.4) characteristics different from the incident radiation, and both of these attributes will also depend on the direction of observation.

If the frequency content of the scattered radiation is analyzed, it will show not only the original frequency, f_I (referred to as Rayleigh scattering, §3.4.2), but also pairs of additional frequencies, $f_S = f_I \pm f_M$ (referred to as Raman¹⁶ scattering), where f_M is an internal frequency that depends on molecular, rotational, and electronic transitions (Fig. 3.4.2). In molecular crystals, the Raman spectrum is further dependent on the crystal symmetry, or point group (§4.3), and the intermolecular interactions, which can result in further splitting of the Raman band. Finally, understanding Raman scattering from crystalline solids requires detailed application of group theory and lattice phonon dynamics; however, in practice, a key challenge is to avoid damage (§5.7) of the specimen under irradiation by the intense laser beam. Such details are beyond the scope of this book (see Sherwood, 1972 for details); it suffices to say that for specific materials, such as diamond, the Raman modes are very good “finger prints” for the confirmation of the structure. Basic principles of Rayleigh scattering and Raman spectroscopy are introduced in §3.6.

1.4.2 Scattering and Diffraction

An electromagnetic radiation can be considered as a continuous wave or a discrete quantum of energy, called photons. Even the quanta are discrete bundles of waves

¹⁶ Sir C. V. Raman received the Nobel prize in Physics in 1930 and was cited for “his work on the scattering of light and for the discovery of the effect named after him.”

¹⁷ It is common in optical spectroscopy to specify the radiation in inverse wavelength or wavenumber, $\nu = 1/\lambda$

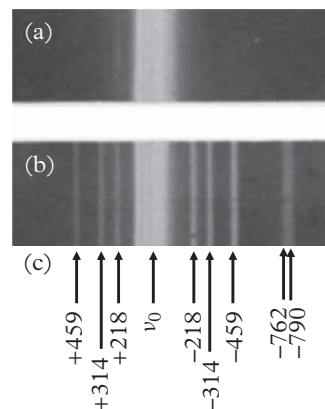


Figure 1.4.6 One of the first published Raman spectra of carbon tetrachloride liquid. (a) Spectrum of the mercury arc lamp in the region of ($\lambda = 435.9$ nm, or wavenumber $\nu_0 = 22938$ cm^{-1})¹⁷ used as the incident probe. (b) Rayleigh and Raman spectrum from liquid CCl_4 . (c) The principal lines from the spectrum of CCl_4 are indexed in wave numbers (cm^{-1}) with respect to $\nu_0 = 22938$ cm^{-1}

Adapted from [14].

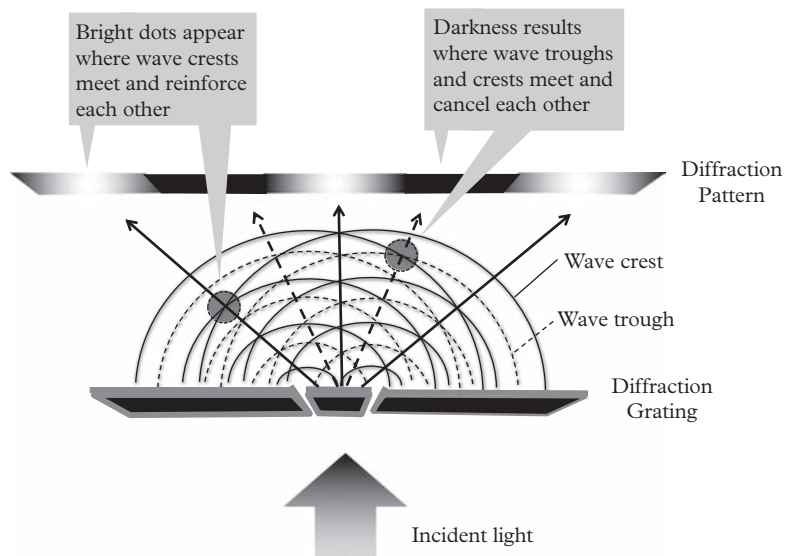


Figure 1.4.7 Interference from a diffraction grating consisting of two slits. Adapted from <https://www.nobelprize.org/prizes/chemistry/2011/press-release/>. For further details of diffraction gratings see §6.6. In the case of crystalline materials, the slits are replaced by a periodic arrangement of atoms.

(Fig. 1.3.5) and their wavelength determines their energy, and in the case of the visible spectrum, their color. When multiple quanta reach the same point in space, they either interfere constructively (become brighter) or destructively (become darker). Simply put, the results of the interference between two waves depend on their phase difference. In the extreme case, if the two waves of the same wavelength are completely in phase (phase difference = $m\pi$, where m is 0 or an even integer) they interfere constructively (addition of amplitudes). Alternatively, if the two waves are out of phase (phase difference = $m\pi$, where m is an odd integer), they interfere destructively (subtraction of amplitudes).

Such an interference effect is illustrated in the high-school physics experiment involving the passage of monochromatic light through two slits: a diffraction grating (Fig. 1.4.7). As the light waves travel through the grating, the waves from the two slits interfere and an alternating dark and light pattern on a screen positioned behind the grating is formed. This diffraction pattern arises, in the general sense, whenever a wave motion (incident radiation) encounters an ordered array of scatterers (such as slits in the grating), which then redirects the incident radiation into relatively well-defined directions. The only requirement for such diffraction to occur is that the wavelength of the incident radiation should be of the same magnitude as the distance between the scattering centers.

In crystalline materials, instead of slits, the gratings are made up of a periodic arrangement of atoms in three dimensions (see discussion at the end of §6.6.2). The repeat distance, or the period, d , in crystalline materials is of the order of 1 \AA (0.1 nm), and so X-rays (Fig. 1.3.2) with similar wavelengths are ideally suited for such diffraction experiments (see Examples 1.4.1 and 1.4.2). Alternatively,

electrons subject to an acceleration potential (high energy, ~ 100 keV, for bulk studies in a transmission electron microscope, or low energy, ~ 100 eV, for surface studies), or neutrons can also be used. The periodic array of atoms in the crystal form well-defined planes that coherently scatter the incident radiation along specific directions, given by Bragg's¹⁸ law

$$\lambda = 2 d \sin \theta \quad (1.4.1)$$

where λ is the wavelength of the incident radiation, d is the interplanar spacing, and θ is measured from the reflecting planes (Fig. 1.4.8). The periodic arrangement of atoms in a 3D crystal describe many such planes with different interplanar spacings, and hence, diffraction peaks or positive interference occurs along several directions (Fig. 1.4.9a). In contrast, amorphous materials show a broad peak (Fig. 1.4.9b) and quasicrystal (§4.4) show unusual fivefold symmetry (Fig. 1.4.9c), a rotational symmetry inconsistent with lattice translations (see §4.1). Diffraction, particularly in reciprocal space is introduced in §4, and discussed in detail, starting in §7 for X-rays and continuing in §8 for electrons and neutrons.

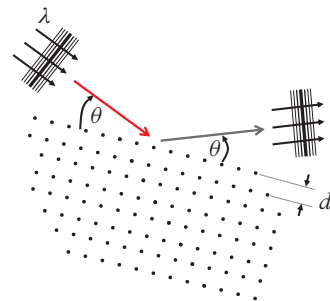


Figure 1.4.8 Diffraction from a periodic arrangement of scattering sites, such as atoms in crystalline materials.

Example 1.4.1: A XRD measurement for NaCl (Fig. 7.9.5) shows the most intense Bragg peak for $d_{hkl} = 2.82 \text{ \AA}$ at $2\theta = 31.69^\circ$. What is the wavelength of the X-ray radiation?

Solution: Applying (1.4.1), we get $\lambda = 2 \cdot 2.82 \sin(15.89) = 1.54 \text{ \AA}$, which is the Cu $K\alpha$ radiation, often used for XRD in the laboratory.

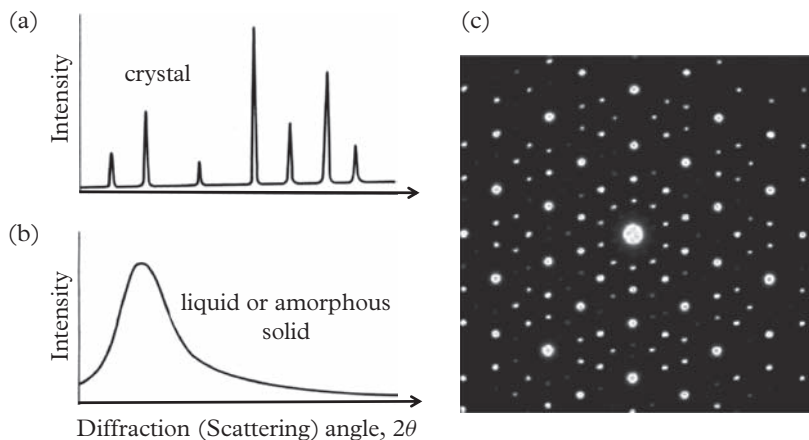
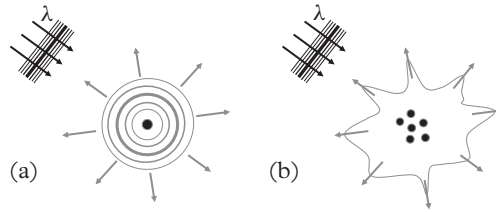


Figure 1.4.9 X-ray diffraction pattern ($\theta - 2\theta$ scan) as a function of angle, 2θ , in (a) crystalline, and (b) amorphous materials. (c) An electron diffraction pattern from a quasicrystalline material, originally identified by Professor Schechtman.¹⁹ Notice the unusual tenfold rotation symmetry—a rotational axis that is inconsistent with lattice translations. Such crystals are mathematically regular but do not repeat themselves periodically.

¹⁸ Sir Lawrence Bragg, at age 25, was the youngest Nobel prize (1915) winner in Physics, and was cited for “services in the analysis of crystal structure by means of X-rays.”

¹⁹ Dan Shechtman won the Nobel prize in Chemistry in 2011, and was cited for “the discovery of quasicrystals.”

Figure 1.4.10 Scattering of incident radiation by (a) point scatterer isotropically in all directions and (b) partially ordered material scattering non-isotropically.



In addition to diffraction, incident radiation can also be redirected over a wide angular range by a point scatterer, such as an individual atom (Fig. 1.4.10a), and by a partially ordered material or a rough surface (Fig. 1.4.10b). The angular distribution of such scattering process is related to the spatial periodicities of the scattering object—obtained from the Fourier transform of its charge density distribution function. Thus, a point object scatters radiation evenly in all directions. In contrast to crystalline materials, in amorphous solids or liquids the atoms are tightly packed together with a preference, statistically speaking, for a specific interatomic spacing but with a general lack of periodicity. Figure 1.4.9 shows representative X-ray scattering from periodic crystals and amorphous solids.

It is worth mentioning here that if a collimated beam of monoenergetic incident particles (typically ^4He ions with MeV energy) are used to probe a solid, the ions are kinematically scattered (§5.3.5.3) following simple rules of conservation of energy and momentum both parallel and perpendicular to the direction of incidence. It can be easily shown that the energy of the ions after scattering is determined by the masses of the particle (^4He ions) and the target atoms in the material, as well as the scattering angle. For direct back-scattering, the energy ratio of the scattered to the incident ion has the lowest value and this geometry is often used in a technique called Rutherford back-scattering spectrometry (RBS, §5.4.1) to determine composition profiles, with depth, of a wide variety of materials. RBS is particularly popular in the analysis of semiconductor heterostructures and further details are discussed in §5.4.

Example 1.4.2: In a low-energy electron diffraction experiment, a peak is observed at $2\theta = 24.42^\circ$ for a specimen with an interplanar spacing of 2.9 \AA . What is the voltage used to accelerate the electron in this experiment?

Solution: Applying Bragg's law, (1.4.1), we solve for the wavelength of the incident electrons:

$$\lambda = 2 d \sin\theta = 2 * 2.9 * \sin(12.21^\circ) = 1.227 \text{ \AA}$$

From the de Broglie relation, (1.3.3), we have

$p = m_e v = h/\lambda$. Thus, the velocity of the of the incident electron is

$$v = \frac{h}{\lambda m_e} = 5.93 \times 10^6 \text{ m/s}$$

Its kinetic energy is

$$E = \frac{1}{2}m_e v^2 = 1.60 \times 10^{-17} \text{ J}$$

Assuming that all this kinetic energy is due to the acceleration potential, V , we get

$$V = E/e = 100 \text{ V, where } e = 1.6 \times 10^{-19} \text{ C is the charge of the electron.}$$

1.4.3 Imaging and Microscopy

Complementing spectroscopy and diffraction/scattering, imaging is the third principal component of materials characterization. Optical microscopy/metallography (§6.8.5) was the first technique developed by Sorby²⁰ to reveal the microstructure of metallic surfaces. From these early observations of steels by optical methods [15], it became apparent that materials not only had structure, but more importantly, that the defects in steels could be related to their properties. This gave rise to the technique of metallography, including related surface preparation (Table 6.8.1) and laid the foundations of structure–property correlations in metallurgy and materials sciences.

To coordinate with the excellent characteristics of data collection and image formation of the human eye (§6.7), optical imaging is optimized for its sensitivity range ($\lambda = 380 - 700 \text{ nm}$), peaking in the green ($\lambda = 560 \text{ nm}$) portion of the visible spectrum. Hence, green filters are commonly used to focus optical microscopes and the viewing screens of TEMs are coated with a green phosphor. Now, the resolution, δ , of a microscope is given by the Rayleigh criterion (§6.8.1):

$$\delta = \frac{0.6\lambda}{n \sin \alpha} \quad (1.4.2)$$

where, λ is the wavelength of the radiation, n is the refractive index of the material, and 2α is the angle that a point source subtends at the lens (Fig. 1.4.11). For a given geometry, fixing 2α , the resolution can be improved by going to smaller wavelengths, λ . Figure 1.4.12 shows a typical example that illustrates the effect of wavelength on resolution. The optical micrograph (a) at $500\times$, of the Toluca iron meteorite is compared with an image (b) of the same meteorite surface taken with a SEM at $2000\times$, with the latter showing substantially greater details. Nevertheless, optical microscopy (§6.8) is a rapid and efficient technique that is the mainstay of materials characterization; further details, including the use of crossed polarizers for non-cubic materials, are discussed in §6.8.

Based on the Rayleigh criterion of resolution, (1.4.2), it is indeed tempting to consider using X-rays of shorter wavelengths than the visible spectrum to improve

²⁰ Henry Clifton Sorby, 1826–1908.

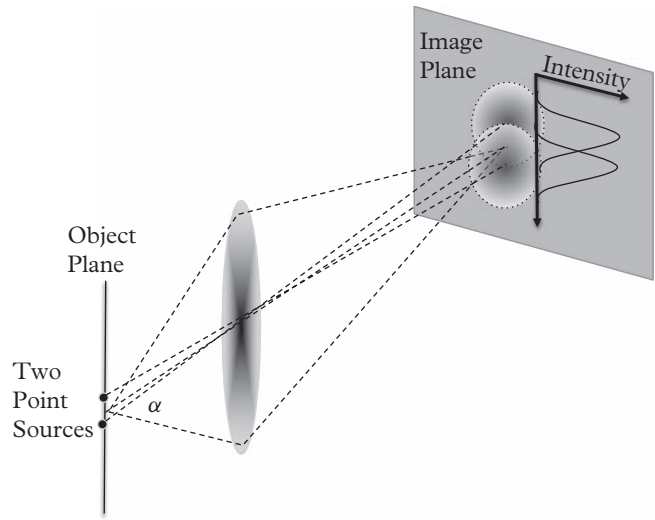
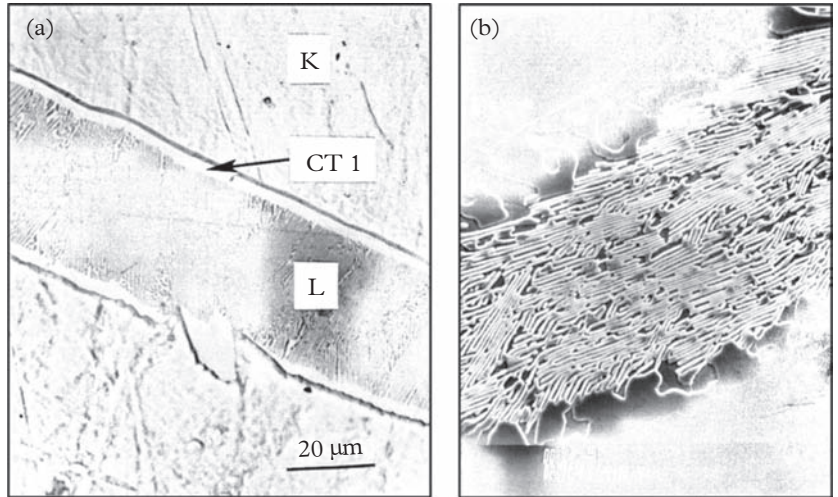


Figure 1.4.11 The Rayleigh criterion, defined by the separation in the image of two point-sources, such that the maxima of one coincides with the first minima of the other.

Figure 1.4.12 (a) The lamellar (L) structure in a high-Ni Taenite (T) phase of the Toluca iron meteorite observed using an optical microscope at 500x magnification. The grey region (CT1) surrounding the lamellar structure is a high-Ni ordered FeNi phase. (b) The same lamellar structure observed in an SEM at 2000x; now the details of the lamellar structure, composed of aligned K and T phases, are clearly resolved.



Adapted from Williams, Pelton, and Gronsky (1991).

resolution. However, optical lenses are based on the simple idea of refraction, i.e. the bending of radiation at the interface between materials of different refractive indices (§6.5). Unfortunately, for EUV and soft X-rays wavelengths, significant refraction cannot be accomplished within a single absorption length. As a result, real images using refraction (lenses) at X-ray wavelengths are not practical. Instead, diffraction techniques using Fresnel zone plate lenses (§6.6.7) are employed for high-resolution soft X-ray ($\lambda = 0.4\text{--}4.4\text{ nm}$) microscopy. There

are two versions of such microscopes: (a) the *full-field* soft X-ray microscope (Fig. 6.6.12), which uses the zone plate lens after the specimen to form a complete image, point by point, much like a common optical microscope, and (b) the *scanning* X-ray microscope, which uses the zone plate to focus a spot of X-ray radiation on the specimen, which is then scanned and the radiation transmitted through the specimen is used to construct its image, pixel by pixel. In addition to recording the absorption as a function of position, it can also record element specific signals, such as emission or fluorescence, giving chemical information as a function of position. Alternatively, using circularly polarized light (Fig. 1.3.4) and X-ray magnetic circular dichroism (XMCD) for magnetic contrast, the magnetic microstructure, or the domain structure, can also be imaged (Fig. 1.4.13). Further discussion of various magnetic imaging methods can be found in Krishnan (2016). XTM, using synchrotron radiation, is introduced in §6.6.7.

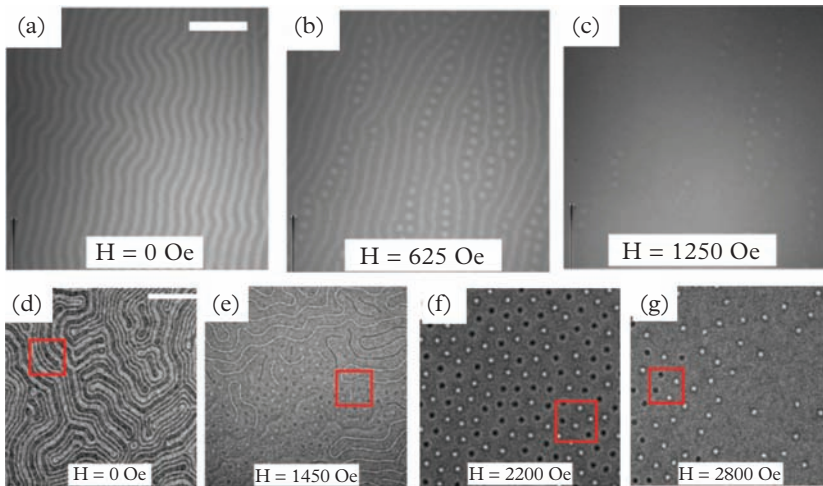


Figure 1.4.13 Magnetic images of $[\text{Fe}_{0.34\text{nm}}\text{Gd}_{0.4\text{nm}}]_{80}$ multilayers under magnetic fields applied perpendicular to the film as indicated. (a-c) Images taken using a full-field soft X-ray transmission microscope (XTM), at the Fe_{L3} edge, with contrast sensitive to the out of plane magnetization. Starting with a stripe domain (a), the domains are pinched to form cylinders in the same space (b), followed by final dissipation (c) of the cylindrical domains. (d-f) Lorentz microscopy images (§9.3.6), recorded at room temperatures, in a FEI Titan microscope equipped with an aberration corrector. Transitions from stripe domains (d), to a magnetic skyrmion²¹ lattice (f), and subsequently to disordered skyrmions (g) are observed. Lorentz microscopy is sensitive to the in-plane magnetic induction only.

Adapted from [16].

²¹ A magnetic skyrmion is a quasiparticle that defines the smallest perturbation to a uniform magnetic field and is visualized as a point-like region of reversed magnetization surrounded by a whirling twist of spins.

Attempts to improve upon the resolution of optical microscopy by using shorter wavelength radiation, such as soft X-rays, have been successful but not easily accessible as they require synchrotron radiation sources (§2.4.3) to generate the X-ray radiation. For routine laboratory use, a more successful optical approach is to reduce the size and intensity of the light source to a sub-micron scale, i.e. using a laser, to generate image signals from individual microscopic spots on the specimen surface. Further, apertures are used to eliminate all light in the image from any plane in the specimen outside the plane of focus. In other words, this method improves resolution and contrast by employing spatial filtering methods to eliminate scattered or reflected light from planes that are out of focus. Two-dimensional images are formed by rastering the spot on the specimen surface; 3D images can be constructed by changing the image plane in the vertical direction. Such confocal scanning optical microscopes (CSOM), described in §6.8.5, have found much use in imaging biological materials (Sheppard and Shotton, 1997).

Following (1.4.2), electrons accelerated at higher voltages (~ 100 kV), are a good alternative to achieving much smaller wavelengths, and thus superior resolutions. However, the electromagnetic lenses required for electron microscopy suffer from various lens aberrations (§9.2.2) that limit the collection angle, α , of electrons to $0.05\text{--}0.5^\circ$ ($10^{-2}\text{--}10^{-3}$ rad). In vacuum, the refractive index, $\mu = 1$, and the Rayleigh criterion for small angles α , gives a resolution $\delta = 1.2\lambda/\mu \sin \alpha = 1.2\lambda/\alpha$. Interatomic distances in solids are of the order of 0.1 nm (see §5.3.5.1 for a discussion of sizes and dimensions); thus, atomic resolution should be attainable for electrons microscopes at ~ 100 kV. Further, taking into consideration the aberrations of electromagnetic lenses, and being mindful of the need to penetrate electron transparent thin foils representative of the bulk material being investigated, atomic resolution was typically achieved in microscopes operating only at higher voltages. However, recent developments in the design and availability of aberration corrected microscopes have made sub-Å resolution in transmission electron microscopy routinely achievable. Figure 1.4.14 provides a very convincing case of the advancement made in image resolution, with successive generations of high-resolution TEMs, using an example of the structural determination of β -SiAlON.

From the first demonstration of a transmission electron microscope in 1933 by Ernst Ruska,²² electron microscopy and diffraction have undergone spectacular development over the years. Further details of this versatile technique, where a single instrument incorporating multiple detectors can provide comprehensive information on the physical, chemical, and magnetic microstructure (Fig. 1.4.13) of the specimen, all at unmatched spatial resolution (Fig. 9.1.2) through diffraction, imaging, and spectroscopy, are discussed in §8 and §9.

Complementing TEM, the SEM (§10), in which the resolution depends on the size of a finely focused probe incident on the specimen, is a versatile instrument

²² Ernst Ruska (1906–1988) was a German physicist who received a much-belated Nobel prize in Physics in 1982; he was cited for “his fundamental work in electron optics, and for the design of the first electron microscope.”

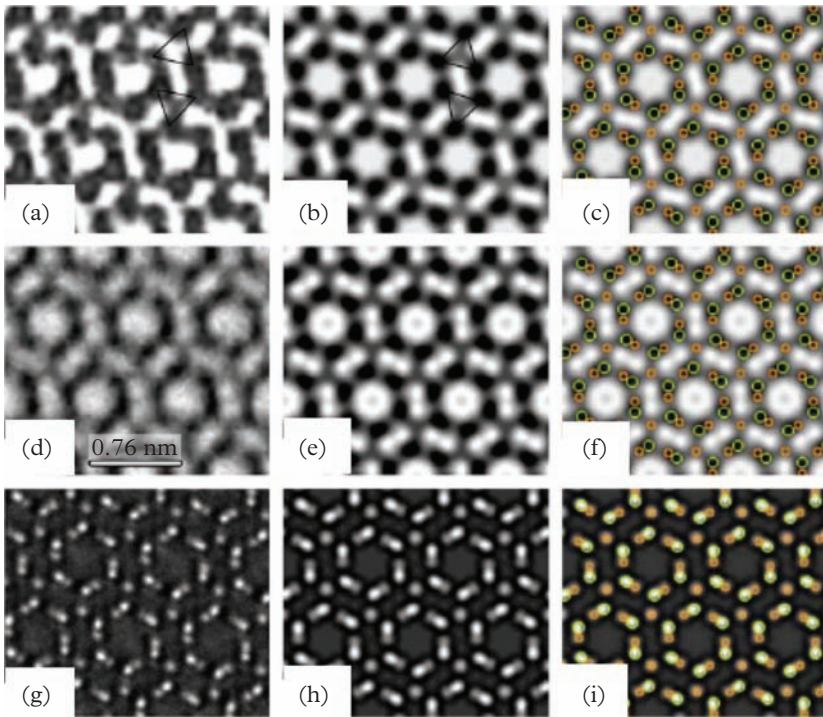


Figure 1.4.14 High resolution atomic structure images of a ceramic material, β' -SiAlON, taken with three generations of transmission electron microscopes at the National Center for Electron Microscopy, Berkeley. Top: The Atomic Resolution Microscope (ARM) designed to achieve atomic resolution using high voltage (1 MeV, $\lambda = 0.00087$ nm) and a spherical aberration coefficient, $C_s = 2$ mm. Middle: The next generation One Ångstrom Microscope (OAM), uses a 300 kV, Schottky emission gun source and a much smaller $C_s = 0.6$ mm. Bottom: The most recent Transmission Electron Aberration-corrected Microscope (TEAM) uses hardware corrections of the aberrations allowing C_s to be tuned at will, and designed for a resolution limit of 0.05 nm. For each microscope, the left column shows the image recorded at Scherzer defocus (§9.2.7.4), with the specimen viewed along the (0001) zone axis of this hexagonal material. The middle column shows a simulation of the structure and the right column shows an overlay of the simulated image on the atomic structure. While all three images (a, d, g) show sixfold symmetry, only the TEAM image shows a direct relationship to the atomic structure. TEM is described in detail in §9.

Adapted from [17].

providing various modes for imaging using secondary or back-scattered electrons. It provides topographic (Fig. 1.4.12b), compositional (Fig. 1.4.15), voltage, and magnetic contrast as well as crystallographic information through channeling patterns (§10.4).

Another elegant way to obtain microstructural information at atomic resolution (Fig. 1.4.16) is to apply a large electric field to a specimen of the material, shaped in the form of a needle, such that the potential barrier, V , for the electrons to leave the specimen can be locally overcome at the tip. Such field emission (§5.2.2) was used to image local variations in the work function. Alternatively, by admitting a small quantity of gas into the chamber and reversing the voltage on the needle (in the first experiments, the material happened to be tungsten) the gas close to the needle surface can be ionized. As the electric field is increased, these ionized gas atoms are repelled from the tip surface towards a fluorescent screen, producing a magnified image of the needle specimen (Fig. 1.4.16) that can clearly delineate the individual atoms. This technique, called field ion microscopy (FIM) [18, 19], has made significant contributions to the study of the structure of interfaces and grain boundaries on the atomic scale [20], but will not be discussed further in this book. A serious limitation of the FIM has been its inability to identify the chemical



Figure 1.4.15 SEM compositional maps, using characteristic X-rays, of a Cu–Zn specimen showing diffusion-induced grain boundary migration. (a) Zn-map, with Zn in white, (b) Cu-map, with 90% Cu being black, and (c) a pseudo-color superposition image with Cu in green and Zn in yellow.

Adapted from Gronsky, Pelton, and Williams (1991).

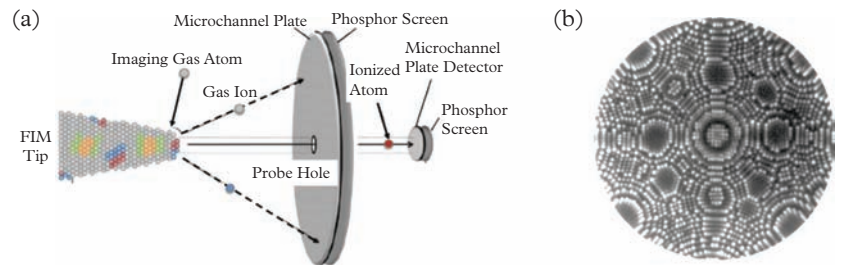


Figure 1.4.16 (a) Schematic of an atom probe field ion microscope (AP-FIM) and (b) FIM image of a Tungsten tip. Note that individual atoms are resolved. FIM was invented by E. R. Müller.

nature of the individually imaged atoms. To overcome this limitation, Müller²³ conceived and built the atom-probe FIM (Fig. 1.4.16a), which is a combination of a probe-hole FIM with a mass spectrometer (§5.4.3) having single particle sensitivity [21]. During observation, the observer selects an atomic site of interest by placing it over a probe hole in the image screen. Pulsed field evaporation sends the chosen particle through the hole and into the spectrometer section. The AP-FIM (see Miller et al., 1996 for a detailed discussion) has undergone numerous major improvements, including the imaging atom probe [22] and the position-sensitive atom probe [23]. The most common geometry currently used is a local electrode atom probe (LEAP) [24], which first appeared commercially in 2002. The current status of atom probe tomography is discussed in [19].

If such a “needle” reverses its role, i.e. it is used as a probe, rather than as the specimen, and is mounted on a flexible cantilever, which is then brought very close—within a few atomic distances—to the specimen surface, a tunneling current can be established between the specimen and the tip. If the tip is now scanned, the specimen surface in vacuum can be imaged at atomic resolution, either by monitoring the tunneling current at constant height, or by monitoring the height at constant tunneling current (§11.2). Such an instrument is called an STM and was invented by Binnig and Rohrer.²⁴ Moreover, the sharp tip can serve as a fine probe to measure a variety of physical properties on the local scale by using a variety of spectroscopic methods. Note that the STM resolves individual atoms on conducting surfaces (Fig. 1.4.17). For resolving individual atoms on insulating surfaces the alternative atomic force microscope (AFM) was introduced [26]. Here, instead of the tunneling current, atomic forces between the needle and the specimen surface, as the tip is scanned, can also be measured



Figure 1.4.17 Large-scale, atomic resolution, topographical STM image of the Si(100) 2×1 surface showing two kinds of steps and various point defects. This is technologically most important as integrated circuits are made on this silicon surface and understanding the local structure on the atomic scale is important for processing and manufacturing of semiconductor microprocessors.

Adapted from [25].

²³ E. R. Müller (1911–1977), German–American physicist.

²⁴ G. Binnig and H. Rohrer shared the 1986 Nobel prize in Physics with E. Ruska, and they were cited for “their design of the scanning tunneling microscope.”

(§11.4). The forces between the tip and surface can have various origins, such as electrostatic, van der Waals, magnetic, etc., giving rise to various variants of these AFMs. These scanning probe instruments and their applications in materials analysis (Weisendanger, 1994; Meyer, Hug, and Bennewitz, 2003) are discussed in §11.

1.4.4 Digital Imaging

As electronic acquisition and analysis of images is now routinely used in materials characterization, it is important to have at least a basic knowledge of digital image acquisition, storage, processing, and analysis methods. While there are excellent textbooks (Gonzales and Woods, 2018; Russ, 1992) and review articles [27–29] that an interested reader can consult for a detailed treatment of the subject, a very brief introduction is included here for completeness.

The sequence of procedures followed in digital imaging is *acquisition* (Fig. 1.4.18a), followed by *processing, analysis, and output* (Fig. 1.4.18b). Typically, an image acquired from a materials characterization source, such as an optical, electron, or scanning probe microscope, is digitized and then stored. By digitization we mean the generation of a digital image, $a[m,n]$, in a 2D *discrete* space that is derived from an analog image, $a(x,y)$, in a 2D *continuous* space through a *sampling* process. The analog image is divided into N rows and M columns and the intersection of a specific row and column, with integer coordinates $[n,m]$, is called a picture element or *pixel*. The value, $a[m,n]$, assigned to each pixel in the digital image is the average brightness in the pixel, rounded to the nearest integer value, with L different gray levels in a process called amplitude

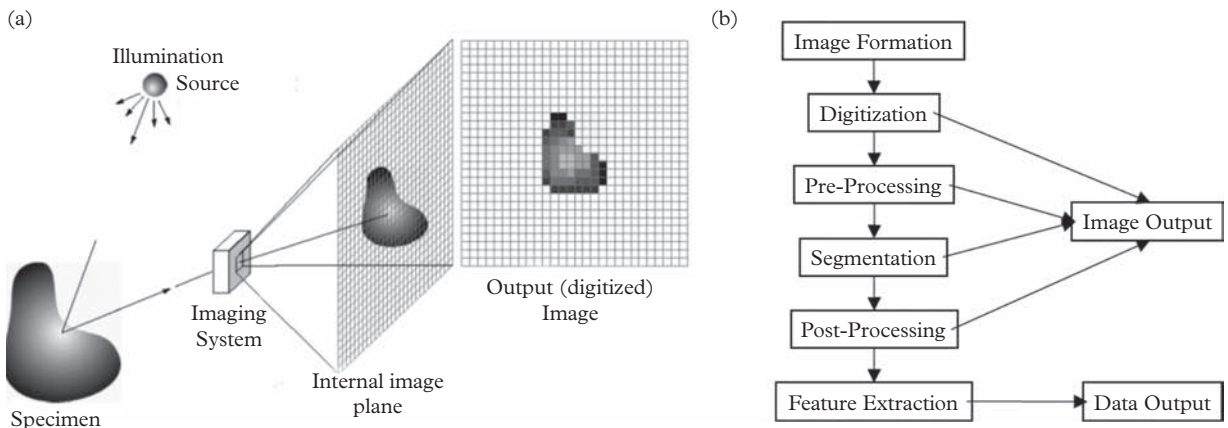


Figure 1.4.18 (a) Schematic illustration of the digital image acquisition process, which include illumination, the specimen, the imaging system and the digitized image. (b) Steps in digital imaging, shown as a flowchart.

(a) Adapted from Gonzalez and Woods (2002). (b) Adapted from [27].

quantization. Usually, $L = 2^B$, where B is the number of bits used to represent the brightness levels in the image; if $B = 1$, we get a binary (black and white) image, and if $B > 1$, we get a gray-scale image.

While the acquired image can itself be the output, it often suffers from defects such as the inclusion of electronic noise, uneven illumination over the field of view, and/or specimen drift. These defects are corrected in the *pre-processing* step. Further analysis of the image for quantitative interpretation requires a sophisticated and complex *segmentation* step, where features of interest in the image are identified and discriminated from the background. Often, the segmentation result requires some *post-processing* correction and then the image, containing the distribution of the desired object(s), is analyzed in the *feature extraction* step to obtain a number of quantitative parameters, including size, position, texture, and (when possible and necessary) appropriate statistical analysis. Here, we introduce only the first three important steps of general interest in digital imaging; the final two steps of post-processing and feature extraction are specific to the particular imaging methods and the characterization problem at hand, and as such are best left for more detailed discussions, readily available in specific textbooks cited earlier.

1.4.4.1 Image Acquisition, Digitization, and Storage

A typical SEM image of a cleaved silicon surface (Fig. 1.4.19) can be used to illustrate the effect of sampling in creating the digital image. The rate at which the signal intensity changes in space is called the spatial frequency; typical features in the image such as edges and small particles represent high spatial frequencies and are best sampled at shorter intervals to improve the quality of the digital image. The sampling frequency in the spatial axis is also known as the *resolution*; in the intensity axis it is known as *quantization*. Figure 1.4.20 shows the effects of resolution and quantization on the quality of the digitized image. While it is obvious that the best-quality image is obtained for largest values of resolution and quantization, this choice often leads to very large data files, which reduces its attractiveness.

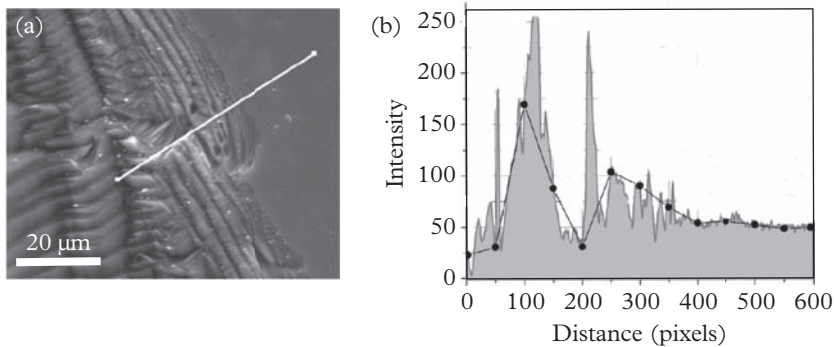


Figure 1.4.19 (a) A scanning electron micrograph of a cleaved silicon wafer, and (b) the intensity trace along the white line shown in the image (a). The image is typically sampled at a specific number of points (black dots) and the digital approximation is shown by the black line.

Adapted from [27].

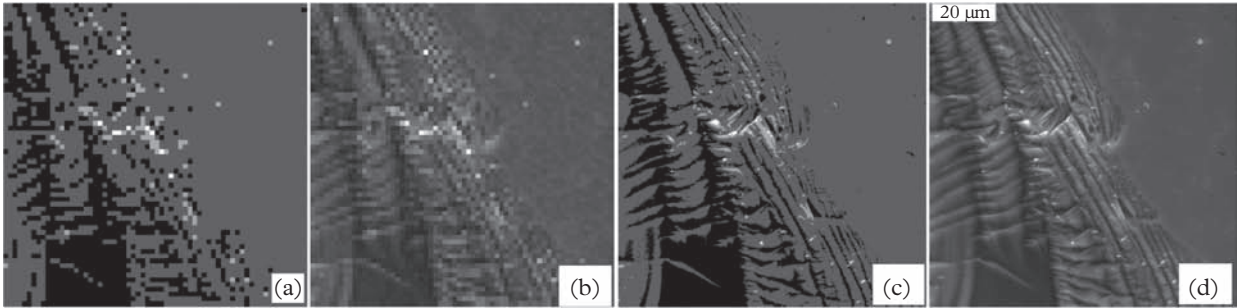


Figure 1.4.20 The effect of resolution and quantization on the digital image. The image from Figure 1.4.19, now shown with (a) 64×64 pixels and four gray levels, (b) 64×64 pixels and 256 gray levels, (c) 512×512 pixels and four gray levels, and (d) 512×512 pixels and 256 gray levels.

Adapted from [27].

The image file size, IFS , is given by

$$IFS = N_x N_y B_{pp} \quad (1.4.3)$$

where N_x and N_y are the number of pixels in the two orthogonal axes, and B_{pp} , which depends on the quantization, is the number of bytes occupied by each pixel. By definition, a byte is composed of 8 binary digits (bits) and a full byte represents 256 values. For examples, a typical gray-scale image with 256 levels corresponds to a digital value ranging from 0 (black) to 255 (white), will require 1 byte/pixel. Such digital images or arrays of numbers can be stored in different file formats, with different compression protocols developed to reduce the file size. TIFF (Tagged Image File Format) is the most flexible format that can be easily exchanged between different computer platforms, and which accepts different kinds of lossless compression methods. It is also the format of choice for many characterization applications. Alternatively, JPEG (Joint Photograph Expert Group) is another standard and commonly used file format that presents images of good visual quality, but often with lossy compression (Fig. 1.4.21). It allows for several levels of data compression, and the higher the level, the smaller the file (more efficient storage) and the greater the loss of information. For scientific and technical purposes, it is important to retain the precision and details of the acquired image and therefore it is best to avoid the JPEG format since the compressions compromise the data.

1.4.4.2 Pre-Processing: Look-Up Tables, Histogram Equalization, Point, and Kernel Operations

An image displayed on a computer monitor need not be a direct mapping of the original image. Generally, a look-up table (LUT) is used to map the image

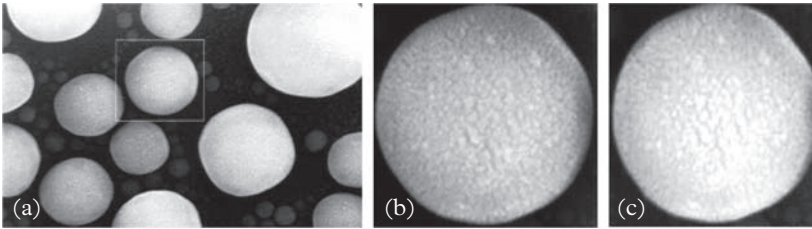


Figure 1.4.21 Storing SEM images of micrometer-size tin spheres. (a) A .TIF file requiring 306 kB of storage. The same file enlarged by a factor of four ($4\times$) using the original image stored as (b) .TIF, and (c) .JPEG requiring only 42 kB of storage. Note that the .JPEG image is degraded and pixelated compared to the .TIF image.

Adapted from Goldstein et al. (2003).

intensity values to the brightness values in the display (Fig. 1.4.22a). If the LUT is linear with unit slope and zero intercept the image is directly mapped to the display. The most common example of a LUT operation is the one used to control the brightness (Fig. 1.4.22b) and contrast (Fig. 1.4.22c) in the displayed image. The functional form of the linear LUT is $g(u) = u + b$ with image values $u \in [0, 1]$. When $b > 0$ (< 0), we get a brightening (darkening) of the image. In addition, the contrast can also be manipulated using a LUT of the form $g(u) = mu + b$, where $b = (1 - m)/2$. Then the contrast is enhanced with a large slope, $m \rightarrow \infty$, and negative intercept, $b \rightarrow -\infty$; alternatively, the contrast is reduced with a small slope, $m \rightarrow 0$ and positive intercept, $b \rightarrow 1/2$. Note that the image is inverted when $m = -1$, $b = 1$. Finally, a nonlinear LUT of the form $g(u) = u^\gamma$, also known as the gamma correction, is often used (Fig. 1.4.22d). Now, when $\gamma < 1$, the function approximates a logarithmic LUT with contrast expansion in the dark region, and when $\gamma > 1$, it approximates an exponential LUT with contrast reduction in the dark region.

In practice, the intensity values of a typical image, plotted as a histogram, are often clustered around the mid-gray value and fall off on either side (Fig. 1.4.21e, top). Such a clustered histogram indicates that the contrast of the image is not maximized. This image is normally transformed so that the distribution of intensity values is such that all intensity values are equally represented in the image. This is known as *histogram equalization* (Fig. 1.4.21e, bottom), and helps optimize image contrast. Modern image acquisition software includes a live window that includes the image and its histogram, and it can be optimally adjusted by changing the illumination and/or exposure time. Needless to say, it can also be adjusted off-line, post image acquisition.

In general, the LUT operations discussed so far are classified as *point operations*, where the intensity, $I_O[m, n]$, of the output image at any pixel with coordinates

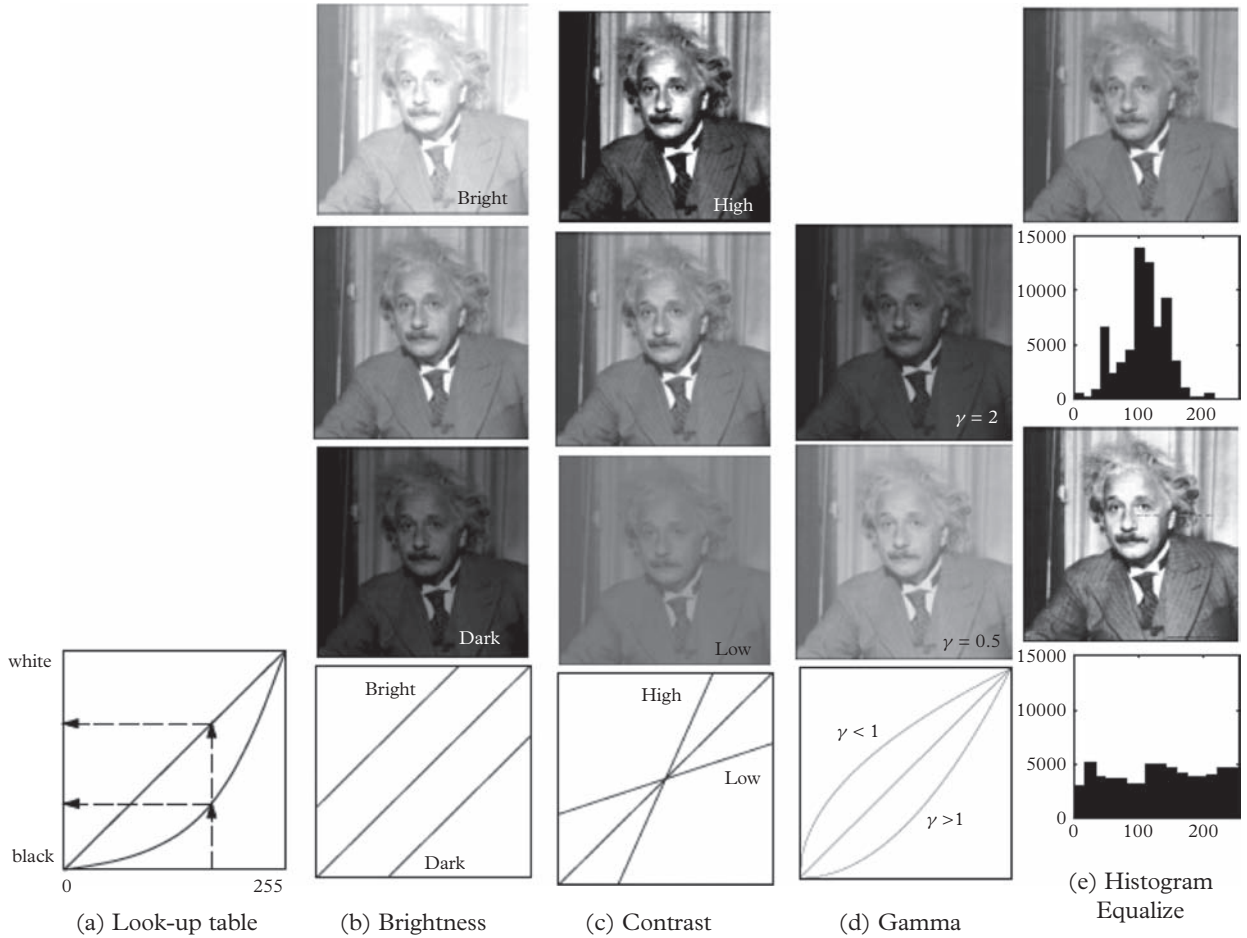


Figure 1.4.22 (a) A look-up table maps the image intensities to the display intensities. A linear LUT can be used to manipulate (b) brightness and (c) contrast in the image. (d) A nonlinear LUT, such as the gamma correction can be used to increase ($\gamma > 1$) or decrease ($\gamma < 1$) contrast. (e) A histogram of the number of pixels in the image at every pixel intensity (0 to 255) is typically clustered (top) around mid-value. By equalizing or stretching the histogram over the entire intensity range, typically improves the contrast in the image.

Adapted from Farid (2010).

$[m,n]$ is dependent only on the input image, $I_I[m,n]$, at the same coordinates. i.e. the two are related by the function, F , such that

$$I_O[m,n] = F(I_I[m,n]) \tag{1.4.4}$$

Such point operations readily lend themselves to algebraic and logic operations on two or more images, in such a way that

$$I_O [m, n] = F (I_1 [m, n], I_2 [m, n]) \quad (1.4.5)$$

where the function, F , relates the intensities at the same pixel position $[m, n]$ in the two input images. The simplest algebraic functions are addition, subtraction, multiplication, and division.

Addition is often used to improve the signal-to-noise ratio (SNR): several fields of the same image are acquired and added together to give an improvement of SNR by the square root of the number of fields. Alternatively, subtraction is used to eliminate contributions from noise or uneven background as may be expected for poor or uneven illumination in an optical microscope (Fig. 1.4.23). Multiplication is used to change pixel intensities using another image as a mask, and division is sometimes used to normalize the response of a CCD camera.

Neighborhood operations differ from point operations, in that their output intensity at any pixel position depends not only on the input intensity at the same pixel position but also on the intensities of its neighbors. Also known as *kernel operations*, they are critically important for applications, which include noise filtering, background subtraction, and edge detection. The example, Figure 1.4.24(i), uses a neighborhood—which is always odd-sided and whose weights are represented as a matrix of 3×3 pixels. The intensity of each pixel is multiplied by a certain weight (kernel), the results are summed together and divided by the total weight for all pixels, and the result is then plotted as the output for the neighborhood center.

Kernels are of two types: (a) those with only positive values, called *low-pass filters*, because they reduce the high-frequency component of the images, and result in reducing *noise* and *blur* in the image, and (b) those with mixed positive and negative values, called *high-pass filters*, because they increase high spatial frequencies in the image, and result in sharpening the image but at the same time increasing the noise. These two filters are also illustrated in Figure 1.4.24(ii), and their effects on an image, i.e. the blurring effect of a low-pass filter, and



Figure 1.4.23 Background subtraction. (a) An optical micrograph of hypereutectic cast iron at $200\times$ BF, 1300×1030 pixels that is unevenly illuminated. (b) The estimated background image intensity. (c) The background subtracted image.

Adapted from [27].

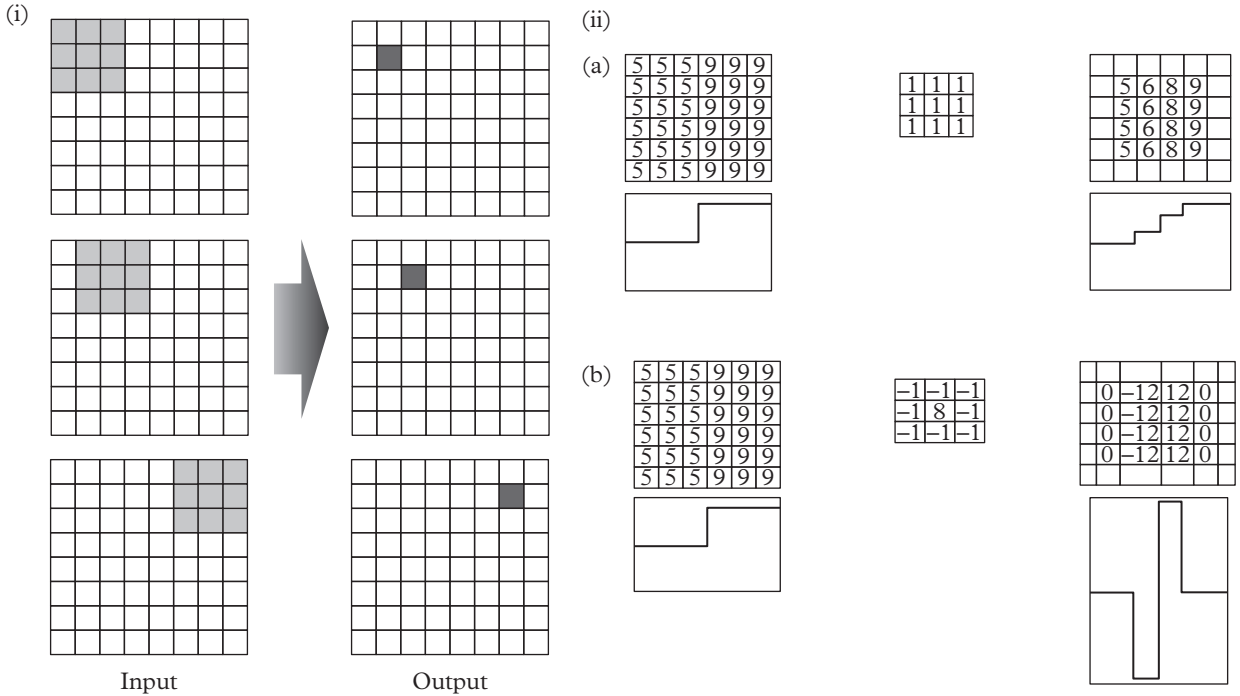


Figure 1.4.24 (i) Sequence used in a neighborhood operation, with the neighborhood analyzed on the left and the calculated output pixel on the right. The process starts at the top and is carried out, column by column, across a line and then line by line, until the entire image is processed. (ii) Application of low-pass and high-pass filter to a simple image. (a) Original image and line profile (left), the low-pass kernel (center), and the output image and line profile (right). (b) Original image and line profile (left), the high-pass kernel (center) and the output image and line profile (right).

Adapted from [27].

the sharpening (edge enhancement) of the high-pass filter, are illustrated in Figure 1.4.25.

Now, consider the filters (kernels) shown in Figure 1.4.26a, which are directional filters that have different effects in different image directions. As it turns out, these kernels are low-pass filters in one direction, and high-pass filters in the orthogonal direction. Hence, they enhance edge directionality, and approximate the derivative of the image in x - and y -directions. In fact, they are the basis of the *Sobel edge detector*, which is often used in segmentation, and corresponds to the intensity gradient in the image. It is given by

$$\text{Sobel}[I(x,y)] = \sqrt{\left(\frac{\partial I(x,y)}{\partial x}\right)^2 + \left(\frac{\partial I(x,y)}{\partial y}\right)^2} \quad (1.4.6)$$

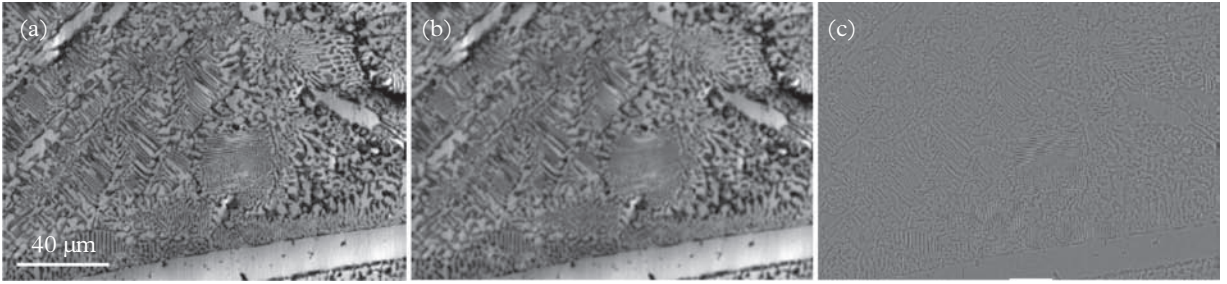


Figure 1.4.25 The effect of low-pass and high-pass filters. (a) The original image. The effect of (b) a 9×9 kernel low-pass filter, and (c) a 3×3 kernel high-pass filter.

Adapted from [27].

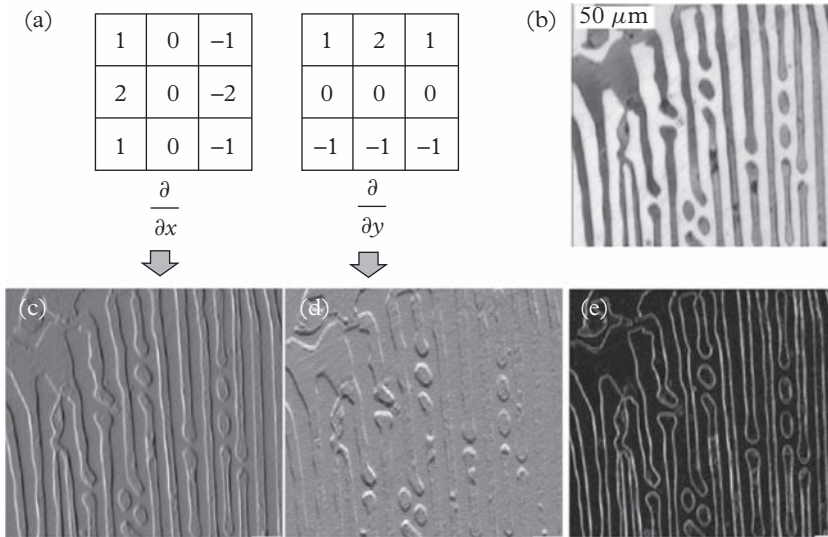


Figure 1.4.26 (a) The kernels for partial x - and y -derivatives. (b) The original image. (c) x -partial derivative image. (d) y -partial derivative image, and (e) Magnitude of the image after the Sobel operation.

Adapted from [27].

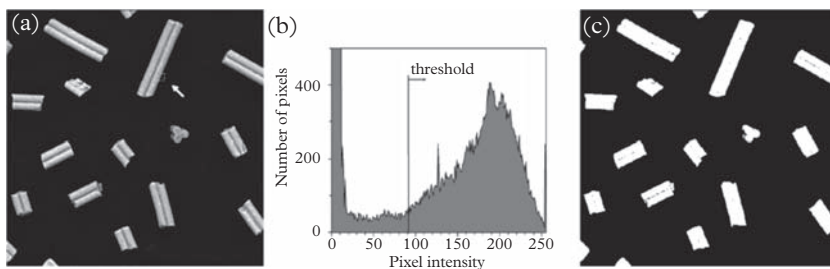
where the partial derivatives correspond to the two kernels in Figure 1.4.26a. The effect of these operations on an image is shown in Figure 1.4.26b–e; in particular, the Sobel operator enhances the edges while the uniform regions become black, and can be used in the segmentation step to discriminate objects in an image.

1.4.4.3 Image Segmentation

This is the most complex step in the digital imaging flow-chart illustrated in Figure 1.4.18b, because it requires the computer to perform cognitive functions similar to the human brain. The latter performs a rapid processing of numerous inputs—specific shape, texture, brightness, boundaries—in association with previous experience, but unfortunately, computers do not have such associative

Figure 1.4.27 (a) An image of catalyst particles. (b) The histogram of intensities and a highlighted threshold level. (c) The segmentation obtained from the thresholding operation.

Adapted from [27].



power, and the classification of an object is done by classifying each pixel of the image as belonging to the object, or not.

The simplest way to segment is to work with the intensities of the pixels; it is considered to be part of the object if its brightness is above a certain level. In the simplest process of intensity thresholding, the choice of the threshold, T , is based on the image histogram, i.e. if $I(x,y) > T$, then the pixel at (x,y) belongs to the object class (Fig. 1.4.27). Alternatively, segmentation can also be based on the contours, and the simplest method is to apply the Sobel edge detector. If such edges form closed boundaries, they can be clearly identified with the object, but if the boundaries or contours are incomplete, it limits the ability to detect the objects of interest. Several other contour-based methods, such as Marr-Hildreth [30] and Canny [31] methods, have been developed to overcome these limitations; however, further details are beyond the introductory nature of this discussion.

The practice of image processing cannot be defined in general terms, as so much of it relates to the actual tasks in mind. For instance, one can include in image processing the task of modeling the background and then subtracting it, which is routinely done in EELS spectroscopy (§9.4.2.3). Examples include the coloring of an image using a well-defined scheme (Fig. 6.8.12), or according to the atomic species in quantitative chemical mapping using EDXS (Fig. 1.4.15). On the other hand, techniques such as particle measurements, closing, erosion, area, moment, counting, and so on are incredibly important at lower resolution, but rarely (if ever) used in high-resolution TEM (§9.3.5). Then, there are the techniques of filters and convolutions, both in real and reciprocal space, which have been introduced, but again, in practice, must be tailored to the actual “question” in mind. Finally, image processing has been covered in all its detail in specialized textbooks (Gonzales and Woods, 2002), but here our interest is limited to providing basic information of general use in characterization.

1.4.5 *In Situ* Methods Across Spatial and Temporal Scales

The emphasis of this book is to describe principles and applications of characterization methods that are broadly applied to studying static and motionless

states of materials. These studies include structural and analytical methods that have provided incredible details of the structure, form, and function of matter, nature, and life. However, matter reacts, undergoes transformations, and routinely exhibits changes in its thermodynamic state. These changes in equilibrium are often unstable and transient in nature. As a result, there is substantial interest in “seeing” how the building blocks of nature, if possible at the atomic length scale, react to external forces, e.g. changes in the thermodynamic state of the material. In other words, a fourth dimension, *time*, now becomes important in characterizing the dynamic behavior of materials. Even though time-resolved studies are not new, and date back to the study of galloping horse in the nineteenth century [36], recent developments permit *in situ* studies at the atomic-length scale and even at femtosecond time scales. In practice, there are many hurdles to carry out these dynamic studies even at slower time scales, much of which revolves around the nature of the specimen, their preparation, and the appropriate specimen environment. We provide very brief introductions to these dynamic methods of materials characterization in this book for X-ray (§7.11.5), neutron (§8.8.3), and electron (§9.5.5) probes, but for those interested in further details, the monograph edited by Ziegler et al. (2014) gives a good overview of time-resolved and *in situ* methods, providing a snapshot of these rapidly developing techniques with particular emphasis on parameters that limit their application.

1.5 Features of Materials Used for Characterization

In general, two principal features of materials, i.e. their electronic structure, including their atomic mass, and crystallography, are used for characterization and are highlighted throughout this text.

For spectroscopy, we probe different aspects of the electronic structure of the material; this can be done starting with the energy levels of its constituent atoms (§2). The core levels, or the inner-shell electron energy levels, are barely perturbed by atomic bonding, and continue to provide valuable chemical information, even in bulk form, for most materials. Techniques that are based on probing such energy levels and related transitions, including the design of simple detectors for measuring X-rays and electrons, are described first (§2). The electronic structure of materials, especially the outer levels, change when the atoms bind into molecules and solids. In addition, molecules exhibit vibrational and rotational modes, whereas crystalline solids develop a bulk band structure, conveniently described by an itinerant or delocalized electron model (Sutton, 1993). The solid also develops acoustic or phonon modes of excitation. Following a conceptual introduction to the relevant electronic structure of molecules and solids, various techniques that are based on probing their rich electronic structures are introduced in §3.

Whenever electromagnetic radiation interacts with matter, some form of scattering always takes place. In particular, the type of scattering that we consider can be simply thought of as arising from the absorption of the incident radiation followed by its re-emission. This model lends itself to both elastic (Rayleigh) and inelastic (Stokes and anti-Stokes) scattering for molecules and atomic arrangements in solids (§3).

An electromagnetic wave, such as an X-ray, can be described by a propagating electric field, which varies sinusoidally with time (Fig. 1.3.4). At any given location, when such an oscillating electric field encounters a charged particle, e.g. an electron in an atom, it will set it also in oscillatory motion about its mean position. An oscillating or accelerating electric charge will emit an electromagnetic radiation. Thus, the atomic electron will not only absorb the incoming radiation but will also re-emit it with the same frequency (f) and wavelength (λ). This process is called scattering, and in X-ray diffraction it is characterized by the re-emitted radiation being coherent with the incident wave. By coherent, we mean a constant phase difference, ϕ , between the incident and scattered radiation, such that in the case of X-rays, $\phi = \lambda/2$. Even if the incident radiation is a parallel beam, the scattered radiation is re-emitted in all directions, with intensities dependent on the angle of scattering (we discuss such Thomson scattering in §7.2.1). Note that in this simple model, the contributions from the positively charged nucleus can be ignored because its mass is much larger ($\sim 1,000$ times) than that of the electron, and as such, it cannot be oscillated to any significant degree by the incident wave. The collection of all electrons in an atom will thus scatter the incident wave in all directions (Fig. 1.4.10). However, for a crystalline material, where atoms are arranged in a well-defined periodic array, their collective scattered radiations interfere constructively only along certain well-defined direction determined by Bragg law, (1.4.1), but destructively interfere for all other directions (§7.4). Further, if the crystal is not perfect, i.e. it includes defects, then the requirement for complete destructive interference is not met, and intensities can be found at angles other than the Bragg angle.

From this brief discussion, it is important to recognize that before we present the physics of diffraction, we need to develop a technical vocabulary to describe the symmetry and periodic arrangement of atoms in crystals as well as their defects. Thus, in §4, we begin with an introduction to crystallography and the general principles of diffraction. We then discuss details of the different kinds of probes and scattering of ions and ion-based characterization methods (§5), and present an introduction to optics, microscopy, and ellipsometry (§6). In the second half of the book, we discuss diffraction in detail for X-rays (§7), and electrons and neutrons (§8). Finally, we discuss imaging with electrons in transmission (§9) and scanning (§10) modes, as well as scanning probe methods (§11), and conclude with a comprehensive set of tables (§12) comparing the different spectroscopy, imaging, and diffraction methods discussed throughout the book.

Summary

Optimizing materials microstructures is central to materials development, enabling new technologies, and in a broad sense, impacting every aspect of our life today. Central to this exercise is materials characterization, which helps relate synthesis and processing of materials to their structure, properties, and performance. The reach of materials characterization is indeed broad and includes, for example, optimization of materials microstructures for advanced technologies, unraveling the structure of biological molecules and complexes, failure analysis, understanding the morphology of rocks and geological processes, and even in the analysis, conservation, and authentication of sculptures or paintings.

Materials characterization typically uses probe and signal radiations to interrogate a specimen. The probe and signal radiations may or may not be the same, and the interactions between the probe and the specimen may be elastic or inelastic, coherent or incoherent. The characterization techniques can be broadly classified as spectroscopy (involving absorption, emission, and/or transitions processes), diffraction and scattering, and imaging and microscopy. The probes are broadly based on the electromagnetic spectrum, and their characteristics (energy, wavelength, momentum, polarization) define their interaction with matter, and determine the nature, scope, and details of the possible methods of characterization. In addition, the probes or signals can also be ions or neutrons. Principal features of the materials, i.e. details of their electronic structure, including atomic mass, composition, and crystallography, contribute to the observable signals and define possible characterization methods that are explored systematically in later chapters.

This introductory chapter provides some basic background, including definitions, on the underlying physics of spectroscopy, diffraction and imaging, interactions of radiations with matter, and a rudimentary introduction to digital imaging. Further, it provides numerous motivational examples of characterization in a variety of different contexts.

FURTHER READING

- Brandon, D., and W. D. Kaplan. *Microstructural Characterization of Materials*. Chichester: Wiley, 2008.
- Brooks, C., and A. Choudhury. *Failure Analysis of Engineering Materials*. New York: McGraw-Hill, 2001.
- Brundle, C. R., C. A. Evans and S. Wilson (eds.). *Encyclopedia of Materials Characterization*. Stoneham: Butterworth-Heinemann, 1992.
- Callister, W. D., Jr., and D. G. Rethwisch. *Materials Science and Engineering: An Introduction*. New York: Wiley, 2009.

- Farid, H. *Fundamentals of Image Processing*. Hanover: Dartmouth College Press, 2010.
- Feldman, L. C., and J. W. Mayer. *Fundamentals of Surface and Thin Film Analysis*. New York: North-Holland, 1986.
- Flewitt, P. E. J., and R. K. Wild. *Physical Methods of Materials Characterization*. Bristol: IoP Press, 2003.
- Goldstein, J., D. Newbury, D. Joy, C. Lyman, P. Echlin, E. Lifshin, L. Sawyer, and J. Michael, *Scanning Electron Microscopy and X-Ray Microanalysis*. New York: Springer, 2003.
- Gonzalez, R. C., and R. E. Woods. *Digital Image Processing*. Upper Saddle River: Prentice-Hall, 2002.
- Hecht, E. *Optics*. Reading: Addison Wesley, 2002.
- Hüfner, S. *Photoelectron Spectroscopy*. Berlin: Springer-Verlag, 2003.
- Krishnan, K. M. *Fundamentals and Applications of Magnetic Materials*. Oxford: Oxford University Press, 2016, Chapter 8.
- Kurzydowski, K. J., and B. Ralph. *The Quantitative Description of the Microstructure of Materials*. Boca Raton: CRC Press, 1995.
- Meyer, E., J. J. Hug, and R. Bennewitz. *Scanning Probe Microscopy—The Lab on a Tip*. Berlin: Springer-Verlag, 2003.
- Miller, M. K., A. Cerezo, M. G. Hetherington, and G. D. W. Smith. *Atom Probe Field Ion Microscopy*. Oxford: Oxford University Press, 1996.
- Owens, F. J., and C. P. Poole Jr., *The Physics and Chemistry of Nanosolids*. Wiley, 2008.
- Russ, J. C. *The Image Processing Handbook*. Boca Raton: CRC Press, 1992.
- Sheppard, C. J. R., C. Sheppard, and D. Shotton. *Confocal Laser Scanning Microscopy*. Abingdon: BIOS Scientific Publishers, 1997.
- Sherwood, P. M. A. *Vibrational Spectroscopy of Solids*. Cambridge: Cambridge University Press, 1972.
- Somorjai, G. A. *Chemistry in Two Dimensions: Surfaces*. New York: Cornell University Press, 1981.
- Stokes, D. E. *Pasteur's Quadrant: Basic Science and Technological Innovation*. Washington, DC: Brookings Institution Press, 1997.
- Sutton, A. P. *Electronic Structure of Materials*. Oxford: Oxford University Press, 1993.
- Vernon, R. H. *A Practical Guide to Rock Microstructure*. Cambridge: Cambridge University Press, 2004.
- Vickerman, J. C., ed. *Surface Analysis—The Principal Techniques*. Chichester: Wiley, 1997.
- Wiesendanger, R. *Scanning Probe Microscopy and Spectroscopy*. Cambridge: Cambridge University Press, 1994.
- Williams, D., A. R. Pelton, and R. Gronsky, eds. *Images of Materials*. Oxford: Oxford University Press, 1991.
- Woodruff, D. P., and T. A. Delchar. *Modern Techniques of Surface Analysis*. Cambridge: Cambridge University Press, 1986.
- Ziegler, A., H. Graafsma, X. F. Zhang, and J. W. M. Frenken, eds. *In-Situ Materials Characterization Across Spatial and Temporal Scales*. New York: Springer, 2014.

.....

REFERENCES

- [1] *Materials Science and Engineering for the 1990s: Maintaining Competitiveness in the Age of Materials*, Washington, DC: The National Academy Press, 1989. A pdf copy of the report is available from <http://nap.edu/758>
- [2] Long, H., S. Mao, Y. Liu, Z. Zhang, and X. Han. “Microstructural and compositional design of Ni-based single crystalline superalloys — A review.” *Journal of Alloys and Compounds* 743 (2018): 203–20.
- [3] Xiang, S., S. Mao, H. Wei, Y. Liu, J. Zhang, Z. Shen, H. Long, H. Zhang, X. Wang, Z. Zhang, and X. Han “Selective Evolution of Secondary γ' Precipitation in a Ni-Based Single Crystal Superalloy Both in the γ Matrix and at the Dislocation Nodes.” *Acta Materialia* 116 (2016): 343–53.
- [4] Liu, M., and S. Nemat-Nasser. “The Microstructure and Boundary Phases of *In-Situ* Reinforced Silicon Nitride.” *Materials Science and Engineering A* 254, (1998): 242–52.
- [5] Clarke, D. R. “Grain Boundaries in Polycrystalline Ceramics.” *Annual Review of Materials Science* 17 (1987): 57.
- [6] Watson, J. D., and F. H. C. Crick. “Molecular Structure of Nucleic Acids: A Structure for Deoxyribose Nucleic Acid.” *Nature* 171 (1953): 737–8.
- [7] Franklin, R. E., and R. G. Gosling. “Evidence for 2-Chain Helix in Crystalline Structure of Sodium Deoxyribonucleate.” *Nature* 172 (1953): 156–7.
- [8] Felkins, K., H. P. Leighly, and A. Jankovic. “The Royal Mail Ship Titanic: Did a Metallurgical Failure Cause a Night to Remember?” *Journal of Metals* 1998: 12–17.
- [9] Götzte, J. “Potential of Cathodoluminescence (CL) Microscopy and Spectroscopy for the Analysis of Minerals and Materials.” *Analytical and Bioanalytical Chemistry* 374 (2002): 703.
- [10] Carson, W. D., and C. Denison. “Mechanisms of Porphyroblast Crystallization: Results from High-Resolution Computed X-ray Tomography.” *Science* 257 (1992): 1236.
- [11] Whitehead, M. E., A. S. A. Karim, M. H. Loretto and R. E. Smallman. “Electron Radiation Damage in H.C.P. Metals—II. The Nature of the Defect Clusters in Zn and Cd Formed by Irradiation in the HVEM.” *Acta Metallurgica* 26, no. 6 (1977): 983–93.
- [12] Li, M., M. A. Kirk, P. M. Baldo, D. Xu and B. D. Wirth. “Study of Defect Evolution by TEM with *In Situ* Ion Irradiation and Coordinated Modelling.” *Philosophical Magazine* 92, no. 16 (2012): 2048–78.
- [13] Krause, M. O. “Atomic Radiative and Radiationless Yields for *K* and *L* Shells.” *Journal of Physical and Chemical Reference Data* 8 (1979): 307.
- [14] Raman, C.V., and K. S. Krishnan. “The Production of New Radiations by Light Scattering. Part I.” *Proc. Roy. Soc.* 122, no. 789 (1929): 23–35.
- [15] Nutall, R. H. “The First Microscopes of Henry Clifton Sorby.” *Technology and Society* 22 (1981): 275–80.
- [16] Montoya, S.A., S. Couture, J. J. Chess, J. C. T. Lee, N. Kent, D. Henze, S. K. Sinha, M.-Y. Im, S. D. Kevan, P. Fischer, B. J. McMorrnan, V. Lomakin,

- S. Roy, and E. E. Fullerton. “Tailoring Magnetic Energies to Form Dipole Skyrmions and Skyrmion Lattices.” *Physical Review B* 95 (2017): 024415.
- [17] Thorel, A., J. Ciston, T. P. Bardel, C. -Y. Song, and U. Dahman. “Observation of the Atomic Structure of β' -SiAlON Using Three Generations of High-Resolution Electron Microscopes.” *Philosophical Magazine A* 93(2013): 1172–81.
- [18] Müller, E. R., and K. Bahadur. “Field Ionization of Gases at a Metal Surface and the Resolution of the Field Ion Microscope.” *Physical Review* 102 (1956): 624.
- [19] Miller, M. K., T. F. Kelly, K. Rajan, and S. P. Ringer. “The Future of Atom Probe Tomography.” *Materials Today* 15, no. 4 (2012): 158–65.
- [20] Amouyal, Y., and G. Schmitz. “Atom Probe Tomography—A Cornerstone in Materials Characterization”. *MRS Bulletin* 41 (2016): 13–18.
- [21] Muller, E. W., J. A. Panitz, and S. B. McLane. “The Atom-Probe Field Ion Microscope.” *Review of Scientific Instruments* 39 (1968): 83.
- [22] Panitz, J.A. “The 10 cm Atom Probe.” *Review of Scientific Instruments* 44 (1973): 1034.
- [23] Cerezo, A., T. J. Godfrey and G. D. W. Smith. “Application of a Position-Sensitive Detector to Atom Probe Microanalysis.” *Review of Scientific Instruments* 59 (1988): 862.
- [24] Kelly, T. F., T. T. Gribb, J. D. Olson, R. L. Martens, J. D. Shepard, S. A. Wiener, T. C. Kunicki, R. M. Ulfig, D. R. Lenz, E. M. Strennen, E. Oltman, J. H. Bunton, and D. R. Strait. “First Data from a Commercial Local Electrode Atom Probe (LEAP).” *Microscopy and Microanalysis* 13 (2004): 373–83.
- [25] Hamers, R. J., R. M. Tromp, and J. E. Demuth. “Electronic and Geometric Structure of Si(111)-(7 × 7) and Si(001) Surfaces.” *Surface Science* 181 (1987): 346–55.
- [26] Binnig, G., C. F. Quate and Ch. Gerber. “Atomic Force Microscope.” *Physical Review Letters* 56 (1986): 930.
- [27] Paciornik, S., and M. H. P. Mauricio. “Digital Imaging.” In: *ASM Handbook, Metallography and Microstructures*, edited by G. F. Vander Voort, Vol. 9, 368–402. Materials Park: ASM International, 2014.
- [28] Russ, J. C. “Fundamentals of Image Processing and Measurement.” In *Encyclopedia of Computer Science and Technology*, 2nd ed., edited by P. A. Laplate. Boca Raton: Taylor & Francis Group, 2016.
- [29] Russ, J. C. “Image Analysis of Foods.” *Journal of Food Science* 80, no. 9 (2015): 1974–87.
- [30] Marr, D., and E. Hildreth. “Theory of Edge Detection.” *Proceedings of the Royal Society of London. Series B, Biological Sciences* 207, no. 1167 (1980): 187–217.
- [31] Canny, J. “A Computational Approach to Edge Detection.” *IEEE Transactions on Pattern Analysis and Machine Intelligence* 8 (1986): 679–698.
- [32] Feynman, R. P. “There’s Plenty of Room at the Bottom (Data Storage).” *Journal of Microelectromechanical Systems* 1, no. 1 (1992): 60–66. doi:10.1109/84.128057. This is a transcript of the talk by Richard Feynman.

- [33] Bednorz, J. G., and K. A. Müller. “Possible High T_c Superconductivity in the Ba–La–Cu–O System.” *Zeitschrift für Physik B Condensed Matter* 64 (1986): 189–93.
- [34] Zhao, J. C., and J. H. Westbrook. “Ultrahigh-Temperature Materials for Jet Engines.” *MRS Bulletin* 28, no. 9 (2003): 622–30.
- [35] Seah, M. P., and W. A. Dench. “Quantitative Electron Spectroscopy of Surfaces: A Standard Data Base for Electron Inelastic Mean Free Paths in Solid.” *Surface and Interface Analysis* 1, no. 1 (1979): 2–11.
- [36] Eadweard Muybridge collections, Stanford University Libraries. Available at: <https://library.stanford.edu/collections/eadweard-muybridge-photographs>.

.....

EXERCISES

A. Test Your Knowledge

There may be more than one, or no, correct answer.

1. Metrology is
 - (a) the study of measurements.
 - (b) the study of weather patterns.
 - (c) not relevant for good materials characterization.
2. Microstructure
 - (a) includes atomic, mesoscopic, and microscopic length scales.
 - (b) is related to materials properties and function.
 - (c) can be observed by the naked eye.
3. Materials characterization involves
 - (a) probes and signals.
 - (b) probes that may damage some materials.
 - (c) probes and signals that are always different radiations.
4. Resolution in the context of materials characterization is
 - (a) a measure of how determined you are to get the job done.
 - (b) only given by the penetration depth of the probe.
 - (c) divided into spatial, depth, and temporal categories.
5. The interaction of a probe with the specimen is
 - (a) elastic if it does not lose any energy.
 - (b) coherent if probe and signal have the same phase.
 - (c) coherent if all the signal is uniformly of the same phase.
6. The electromagnetic spectrum
 - (a) provides a rich source of probes for materials analysis.
 - (b) includes scanning probes.
 - (c) can be displayed in terms of energy, frequency, or wavelength.
 - (d) matches with critical length scales that describe the microstructure of materials.

7. Light
 - (a) is always unpolarized.
 - (b) is a transverse wave with **E** and **H** propagating in orthogonal planes.
 - (c) can be linearly, elliptically or circularly polarized.
8. A photon is a quantum of light that
 - (a) behaves as a particle.
 - (b) behaves as a wave packet.
 - (c) can be divided into smaller units of energy.
9. Interaction of a probe with matter
 - (a) will generally not perturb the material.
 - (b) can cause damage.
 - (c) is characterized by a penetration depth and a mean free path length.
10. The Planck constant
 - (a) is used to strengthen your abs.
 - (b) is a very large number.
 - (c) relates the energy of a photon to its frequency.
 - (d) can be used to calculate the wavelength of an object if its velocity is known.
11. Spectroscopy can involve
 - (a) absorption, emission, and transition processes.
 - (b) non-radiative processes.
 - (c) energy levels associated with molecular vibrations and rotations.
12. X-ray diffraction
 - (a) of crystals involves Bragg law.
 - (b) is dominated by the interaction only with atomic electrons.
 - (d) includes contributions from the electrons, protons and neutrons of the atoms.
13. The resolution of a microscope
 - (a) is given by the Rayleigh criterion.
 - (b) can be improved by reducing the wavelength of the probe.
 - (c) can be improved by increasing the refractive index of the medium.
14. Images with *atomic resolution* can be obtained by _____ microscopy.
 - (a) optical
 - (b) scanning probe
 - (c) scanning tunneling
 - (d) high resolution transmission electron
 - (e) field ion
 - (f) scanning electron
15. A *digitized* image
 - (a) generates an image in *discrete* space.
 - (b) is often derived from an image in continuous space.
 - (c) typically involves a *sampling* process.

16. A *pixel*
 - (a) stands for a picture element.
 - (b) has an *averagebrightness* value.
 - (c) has binary values (1 or 0) for a grey scale image.
17. In a digital image, the *sampling frequency*
 - (a) in the spatial axis gives the resolution.
 - (b) in the intensity axis is known as quantization.
 - (c) depends on the number of specimens imaged.
18. *File formats* in digital imaging include
 - (a) TIFF, which is flexible and involves loss-free compression.
 - (b) JPEG, which is common but has lossy compression.
 - (c) no other formats because they are not discussed here.
19. A *look-up table*
 - (a) maps the image intensities to the display intensities.
 - (b) if linear, can routinely manipulate contrast and brightness.
 - (c) can be non-linear.
 - (d) operation, in general, is NOT a *point operation*.
20. *Kernel* operations in digital imaging
 - (a) are neighborhood operations.
 - (b) only allow low-pass filters.
 - (c) can produce derivatives of images.

B. Problems

1. What do you understand by the term “microstructure of materials?” Write a brief (50–100 word) definition of “microstructure.”
2. What is meant by “materials characterization?” In your own words, briefly (50–100 word) define “materials characterization.”
3. What is meant by “sensitivity” or “detection limit” of a characterization technique?
4. Is it possible to damage a material in the process of characterizing it? Explain, in your own words, using appropriate examples.
5. What is the difference between *spatial* and *temporal* resolution?
6. A dust particle of mass 1 μg travels at a velocity of 25,000 kph. Calculate its wavelength.
7. What is the kinetic energy in Joules of an electron accelerated from rest through a potential of 5 kV?
8. What is the de Broglie wavelength of
 - (i) hydrogen atoms ($m = 1.67 \times 10^{-27}$ kg) moving with velocity = 10^3 m/s?
 - (ii) electrons accelerated by 5,000 V in a SEM?
 - (iii) tennis balls (100 g) traveling with a velocity of 20 m/s?
 - (iv) $^4\text{He}^+$ ions accelerated through 1 MV for RBS experiments?

9. If the wavelength of an electron is infinite, the electron must be stationary. True or false? Justify your answer.
10. Please do some general reading and complete as much of the following table as possible.

Characterization Technique	Probe in	Probe out	Resolution, sensitivity	Depth probed	Highlights or comments
Light Microscopy				
Scanning electron microscopy (SEM)					
Transmission electron microscopy (TEM)					
Energy dispersive X-ray spectrometry (EDS)					
Auger electron spectrometry (AES)					
X-ray photoelectron spectroscopy (XPS)					
Fourier transform infrared spectroscopy (FTIR)					
Raman spectroscopy					
Ultraviolet and visible spectrometry (UV-Vis)					
Rutherford back-scattering spectroscopy (RBS)					
X-ray diffraction (XRD)					
X-ray fluorescence (XRF)					
Scanning tunneling microscopy (STM)					
Atomic force microscopy (AFM)					
Nuclear magnetic resonance (NMR)					
Secondary ion mass spectrometry (SIMS)					
Inductively coupled plasma mass spectrometry (ICP-MS)					
Field ion microscopy					

11. For $\text{Cu}_{K\alpha}$ radiation, how many photons are required to deliver 1 Joule of energy? What is the flux (photons/s) required to deliver a power of 1 watt?